

Neural Dynamics of Planned Arm Movements: Emergent Invariants and Speed-Accuracy Properties During Trajectory Formation

Daniel Bullock and Stephen Grossberg
Center for Adaptive Systems
Department of Mathematics
Boston University

A real-time neural network model, called the vector-integration-to-endpoint (VITE) model is developed and used to simulate quantitatively behavioral and neural data about planned and passive arm movements. Invariants of arm movements emerge through network interactions rather than through an explicitly precomputed trajectory. Motor planning occurs in the form of a target position command (TPC), which specifies where the arm intends to move, and an independently controlled GO command, which specifies the movement's overall speed. Automatic processes convert this information into an arm trajectory with invariant properties. These automatic processes include computation of a present position command (PPC) and a difference vector (DV). The DV is the difference between the PPC and the TPC at any time. The PPC is gradually updated by integrating the DV through time. The GO signal multiplies the DV before it is integrated by the PPC. The PPC generates an outflow movement command to its target muscle groups. Opponent interactions regulate the PPCs to agonist and antagonist muscle groups. This system generates synchronous movements across synergetic muscles by automatically compensating for the different total contractions that each muscle group must undergo. Quantitative simulations are provided of Woodworth's law, of the speed-accuracy trade-off known as Fitts's law, of isotonic arm-movement properties before and after deafferentation, of synchronous and compensatory "central-error-correction" properties of isometric contractions, of velocity amplification during target switching, of velocity profile invariance and asymmetry, of the changes in velocity profile asymmetry at higher movement speeds, of the automatic compensation for staggered onset times of synergetic muscles, of vector cell properties in precentral motor cortex, of the inverse relation between movement duration and peak velocity, and of peak acceleration as a function of movement amplitude and duration. It is shown that TPC, PPC, and DV computations are needed to actively modulate, or gate, the learning of associative maps between TPCs of different modalities, such as between the eye-head system and the hand-arm system. By using such an associative map, looking at an object can activate a TPC of the hand-arm system, as Piaget noted. Then a VITE circuit can translate this TPC into an invariant movement trajectory. An auxiliary circuit, called the Passive Update of Position (PUP) model is described for using inflow signals to update the PPC during passive arm movements owing to external forces. Other uses of outflow and inflow signals are also noted, such as for adaptive linearization of a nonlinear muscle plant, and sequential readout of TPCs during a serial plan, as in reaching and grasping. Comparisons are made with other models of motor control, such as the mass-spring and minimum-jerk models.

The subjective ease with which we carry out simple action plans—rotating a wristwatch into view, lifting a coffee cup, or making a downstroke while writing—masks the enormously complex integrative apparatus needed to achieve and maintain coordination among the thousands of sensors, neurons, and

skeleto-motor units that contribute to any act's planning and execution. Moreover, recent studies of the kinematics of planned arm movements (Abend, Bizzi, & Morasso, 1982; Atkeson & Hollerbach, 1985; Howarth & Beggs, 1981) have shown that the integrative action of all these separate contributors produces velocity profiles whose global shape is remarkably invariant over a wide range of movement sizes and speeds. This raises a fundamental question for the theory of sensorimotor control and for the neurosciences in general: How can the integrated activity of thousands of separate elements produce globally invariant properties?

This research was supported in part by National Science Foundation Grant IST-84-17756 and by Air Force Office of Scientific Research Grants 85-0149 and F49620-86-C-0037.

We wish to thank Carol Yanakakis and Cynthia Suchta for their valuable assistance in the preparation of the article and illustrations.

Correspondence concerning this article should be addressed to Daniel Bullock, Center for Adaptive Systems, Department of Mathematics, Boston University, 111 Cummington Street, Second Floor, Boston, Massachusetts 02215.

Two broad species of answers to this question can be contemplated. The first includes theories that posit the existence of a high-level stage involving explicit computation and internal representation of the invariant, in this case the velocity profile, as a whole. This representation is then used as a basis for per-

forming the desired action. Such theories have been favored recently by many workers in the field of robotics, and at least one theory of this type has already been partially formulated to accommodate kinematic data on human movements: the *minimized Cartesian jerk theory* (Flash & Hogan, 1985; Hogan, 1984), which is a special case of global optimization analysis. The second species of answers includes theories in which no need arises for explicit computation and representation of the invariant trajectory as a whole (Sections 6 and 15). In models associated with such theories, a trajectory with globally invariant properties emerges in real time as the result of events distributed across many interacting sensory, neural, and muscular loci.

In this article we describe a theory of arm trajectory invariants that conforms to the latter ideal (Bullock & Grossberg, 1986). Our analysis suggests that trajectory invariants are best understood not by focusing on velocity profiles as such, but by pursuing more fundamental questions: What principles of adaptive behavioral organization constrain the system design that governs planned arm movements? What mechanisms are needed to realize these principles as a real-time neural network? Our development of this topic proceeds via analyses of learned eye-hand coordination, synchronization among synergists, intermediate position control during movement, and variable velocity control. These analyses disclose a neural network design whose qualitative and quantitative operating characteristics match those observed in a wide range of experiments on human movement. Because velocity profile invariance, as well as speed-dependent changes in velocity profile asymmetry ignored by prior models (Section 11), are among the neural network's emergent operating characteristics, our work shows that neither an explicit trajectory nor a kinematic invariant need be explicitly represented within a motor-control system at any time. Thus our work supports a critical insight of workers in the mass-spring modeling tradition that movement kinematics need not be explicitly preprogrammed. By the same token, our results reject a mass-spring model in its customary form and argue against models based on optimization theory. Instead we show how a movement-control system may be adaptive without necessarily optimizing an explicit cost function.

To support these conclusions further, we use the neural model to simulate quantitatively Woodworth's law and Fitts's law, the empirically derived speed-accuracy trade-off function relating error magnitudes, movement distances, and movement durations; isotonic arm-movement properties before and after deafferentation (Bizzi, Accornero, Chapple, & Hogan, 1982, 1984; Evarts & Fromm, 1978; Polit & Bizzi, 1978); synchronous and compensatory central-error-correction properties of isometric contractions (Freund & Büdingen, 1978; Ghez & Vicario, 1978; Gordon & Ghez, 1984, 1987a, 1987b); velocity amplification during target switching (Georgopoulos, Kalaska, & Massey, 1981); velocity profile invariance and asymmetry (Abend et al., 1982; Atkeson & Hollerbach, 1985; Beggs & Howarth, 1972; Georgopoulos et al., 1981; Morasso, 1981; Soechting & Lacquaniti, 1981); the changes in velocity profile asymmetry at higher movement speeds (Beggs & Howarth, 1972; Zelaznik, Schmidt, & Gielen, 1986); vector cell properties in precentral motor cortex (Evarts & Tanji, 1974; Georgo-

poulos, Kalaska, Caminiti, & Massey, 1982; Georgopoulos, Kalaska, Crutcher, Caminiti, & Massey, 1984; Kalaska, Caminiti, & Georgopoulos, 1983; Tanji & Evarts, 1976); the inverse relation between movement duration and peak velocity (Lestienne, 1979); and peak acceleration as a function of movement amplitude and time (Bizzi et al., 1984). In addition, the work reported here extends a broader program of research on adaptive sensorimotor control (Grossberg, 1978, 1986, 1987b, 1987c; Grossberg & Kuperstein, 1986), which enables functional and mechanistic comparisons to be made between the neural systems governing arm and eye movements, suggests how eye-hand coordination is accomplished, and provides a foundation for work on mechanisms of trajectory realization that compensate for the mechanical effects generated by variable loads and movement velocities (Bullock & Grossberg, 1987).

1. Flexible Organization of Muscle Groups Into Synergies

To move a part of the body, whether an eye, head, arm, or leg, many muscles must work together. For example, muscles controlling several different joints—shoulder, elbow, wrist, and fingers—may contract or relax cooperatively to perform a reaching movement. When groups of muscles cooperate in this way, they are said to form a *synergy* (Bernstein, 1967; Kelso, 1982).

Muscle groups may be incorporated into synergies in a flexible and dynamic fashion. Whereas muscles controlling shoulder, elbow, wrist, and fingers may all contract or relax synergetically to produce a reaching movement, muscles of the fingers and wrist may form a synergy to perform a grasping movement. Thus one synergy may activate shoulder, elbow, wrist, and finger muscles to reach toward an object, and another synergy may then activate only finger and wrist muscles to grasp the object while maintaining postural control over the shoulder and elbow muscles. Groups of fingers may move together synergetically to play a chord on the piano, or separate fingers may be successively activated to play arpeggios.

One of the basic problems of motor control is to understand how neural control structures quickly and flexibly reorganize the set of muscle groups needed to cooperate synergetically in the next movement sequence. Once one squarely faces the problem that many behaviorally important synergies are not hardwired, but are dynamically coupled and decoupled through time in ways that depend on the actor's experience and training, the prospect that the trajectories of all synergists are explicitly preplanned seems remote at best. In support of a dynamic conception of synergy formation, Buchanan, Almdale, Lewis, and Rymer (1986) concluded from their experiments on isometric contractions of human elbow muscles that "the complexity of these patterns raises the possibility that synergies are determined by the tasks and may have no independent existence" (p. 1225).

2. Synchronous Movement of Synergies

When neural commands organize a group of muscles into a synergy, the action of these muscles often occurs synchronously

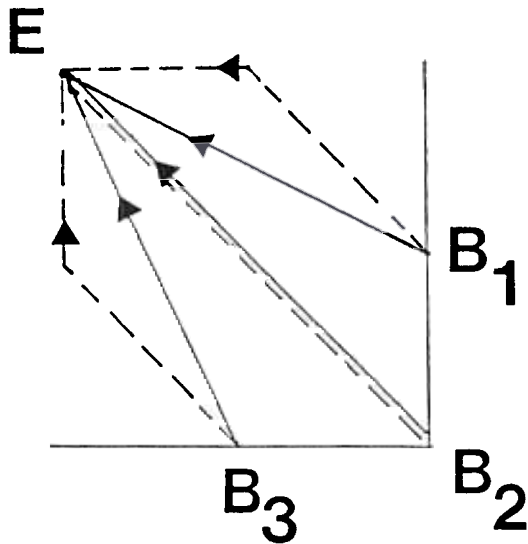


Figure 1. Consequences of two motor-control schemes. (Dashed lines represent movement paths generated when a synergist producing vertical motion and a synergist producing horizontal motion contract in parallel and at equal rates to effect movements from various beginning points [B_i] to the common endpoint E . Solid lines represent movement paths generated when the synergists' contraction rates are adjusted to compensate for differences in the lengths of the vertical and horizontal components of the movement.)

through time. It is partly for this reason that the complexity of the neural commands controlling many movements often goes unnoticed. These movements seem to occur in a single gesture, rather than as the sum of many asynchronous components.

To understand the type of control problem that must be solved to generate synchronous movement, consider a typical arm movement of reaching forward and across the body midline with the right hand in a plane parallel to the ground. Suppose, for simplicity, that the synergist acting at the shoulder is responsible for across-midline motion, that the synergist acting at the elbow is responsible for forward motion, and that the hand is to be moved from Points B_1 , B_2 , or B_3 to Point E . Figure 1 illustrates the effects of two distinct control schemes that might be used to produce these three movements. In the first scheme, the two synergists begin their contractions synchronously, contract at the same rate, and cease contracting when their respective motion component is complete. This typically results in asynchronous contraction terminations and in bent-line movements because the synergist responsible for the longer motion component takes more time to complete its contribution. With this scheme, approximately straight-line motions and synchronous contraction terminations occur only in cases like the B_2 - E movement, for which the component motions happen to be of equal length. In the second scheme, the two synergists contract, not at equal rates, but at rates that have been adjusted to compensate for any differences in length of the component motions. This results in synchronous contraction terminations. Normal arm-movement paths are similar to those implied by the second control scheme (e.g., Morasso,

1981), and experimental studies (Freund & Büdingen, 1978) have shown that contraction rates are made unequal in a way that compensates for inequalities of distance.

What types of adaptive problems are solved by synchronization of synergists? Figure 1 provides some insight into this issue. Without synchronization, the direction of the first part of the movement path may change abruptly several times before the direction of the last part of the movement path is generated (Figure 1). This creates a problem because transporting an object from one place to another with the arm may destabilize the body unless one can predict, and anticipatorily compensate for, the arm movement's destabilizing effects, which are always directional. In the same way, many actions require that forces be applied to surfaces in particular directions. The first control scheme makes the direction in which force is applied difficult to predict and control. Both of these problems are eliminated by the approximately straight-line movement paths that become possible when synergists contract synchronously. Finally, if the various motions composing a movement failed to end synchronously, it would become difficult to ensure smooth transitions between sequentially ordered movements.

In summary, the untoward effects of asynchrony place strong constraints on the mechanisms of movement control: Across the set of muscles whose synergistic action produces a multi-joint movement, contraction durations must be roughly equal, and because contraction distances are typically unequal, contraction rates must be made unequal in a way that compensates for inequalities of distance.

3. Factoring Target Position and Velocity Control

Inequalities of distance are translated into neural commands as differences in the total amounts of contraction by the muscles forming the synergy and, thereby, into mechanical terms as the total amounts of change in the angles between joints (Hollerbach, Moore, & Atkeson, 1986). To compensate for differences in contraction, information must be available that is sufficient to compute the total amounts of contraction that are required. Thus a representation of the initial contraction level of each muscle must be compared with a representation of the target, expected, or final contraction level of the muscle. A primary goal of this article is to specify how this comparison is made. Although information about target position and initial position are both needed to control the total contraction of a muscle group, these two types of information are computed and updated in different ways, a fact that we believe has caused much confusion about whether only target position needs to be coded (Section 6). In particular, we reject the common assumption (Adams, 1971) that the representation of initial contraction used in the comparison is based on afferent feedback from the limbs. We propose instead that it is based primarily on feedback from an outflow-command integrator located along the pathway between the precentral motor cortex and the spinal motoneurons.

Another source of confusion has arisen because target-position information is needed to form a trajectory. This is the type of information that invites concepts of motor planning and expectation. However tempting it may be to so infer, concepts of

motor planning and expectation do not imply that the whole trajectory is explicitly planned.

A second aspect of planning enters into trajectory formation that also does not imply the existence of explicit trajectory planning. This aspect is noticed by considering that the hand-arm system can be moved between fixed initial and target positions at many different velocities. When, as a result of a changed velocity, the overall movement duration changes, the component motions occurring around the various joints must nonetheless remain synchronous. Because fixed differences in initial and target positions can be converted into synchronous motions at a wide range of velocities, there must exist an independently controlled velocity, or GO signal (Section 10). The independent control of target-position commands (TPCs) and velocity commands (GO signals) is a special case of a general neural design that has been called the *factorization of pattern and energy* (Grossberg, 1978, 1982).

4. Synchrony Versus Fitts's Law: The Need for a Neural Analysis of Synergy Formation

Our discussion of synchronous performance of synergies has thus far emphasized that different muscles of the hand-arm system may need to contract by different amounts in equal time in order to move a hand through a fixed distance. When movement of a hand over different distances is considered, a striking contrast between behavioral and neural properties of movement becomes evident. This difference emphasizes that synergies are assembled and disassembled through time in a flexible and dynamic way.

Fitts's law (Fitts, 1954; Fitts & Peterson, 1964) states that movement time (MT) of the arm is related to distance moved (D) and to width of target (W) by the equation

$$MT = a + b \log_2 \left(\frac{2D}{W} \right), \quad (1)$$

where a and b are empirically derived constants. Keele (1981) has reviewed a variety of experiments showing that Fitts's law is remarkably well obeyed despite its simplicity. For example, the law describes movement time for linear arm movements (Fitts, 1954), rotary movements of the wrist (Knight & Dagnall, 1967), back-and-forth movements like dart throwing (Kerr & Langolf, 1977), head movements (Jagacinski & Monk, 1985), movements of young and old people (Welford, Norris, & Schock, 1969), and movements of monkeys as well as humans (Brooks, 1979).

Equation 1 asserts that movement time (MT) increases as the logarithm of distance moved (D), other things being equal. The width parameter (W) in Equation 1 is interpreted as a measure of movement accuracy (Section 27). Although movement distance and time may covary on the behavioral level that describes the aggregate effect of many muscle contractions, such a relation does not necessarily hold on the neural level, where individual muscles may contract by variable amounts, or distances, to achieve synchronous contraction within a constant movement time.

A fundamental issue is raised by this comparison of behav-

ioral and neural constraints. This issue can be better understood by considering the following gedanken example. When each of two fingers is moved separately through different distances, each finger may separately obey Fitts's law. Then the finger that moves a longer distance should take more time to move, other things being equal. In contrast, when the two fingers move the aforementioned distances as part of a single synergy, then each finger should complete its movement in the same time in order to guarantee synergetic synchrony. Thus either one of the fingers must violate Fitts's law, or it must reach its target with a different level of accuracy. Kelso, Southard, and Goodman (1979) and Marteniuk and MacKenzie (1980) have experimentally studied this type of synchronous behavior in experiments on one- or two-handed movements and have documented within-synergy violations of Fitts's law.

Such examples suggest that Fitts's law holds for the aggregate behavior of the largest collection of motor units that form a synergy during a given time interval. Fitts's law need not hold for all subsets of the motor units that compose a synergy. These subsets may, in principle, violate Fitts's law by traveling variable distances in equal time to achieve synchrony of the aggregate movement. To understand how Fitts's law can be reconciled with movement synchrony thus requires an analysis of the neural control mechanisms that flexibly bind muscle groups, such as those controlling different fingers, into a single motor synergy. If such a binding action does not involve explicit planning of a complete trajectory, yet does require activation of a target position command and a GO command, then neural machinery must exist that is capable of automatically converting such commands into complete trajectories with synchronous and invariant properties. One of the primary tasks of this article is to describe the circuit design of this neural machinery and to explain how it works.

5. Some General Issues in Sensorimotor Planning: Multiple Uses of Outflow Versus Inflow Signals

Before beginning a mechanistic analysis of these circuits, we summarize several general issues about motor planning to place the model developed in this article within a broader conceptual framework. In Sections 7 through 12 and 26 through 28, a number of key experiments are reviewed to constrain more sharply the theoretical analysis. In Sections 21 through 28, computer simulations of these data properties are reported.

Neural circuitry automates the production of skilled movements in several mechanistically distinct ways. Perhaps the most general observation is that animals and humans perform marvelously dexterous acts in a world governed by Newton's laws, yet they can go through life without ever learning Newton's laws and, indeed, may have a great deal of difficulty learning them when they try. The phenomenal world of movements is a world governed by motor plans and intentions, rather than by kinematic and inertial laws. A major challenge to theories of biological movement control is to explain how people move so well within a world whose laws they may so poorly understand.

The computation of a hand's or arm's present position illustrates the complexity of this problem. Two general types of present-position signals have been identified in discussions of motor

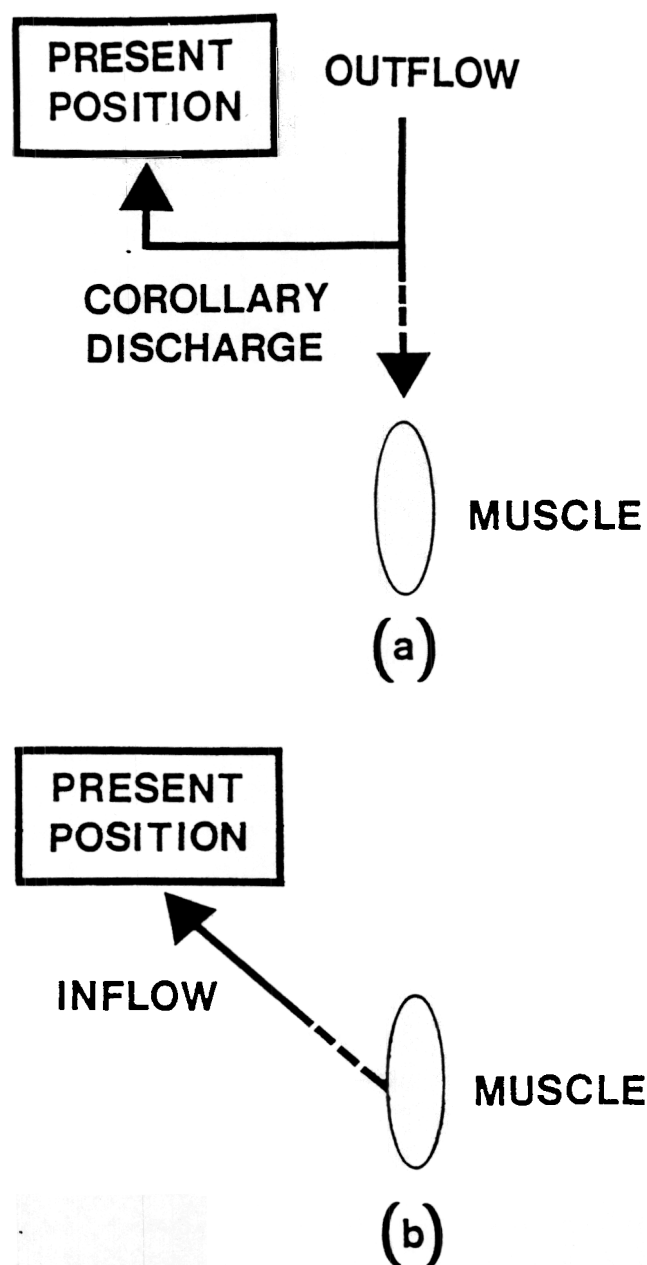


Figure 2. Both outflow and inflow signals contribute to the brain's estimate of the limb's present position, but in different ways.

control: *outflow* signals and *inflow* signals. Figure 2 schematizes the difference between these signal sources. An outflow signal carries a movement command from the brain to a muscle (Figure 2a). Signals that branch off from the efferent brain-to-muscle pathway to register present-position signals are called *corollary discharges* (von Helmholtz, 1866; von Holst & Mittelstaedt, 1950). An inflow signal carries present-position information from a muscle to the brain (Figure 2b). A primary difference between outflow and inflow is that a change in out-

flow signals is triggered only when an observer's brain generates a new movement command. A new inflow signal can, in contrast, be generated by passive movements of the limb. Evidence for influences of both outflow (Helmholtz, 1866) and inflow (Ruffini, 1898; Sherrington, 1894) has accumulated over the past century. Disentangling the different roles played by outflow and inflow signals has remained one of the major problems in motor control. This is a confusing issue because both outflow and inflow signals are used in multiple ways to provide different types of information about present position. The following summary itemizes some of the ways in which these signals are used in our theory.

Although one role of an outflow signal is to move a limb by contracting its target muscles, the operating characteristics of the muscle plant are not known a priori to the outflow source. It is therefore not known a priori how much the muscle will actually contract in response to an outflow signal of prescribed size. It is also not known how much the limb will move in response to a prescribed muscle contraction. In addition, even if the outflow system somehow possessed this information at one time, it might turn out to be the wrong information at a later time, inasmuch as muscle plant characteristics can change through time because of development, aging, exercise, changes in blood supply, or minor tears. Thus the relation between the size of an outflow movement command and the amount of muscle contraction is, in principle, undeterminable without additional information that characterizes the muscle plant's actual response to outflow signals.

To establish a satisfactory correspondence between outflow movement signals and actual muscle contractions, the motor system needs to compute reliable present-position signals that represent where the outflow command tells the muscle to move, as well as reliable present-position signals that represent the state of contraction of the muscle. Corollary discharges and inflow signals can provide these different types of information. Grossberg and Kuperstein (1986) have shown how a comparison, or match, between corollary discharges and inflow signals can be used to modify, through an automatic learning process, the total outflow signal to the muscle in a way that effectively compensates for changes in the muscle plant. Such automatic gain control produces a linear correspondence between an outflow movement command and the amount of muscle contraction even if the muscle plant is nonlinear. The process that matches outflow and inflow signals to linearize the muscle plant response through learning is called *adaptive linearization* of the muscle plant. The cerebellum is implicated by both the theoretically derived circuit and experimental evidence as the site of learning (Albus, 1971; Brindley, 1964; Fujita, 1982a, 1982b; Grossberg, 1969, 1972; Ito, 1974, 1982, 1984; Marr, 1969; McCormick & Thompson, 1984; Optican & Robinson, 1980; Ron & Robinson, 1973; Villis & Hore, 1986; Vilis, Snow, & Hore, 1983).

Given that corollary discharges are matched with inflow signals to linearize the relation between muscle plant contraction and outflow signal size, outflow signals can also be used in yet other ways to provide information about present position. In Sections 16 through 22, we show how outflow signals are matched with target-position signals to generate a trajectory

with synchronous and invariant properties. Thus outflow signals are used in at least three ways, and all of these ways are automatically registered: They send movement signals to target muscles; they generate corollary discharges that are matched with inflow signals to guarantee linear muscle contractions even if the muscle plant is nonlinear; and they generate corollary discharges that are matched with target-position signals to generate synchronous trajectories with invariant properties.

Inflow signals are also used in several ways. One way has already been itemized. A second use of inflow signals is suggested by the following *gedanken* example. When you are sitting in an armchair, let your hands drop passively toward your sides. Depending on a multitude of accidental factors, your hands and arms can end up in any of infinitely many final positions. If you are then called on to make a precise movement with your arm-hand system, this can be done with the usual exquisite accuracy. Thus the fact that your hands and arms start this movement from an initial position that was not reached under active control by an outflow signal does not impair the accuracy of the movement.

A wealth of evidence suggests, however, that comparison between target-position and present-position information is used to move the arms. Moreover, as will be shown later, this present-position information is computed from outflow signals. In contrast, during the passive fall of an arm under the influence of gravity, changes in outflow signal commands are not responsible for the changes in position of the limb. This observation identifies the key issue: How is the outflow signal updated because of passive movement of a limb so that the next active movement can accurately be made? Inasmuch as the final position of a passively falling limb cannot be predicted in advance, it is clear that inflow signals must be used to update present position when an arm is moved passively by an external force.

This conclusion calls attention to a closely related issue that must be dealt with to understand the neural bases of skilled movement: How does the motor system know that the arm is being moved passively because of an external force, and not actively because of a changing outflow command? Such a distinction is needed to prevent inflow information from contaminating outflow commands when the arm is being actively moved. The motor system must use internally generated signals to make the distinction between active movement and passive movement, or postural, conditions. Computational gates must be open and shut on the basis of whether these internally generated signals are on or off (Grossberg & Kuperstein, 1986).

A third role for inflow signals is needed because arms can move at variable velocities while carrying variable loads. Because an arm is a mechanical system embedded in a Newtonian world, an arm can generate unexpected amounts of inertia and acceleration when it tries to move novel loads at novel velocities. During such a novel motion, the commanded outflow position of the arm and its actual position may significantly diverge. Inflow signals are needed to compute mismatches leading to partial compensation for this uncontrolled component of the movement.

Such novel movements differ from our movements when we pick up a familiar fountain pen or briefcase. When the object is familiar, we can predictively adjust the gain of the movement

to compensate for the expected mass of the object. This type of automatic gain control can, moreover, be flexibly switched on and off using signal pathways that can be activated by visual recognition of a familiar object. Inflow signals are used in the learning process, enabling such automatic gain-control signals to be activated in an anticipatory fashion in response to familiar objects (Bullock & Grossberg, 1987).

This listing of multiple uses for outflow and inflow signals invites comparison between how the arm movement system and other movement systems use outflow and inflow signals. Grossberg and Kuperstein (1986) have identified and suggested neural circuit solutions to analogous problems of sensorimotor control within the specialized domain of the saccadic eye-movement system. Several of the problems to which we will suggest circuit solutions in our articles on arm movements have analogs with the saccadic circuits developed by Grossberg and Kuperstein (1986). Together these investigations suggest that several movement systems contain neural circuits that solve similar general problems. Differences between these circuits can be traced to functional specializations in the way these movement systems solve their shared movement problems.

For example, whereas saccades are ballistic movements, arm movements can be made under both continuous and ballistic control. Whereas the eyes normally come to rest in a head-centered position, the arms can come to rest in any of infinitely many positions. Whereas the eyes are typically not subjected to unexpected or variable external loads, the arms are routinely subjected to such loads. Whereas the eyes typically generate a stereotyped velocity profile between a fixed pair of initial and target positions, the arms can move with a continuum of velocity profiles between a fixed pair of initial and target positions. Our analyses show how the arm system is specialized to cope with all of these differences between its behaviors and those of the saccadic eye-movement system.

6. Neural Control of Arm-Position Changes: Beyond the Spring-to-Endpoint Model

A number of further specialized constraints on the mechanisms controlling planned arm movements can be clarified by summarizing shortcomings of the simplest example of a "mass-spring" model of movement generation, which we will call the spring-to-endpoint (STE) model, to distinguish it from other members of the potentially large family of models that exploit mass-spring properties of biological limbs (e.g., Bizzi, 1980; Cooke, 1980; Feldman, 1974, 1986; Humphrey & Reed, 1983; Kelso & Holt, 1980; Sakitt, 1980). As Nichols (1985) and Feldman (1986) have recently noted, past discussions of mass-spring properties have mistakenly lumped together quite different proposals regarding how much properties might be exploited during trajectory formation. Our treatment in this section is meant to serve a pedagogical function, and our criticisms pertain only to the STE model explicitly specified in this section. In particular, no part of our critique denies that the peripheral motor system has mass-spring properties that may be critical to overall motor function. Indeed, in Bullock and Grossberg (1987), we analyzed neural command circuits that exploit mass-spring muscle properties to generate well-controlled movements.

The components of the STE model for movement control can be summarized as follows. Imagine that the eye fixates some object that lies within reach. To touch the object, it is necessary to move the tip of the index finger from its current position to the target position on the object's nearest surface. The STE model suggests that this is accomplished by simply replacing the arm-position command that specifies the arm's present posture with a new arm-position command that specifies the posture the arm would have to assume for the index finger to touch the chosen object surface.

Instatement of the new arm-position command is suggested to generate the desired movement as follows. The arm is held in any position by balancing the muscular and other forces (e.g., gravity) currently acting on the limb. Instatement of a new command changes the pattern of outflow signals that contract the arm muscles. A step change in the pattern of contraction creates a force imbalance that causes the limb to spring in the direction of the larger force at a rate proportional to the force difference. The limb comes to rest when all the forces acting on it are once again balanced. Despite its elegance, the STE model exhibits several deficiencies that highlight properties that an adequate control system needs to have. We briefly summarize two fundamental problems: (a) confounding of speed and distance control and (b) inability to terminate quickly movement at an intermediate position.

The first problem, the speed-distance confound, follows from the dependence of movement rate on the force difference, which in turn depends on the distance between the starting and final positions. At first this might seem to be a desirable property, because it appears to compensate for different distances in the manner needed to ensure synchronization of synergists (Section 2). However, consider also the need to vary the speed of a fixed movement. An actor seeking to perform the same movement at a faster speed would have to follow a two-part movement plan: Early in the movement, instate a virtual target position that is well beyond the desired endpoint and along a line drawn from the initial through the true target position. This command will create a very large initial force imbalance and launch the limb at a high speed. Then, at some point during the movement, instate the true target-position command and let the arm coast to the final position. This example illustrates that the STE model requires a complex and neurally implausible scheme for achieving variable speed control for movements of fixed length.

Cooke (1980) suggested that variable speed control by an STE model can be achieved by abruptly changing the stiffness of agonist and antagonist muscles to achieve differences in distance and speed. This model has not yet been shown to produce velocity profiles with the parameteric properties of the data (Section 11). In addition, Houk and Rymer (1981) and Feldman (1986) have shown that the stiffness of individual muscles is typically maintained at a nearly constant level.

A second problem with the STE model concerns the critical need to abort quickly an evolving movement and stabilize current arm position. Such a need arises, for example, when an animal wishes to freeze upon detection of a predator who uses motion cues to locate prey. It also arises when an action, such as transporting a large mass, begins to destabilize an animal's

overall state of balance. At such times, it is often adaptive to freeze quickly and maintain the current arm position. Freezing could then be quickly achieved by preventing further changes in the currently commanded position. In an STE model, this simple freeze strategy is unavailable because a large discrepancy exists between present arm position and the target-position command throughout much of the trajectory. To implement a freezing response using the STE model, the system would somehow have to determine quickly and instate a new target-position command capable of maintaining the arm's present position. But this is precisely the type of information whose relevance is denied by the STE model.

7. Gradual Updating of Present-Position Commands During Trajectory Formation

Several lines of experimental evidence point to deficiencies of the STE model. One line of evidence, attributable to Bizzi and his colleagues, demonstrates that a type of gradual updating of the movement command occurs that is inconsistent with the STE model. Earlier studies from the Bizzi lab partially supported the STE model.

In their experiments, Polit and Bizzi (1978) studied monkeys trained to move their forearms, without visual feedback of hand position, from a canonical starting position to the position of one of several lights. The monkeys' arm movements were studied both before and after a dorsal rhizotomy was performed to remove all sensory feedback from the arm. Before deafferentation, the monkey could move its hand to the target's position without visual feedback, even if its accustomed position with respect to the arm apparatus was changed. After deafferentation, so long as the spatial conditions of training were maintained—in particular the canonical starting orientation and position with respect to the known target array—the animal remained able to move its hand to the target position. However, if the initial position of the upper arm and elbow of the deafferented arm was passively shifted from the position used throughout training, then the animal's forearm movements terminated at a position shifted by an equal amount away from the target position. Thus the movement of the forearm did not compensate for the change in initial position of the upper arm. Instead the same final synergy of forearm-controlling muscles was generated in both cases.

The fact that deafferented monkeys moved to shifted positions emphasized the critical role of the target position command in setting up the movement trajectory. The fact that normal monkeys could compensate for rotation in a way that deafferented monkeys could not indicated an additional role for inflow signals when the arm is moved passively by an external force (Section 29).

Bizzi et al.'s (1982, 1984) later experiments included an additional manipulation. The results of these experiments are inconsistent with the STE assumption that the arm's motion is governed exclusively by the springlike contraction of its muscles toward the position specified by a new target-position command. In these experiments, the monkey was again deprived of visual and inflow feedback and was placed in its canonical starting position. In addition, its deafferented arm was surrepti-

tiously held at the target position, then released at variable intervals after activation of the target light. Under these circumstances, the arm traveled back toward the canonical starting position, before reversing direction and proceeding to the target. The arm traveled further backward toward the starting position the sooner it was released after target activation. Moreover, when the arm was moved to the target position and then released in the absence of any target presentation, it sprang back to its canonical starting position. Bizzi et al. (1984, p. 2742) concluded that "the CNS had programmed a slow, gradual shift of the equilibrium point, a fact which is not consistent with the 'final position control' [read STE] hypothesis."

The Bizzi et al. (1984) description of their results as a "gradual shift of the equilibrium point" carries the language of the STE model into a context where it may cause confusion. From a mathematical perspective, the intermediate positions of a movement trajectory are not, by definition, equilibrium points. To explicate the Bizzi et al. (1984) data, we show how three quantities are computed and updated through time: a TPC that is switched on once and for all before the movement; an outflow movement command, called the present-position command (PPC), which is continuously updated until it matches the TPC; and the arm position that closely corresponds to the PPC. We use these concepts to explain data from the Bizzi lab in both normal and deafferented conditions.

We call a movement for which a single TPC is switched on before the movement begins an *elementary* movement. Once it is seen how a single TPC can cause gradual updating of the PPC, movements can also be analyzed during which a sequence of TPCs is switched on, either under the control of visual feedback or from a movement-planning network that can store and release sequences of TPCs from memory with the proper order and timing (Grossberg & Kuperstein, 1986).

Our analysis of how the PPC is gradually updated during an elementary movement partially supports the Bizzi et al. (1984) description of a "gradual shift of the equilibrium point" by showing that the arm remains in approximate equilibrium with respect to the PPC, even though none of these intermediate arm positions is an equilibrium point of the system. The only equilibrium point of the system is reached when both the neural control circuit and the arm itself reach equilibrium. That happens when the PPC matches the TPC, thereby preventing further changes in the PPC and allowing the arm to come to rest.

These conclusions refine, rather than totally contradict, the main insight of the STE model. Instead of concluding that the arm springs to the position coded by the TPC, we suggest that the springlike arm tracks the series of positions specified by the PPC as it approaches the TPC. This conception of trajectory formation contrasts sharply with that suggested by Brooks (1986, p. 138) in response to the Bizzi et al. data. Brooks inferred that

animals learn not only the end points and their stiffness, but also a series of intermediate equilibrium positions. In other words, they learn an internal "reference" trajectory that determines the path to be followed and generates torques appropriately to reduce mismatch between the intended and actual events.

In a similar fashion, Hollerbach (1982, p. 192) suggested that

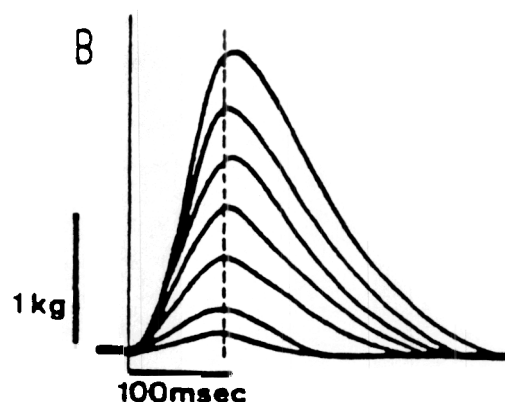


Figure 3. Curves for subjects' approach to various targeted force levels. (Targeted, or peak, levels are reached at nearly the same time, indicating duration invariance across different force "distances." Only the initial part of each curve represents active movement. Postpeak portions represent passive relaxation back to baseline. Reprinted with permission from Freund and Büdingen, 1978.)

we practice movements to "learn the basic torque profiles." In contrast, we suggest that the readout of the TPC is learned, but that the gradual updating of the PPC is automatic. A number of auxiliary learning processes are also needed to update the PPC after passive movements because of an external force (Section 29), to linearize adaptively the response of a nonlinear muscle plant (Grossberg & Kuperstein, 1986), and to compensate adaptively for the inertial effects of variable loads and velocities (Bullock & Grossberg, 1987). These additional learning processes enable the automatic updating of the PPC to generate controllable movements without requiring that the entire trajectory be learned.

8. Duration Invariance During Isotonic Movements and Isometric Contractions

Further information concerning the gradual updating process whereby PPCs match a TPC can be inferred from the detailed spatiotemporal properties of arm trajectory formation. Freund and Büdingen (1978) have studied

the relationship between the speed of the fastest possible voluntary contractions and their amplitudes for several hand and forearm muscles under both isotonic and isometric conditions. These experiments showed the larger the amplitude, the faster the contraction. The increase of the rate of rise of isometric tension or of the velocity of isotonic movements with rising amplitude was linear. The slope of this relationship was the same for three different hand and forearm muscles examined . . . the skeleto-motor speed control system operates by adjusting the velocity of a contraction to its amplitude in such a way that the contraction time remains approximately constant . . . this type of speed control is a necessary requirement for the synchrony of synergistic muscle contractions (p. 1).

This study raises two main issues. First, it must be explained why, "comparing isotonic movements and isometric contractions, the time from onset to peak was similar in the two conditions" (p. 7). Figure 3 shows the fastest voluntary isometric con-

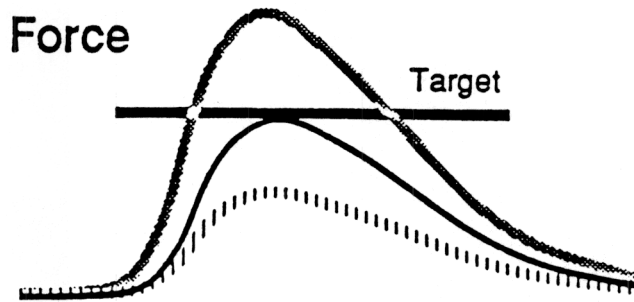


Figure 4. Overshooting (gray curve), hitting (black curve), and undershooting (dashed line) a force-level target (horizontal line) in an isometric task. (Reprinted with permission from Gordon & Ghez, 1987b.)

tractions of the extensor indices muscle. Second, it must be explained why the force develops gradually in time with the shapes depicted in Figure 3. Below it is shown that both duration invariance and the force development through time are emergent properties of the PPC updating process (see Section 21).

9. Compensatory Properties of the PPC Updating Process

Ghez and his colleagues (Ghez & Vicario, 1978; Gordon & Ghez, 1984, 1987a, 1987b) have confirmed the duration invariance reported by Freund and Büdingen (1978) in an isometric paradigm that also disclosed finer properties of the PPC updating process. These authors have suggested that "compensatory adjustments add to preprogrammed specification of rapid force impulses to achieve more accurately targeted responses" (Gordon & Ghez, 1987b, p. 267).

In their isometric task, subjects were instructed to maintain superposition of two lines on a CRT screen. The experimenter could cause one of the lines to jump to any of three positions. Subjects could exert force on an immobile lever to move the other line toward the target line. Equal increments of force produced equal displacements of the line. Thus more isometric force was needed to move the line over a larger distance to the target line.

Figure 4 defines the major variables of their analysis. The force target is represented by the solid black horizontal line. If the subject performs errorlessly—that is, reaches target without overshoot—the value of the peak force will equal the value of the force target, as in the black curve. Overshoots and undershoots in force are represented by the gray and dashed curves, respectively. Figure 5 plots Gordon and Ghez's (1987b) data in a way that illustrates duration invariance. The horizontal line through the data points shows that force rise time is essentially independent of peak force acceleration (d^2F/dt^2) for all the target distances.

Gordon and Ghez (1987b) separately analyzed the data for each of the three target distances and thereby derived the three oblique lines in Figure 5. They interpreted these lines as evidence for an "error-correction" process because a negative correlation exists between peak acceleration and the force rise time, or duration. Thus, if the acceleration for a small target

distance was too high early in a movement, the trajectory was "corrected" by shortening the rise time. Had this compensation not occurred, the high acceleration could have produced a peak force appropriate for a larger target distance.

Gordon and Ghez (1987b) assumed that trajectories are preplanned and that their peak accelerations are a signature indicating which trajectory has been preplanned. It is from this perspective that they interpreted the compensatory effect shown in Figure 5 as an error-correction process. In contrast, we suggest in Sections 12 and 20 that this compensatory effect is one of the automatic properties whereby PPCs are gradually updated. We hereby provide an explanation of the compensatory effect that avoids invoking a special mechanism of error correction for a movement that does not generate an error in achieving its target. In addition, this explanation provides a unified analysis of the Bizzi et al. (1984) data on isotonic movements and the Gordon and Ghez (1987b) data on isometric contractions.

10. Target-Switching Experiments: Velocity Amplification, GO Signal, and Fitts's Law

Our explanation of the Freund and Büdingen (1978) and Gordon and Ghez (1987a) data considers how a single GO signal, which initiates and drives all movements to completion, ensures duration invariance when applied to all components of the synergy defined by a TPC. Georgopoulos et al. (1981) have collected data that provide further evidence pertinent to the hypothesized interaction of a GO signal with the process that instates a TPC and thereby updates the PPC. In their experiments, monkeys were trained to move a lever from a start position to one of eight target positions radially situated on a planar surface. Then the original target position was switched to a new target position at variable delays after presentation of the first target.

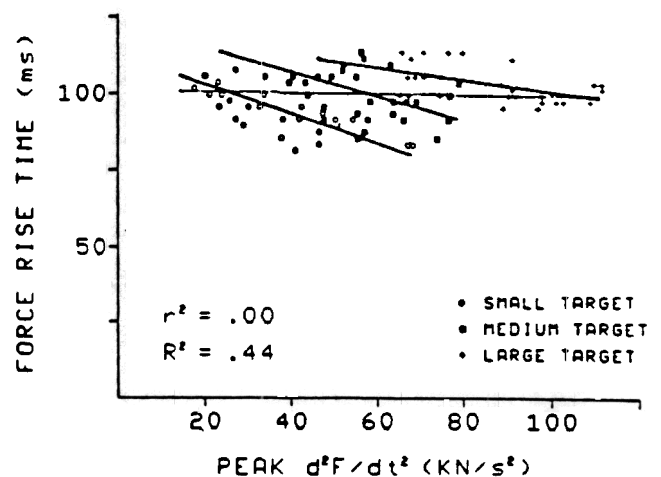


Figure 5. Duration invariance across three force-target levels. (Oblique lines indicate an inverse relation between rise time—duration—and peak acceleration across trials with the same force target level. These trends overlay a direct relation between target level and peak acceleration. Reprinted with permission from Gordon & Ghez, 1987b.)

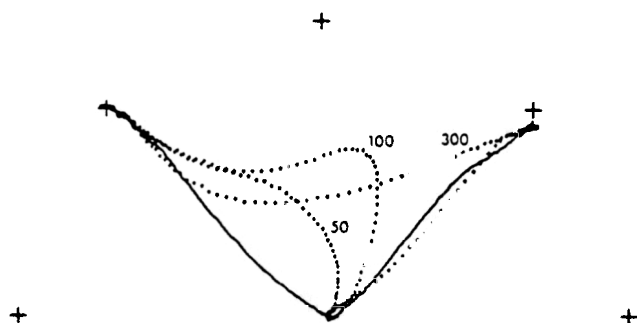


Figure 6. Monkeys seamlessly transformed a movement initiated toward the 2 o'clock target into a movement toward the 10 o'clock target when the latter target was substituted 50 or 100 ms after activation of the 2 o'clock target light. (Reprinted with permission from Georgopoulos, Kalaska, & Massey, 1981.)

Part of the data confirms the fact that

the aimed motor command is emitted in a continuous, ongoing fashion as a real-time process that can be interrupted at any time by the substitution of the original target by the new one. The effects of this change on the ensuing movement appear promptly, without delays beyond the usual reaction time (p. 725).

Figure 6 depicts movement paths found during the target-switching condition. We explain these data in terms of how instatement of a second TPC can rapidly modify the future updating of the PPC.

In addition, Georgopoulos et al. (1981) found a remarkable amplification of peak velocity during the switched component of the movement:

The peak velocity attained on the way to the second target was generally much higher (up to threefold) than that of the control . . . these high velocities cannot be accounted for exclusively by a mechanism that adjusts peak velocity to the amplitude of movements. . . . The cause of this phenomenon is unclear (pp. 732-733).

In Section 24, we explain this phenomenon in terms of the independent control, or factorization, of the GO mechanism and the TPC-switching mechanism described in Section 3. In particular, the GO signal builds up continuously in time. When the TPC is switched to a new target, the PPC can be updated much more quickly because the GO signal that drives it is already large. The more rapid updating of the PPC translates into higher velocities.

These target-switching data call attention to a more subtle property of how a GO signal energizes PPC updating, indeed, a property that has tended to mask the very existence of the GO signal: How can a GO signal that was activated with a previous TPC interact with a later TPC without causing errors in the ability of the PPC to track the later TPC? How does the energizing effect of a GO signal transfer to any TPC? A solution to this problem is suggested in Section 17.

The fact that peak velocity is amplified without affecting movement accuracy during target switching implies a violation of Fitts's law, as Massey, Schwartz, and Georgopoulos (1986)

have noted. Our mechanistic analysis of synergetic binding via instatement of a TPC and of subsequent PPC updating energized by a previously activated GO signal provides an explanation of this Fitts's law violation as well as of Fitts's law itself (Section 27).

Our model also suggests an explanation of why the position of maximal curvature and the time of minimal velocity are correlated during two-part arm movements (Abend et al., 1982; Feters & Todd, 1987; Viviani & Terzuolo, 1980). This correlation arises in the model if the second TPC is switched on only after the PPC approaches the first TPC. In the Georgopoulos et al. (1981) experiment, in contrast, the second TPC is switched on because of the second light before the arm reaches the first target. An unanswered question of considerable interest is whether a second GO signal is switched on gradually with the second TPC in the Abend et al. (1982) paradigm, or whether the reduction in velocity at the turning point is due entirely to nulling of the difference between the PPC and the first TPC while the GO signal maintains an approximately constant value. These alternatives can be tested by measuring the velocities and accelerations subsequent to the position of the turning point.

11. Velocity Profile Invariance and Asymmetry

Many investigators have noted that the velocity profiles of simple arm movements are approximately bell shaped (Abend et al., 1982; Atkeson & Hollerbach, 1985; Beggs & Howarth, 1972; Georgopoulos et al., 1981; Howarth & Beggs, 1971; Morasso, 1981; Soechting & Lacquaniti, 1981). Moreover, the shape of the bell, if rescaled appropriately, is approximately preserved for movements that vary in duration, distance, or peak velocity. Figure 7 shows rescaled velocity profiles from Atkeson and Hollerbach's (1985) experiment. These velocity profiles were generated over a fixed distance at several different velocities. Thus both the duration scale and the velocity scale were modified to superimpose the curves shown in Figure 7.

On the other hand, Beggs and Howarth (1972) showed that "at high speeds the approach curves of the practiced subjects are more symmetrical than at low speeds" (p. 451), and Zelaznik et al. (1986) have shown that at very high speeds the direction of asymmetry actually reverses. Thus the trend documented by Beggs and Howarth continues beyond the range of speeds they sampled. Because velocity profiles associated with slow movements are more asymmetric than those associated with fast movements, they cannot be exactly superimposed. All the velocity profiles shown in Figure 7 are taken from slow (1 to 1.6 s) movements and exhibit the sort of more gradual deceleration than acceleration that Beggs and Howarth (1972) reported for such movements.

Asymmetry, its degree, and changes in its direction are of major theoretical importance. For example, Hogan's (1984) minimum-jerk model predicts symmetric velocity profiles. More generally, superimposability of velocity profiles after time-axis rescaling is a defining characteristic of generalized motor-program models (Hogan, 1984; Meyer, Smith, & Wright, 1982; Schmidt, Zelaznik, & Frank, 1978), which therefore cannot explain how the degree of velocity profile asymmetry varies with

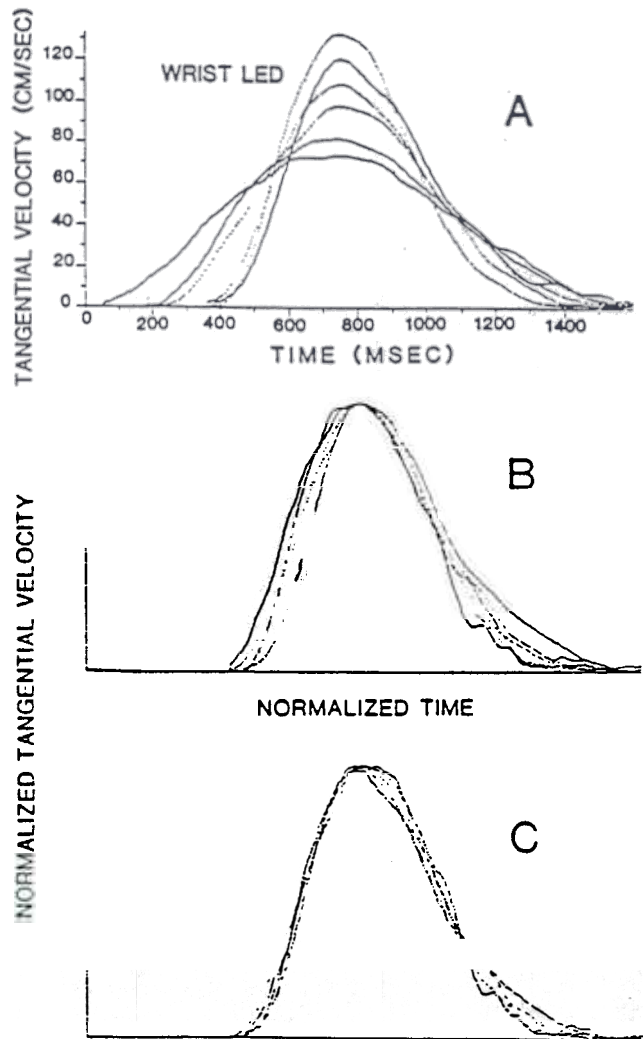


Figure 7. Velocity profiles from movements of similar duration are approximately superimposable following velocity and time axis rescaling. (Reprinted with permission from Atkeson & Hollerbach, 1985.)

overall movement speed. In contrast, our model shows how the gradual updating of the PPC can generate velocity profiles that exhibit the type of speed-dependent asymmetry that is found in the data (Section 22).

Both the existence of asymmetry in velocity profiles and the dependence of degree and direction of asymmetry on movement speed indicate the need for an analysis of the neural dynamics whereby a trajectory unfolds in real time. In contrast, the Hogan (1984) model's global optimization criterion forces strict superimposability of rescaled velocity profiles because it does not represent a process of temporal unfolding. Beggs and Howarth (1972) suggested that the asymmetry reflects a learned strategy of approaching the target as quickly as possible before making corrective movements near the target. For example, these corrective movements could be made under visual guidance by instating a corrected TPC as the arm approached the

target. The approach to such a new TPC would take more time, on the average, than the final approach to the previously tracked TPC, thereby causing greater velocity profile asymmetry. In our simulation results, velocity profiles become more symmetric as movement speed increases and eventually exhibit a symmetry reversal even in the absence of newly instated TPCs. Thus the greater symmetry of velocity profiles at higher speeds may be due to the combined effects of PPC updating properties as the GO signal is parametrically increased, and to the consequent elimination of corrective TPCs as the target is rapidly approached. In support of this analysis, Jeannerod (1984, p. 252) noted that

the low velocity phase is still observed in the absence of visual feedback, and even in the no-vision situation. This finding, however, does not preclude that visual feedback, when present, will be incorporated. . . . In the present study, movement duration and low-velocity phase duration were found to be increased in the visual feedback situation.

In summary, our explanation of these data shows how a circuit capable of flexibly binding muscle groups into synchronous synergies automatically implies the trends observed in data on velocity profile asymmetry. Thus we suggest an explanation of movement invariants, such as duration invariance and synchrony, using a control circuit that never computes an explicit trajectory and whose outputs exhibit a type of speed-dependent asymmetry that other models have not been able to explain.

12. Vector Cells in Motor Cortex

Before quantitatively developing our model, we need to indicate how the PPC is gradually updated until it matches a fixed TPC. Sections 14 through 17 motivate this mechanism through an analysis of the types of information that can be used by a developing system to learn TPCs. The summary here is merely descriptive and is made to link these introductory remarks to supportive neural data.

When a new TPC is switched on, its relation to the current PPC can be arbitrary. Any realizable pair of positions can be coded by the TPC and the PPC. To track the TPC, the PPC needs to change in a *direction* determined by the difference between the TPC and the PPC. In addition, the *amount* of required change is also determined by this difference. An array that measures both the direction and the distance between a pair of arrays, TPC and PPC, is called a *difference vector* (DV). At any given time, the DV between the TPC and the PPC—namely, $DV = TPC - PPC$ —is computed at a match interface (Figure 8).

How does such a DV update the current PPC? Clearly the PPC must be updated in the direction specified by the DV. Hence we assume that the PPC cumulatively adds, or integrates, through time all the DVs that arise at the match interface. Because of this arrangement, the PPC gradually approaches the TPC. At a time when the PPC equals the TPC, the DV equals zero; hence, although the PPC may continue to integrate DVs, it will not change further until either the switching on of a new TPC creates a nonzero DV or the PPC is updated by inflow information during a passive movement (Section 29). To sum-

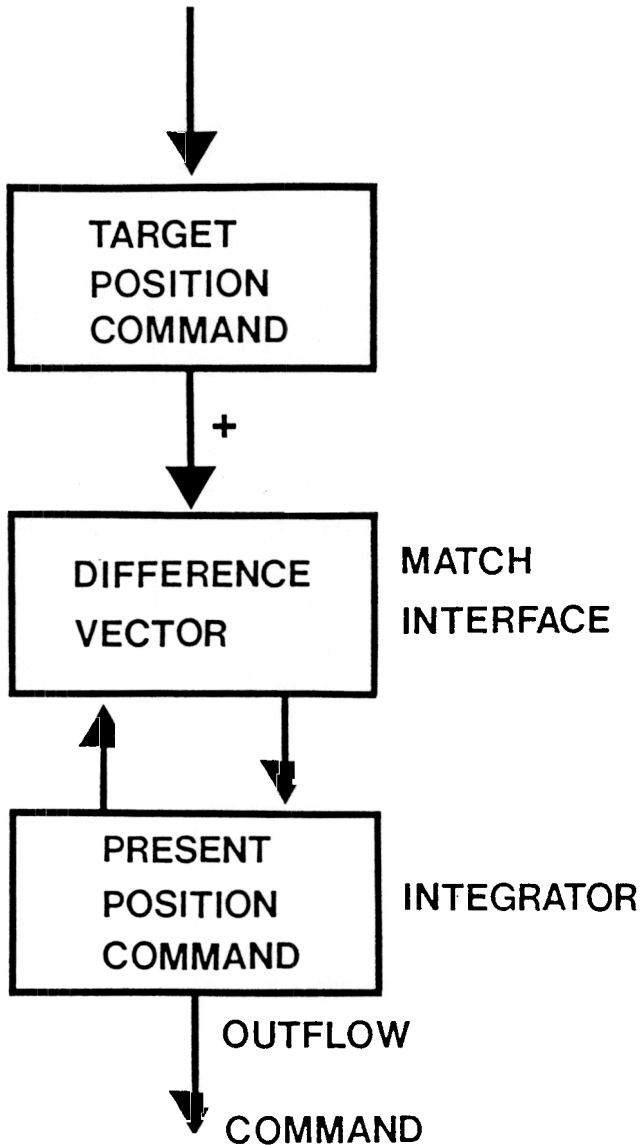


Figure 8. A match interface within the motor command channel continuously computes the difference between the target position and present position and adds the difference to the present-position command.

marize these relations, we call our model the vector-integration-to-endpoint (VITE) model.

Georgopoulos and his colleagues (Georgopoulos et al., 1982; Georgopoulos et al., 1984) have found cell populations in the motor cortex whose collective properties mirror those of the vector-computing nodes at the match interface of our model (Figure 8). The activity of each such node models the average potential of a population of neural cells with similar receptive-field properties. Figure 9 shows a histogram of the average number of spikes per unit time recorded from a single such neuron. This temporal behavior closely matches that of a DV cell population in the model (Figure 18). The vector cells in motor cortex, just like the DV cell populations in the model, are very

broadly tuned to direction (Figure 10a); that is, there exists a broad range of directions in which a given component of the model DV is positive.

Figure 11 further explicates these properties. Figure 11a clarifies why cells at the DV stage may be called vector cells at all. For simple movements, at increasing times $t_0 < t_1 < t_2 < \dots$, the relative sizes of the activities across the DV populations do not change. Hence these populations code a vector direction, even though their individual absolute activities sweep out an approximately bell-shaped curve through time. Figure 11b illustrates that as movement direction is parametrically changed, the relative activations of an agonist-antagonist pair of DV populations change systematically in such a way that individual populations may remain active over a broad range of directions, as in Figure 10a. Figure 11b also schematizes the fact that different agonist muscles may remain active over different ranges of direction, depending on the movement in question. Although Figure 11a schematizes a formal DV, this DV may have many components because it controls many muscle groups. In contrast, the three-dimensional vector that represents the direction of the arm's movement in Euclidean space has only three components. One of the major outstanding problems in arm-movement control is to relate the geometry of the high-dimensional muscle space with the geometry of Euclidean space.

Because of the importance of explaining why each DV population is sensitive to a broad range of directions, we will comment on this property further. The PPC outflow channels must control several different muscle groups at each joint and several different joints in each arm. Because of the opponent organization of the muscles (Figure 11b), up to one half of the cellular components composing the DV stage will have positive activities during a given movement.

Each initial positive-valued component, $DV_i(0) = TPC_i(0) - PPC_i(0) > 0$, of the DV corresponds to an expected change in length of one of the many muscle groups whose shortening contributes a motion component to the overall limb movement. If there were only one active agonist-antagonist muscle pair driving the movement, the movement would always tend to follow a preferred direction. Where more than one agonist-antagonist pair guides the movement, however, a muscle can facilitate motion along directions other than its preferred direction. In this case, the net direction of limb motion depends on the relative sizes $DV_i(0) > 0$ of the cooperating agonists, so that each DV_i population can be active across a broad range of movement directions, as in Figure 11b. Because the net movement direction shifts continuously with the relative sizes $DV_i(0)$ of the cooperating agonists, it should be possible to predict the direction of a forthcoming limb movement.

Both of these conclusions have been supported by Georgopoulos et al. (1984) and Georgopoulos, Schwartz, and Kettner (1986). Figure 10a illustrates that vector cells in motor cortex are, indeed, broadly tuned to direction. Figure 10b illustrates that the aggregate activity of a large sample of active vector cells (read, cells from different DV_i populations) can be used to predict accurately the direction of the forthcoming movement.

Figure 12 plots data from a vector cell population in vivo alongside the velocity profile of the corresponding movement.

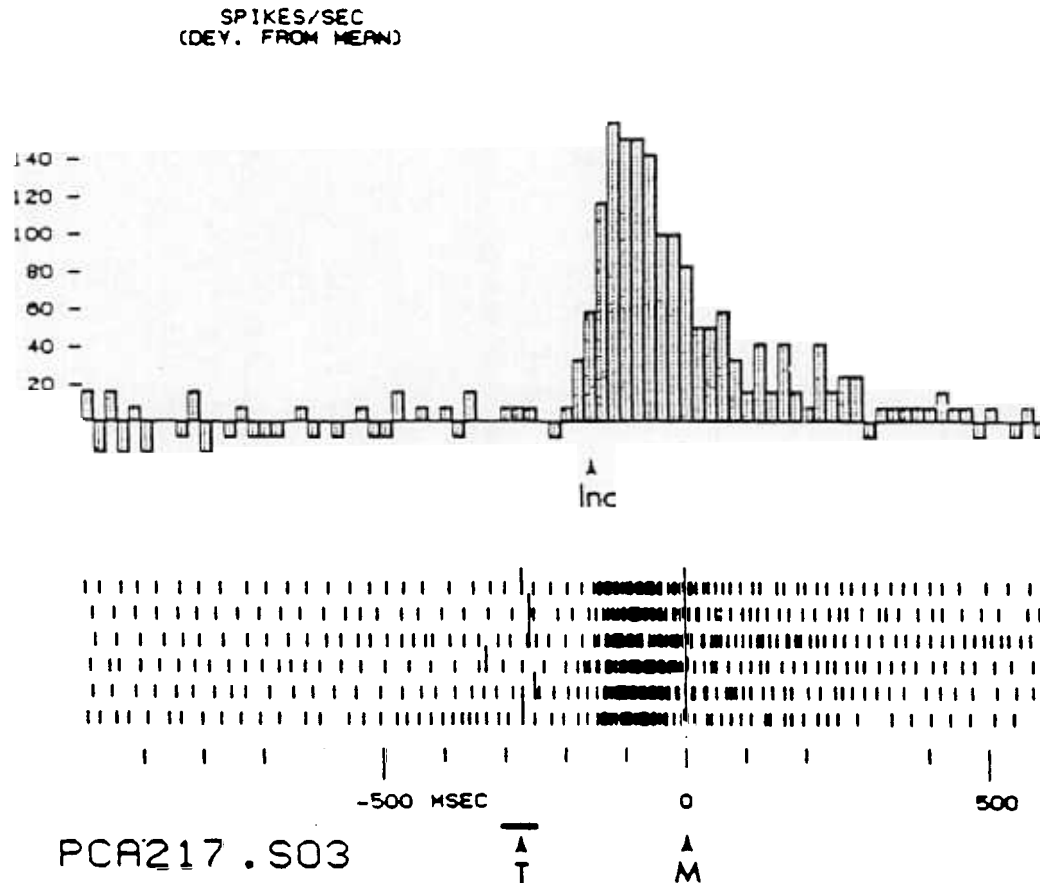


Figure 9. Quick buildup and gradual decline of activity in motor-cortical vector cells.
(Reprinted with permission from Georgopoulos, Kalaska, Caminiti, & Massey, 1982.)

Note that the asymmetry in the velocity profile is in the same direction as the asymmetry in the vector-cell population profile. This correspondence suggests that the velocity asymmetry is related to the neural control circuit, as our model also suggests.

Georgopoulos et al. (1984, p. 510) also noted the following:

No obvious invariance in cell discharge was observed when the final position was the same. . . these results show that, at the level of motor cortex, it is the direction of movement and not its endpoint that is the principle determinant of cell discharge during the initiation and execution of movement. Therefore, if the hypothesis be true that the endpoint of the movement is the controlled spatial variable (Polit & Bizzi, 1979) then the motor cortex seems to be distal to that end-point specifying process.

In other words, if one accepts the STE model, these data suggest that the TPC cells occur closer to the periphery than the DV cells. On the other hand, if one accepts our model, these data imply that the PPC cells occur closer to the periphery than the DV cells, but that the TPC cells occur more central than the DV cells. A combination of anatomical and physiological experiments can be used to test this prediction. Also note, however, that the STE model on which the conclusion of Georgopoulos et al. (1984) is based is inconsistent with the very exist-

tence of vector cells because the springlike properties of the muscles themselves, rather than a neural computation of vectors, determine the direction and length of movement in the STE model.

Several additional properties of cells in precentral motor cortex, documented by Evarts and Tanji (1974; Tanji & Evarts, 1976), lend support to identifying them with the vector cells in our model. In their experiments, monkeys were trained to either push or pull a lever. During each trial (schematized in Figure 13a) animals first held the lever in a medial position for 2 to 4 s. Then either a green or a red *priming* signal was illuminated. If green, the forthcoming movement required for reward was a push; if red, a pull. Finally, 0.6 to 1.2 s after the priming signal, the *release* signal occurred. This release signal took the form of an externally imposed push or pull on the lever held by the monkey. It both cued movement onset and perturbed the position of the lever so as to increase or decrease its initial distance from target.

Figure 13b summarizes operating characteristics of two cells. The first cell increased its activity after a "push" priming signal, but was inhibited by a "pull" priming signal; the second cell showed the opposite response. From these data alone, it would

(A)

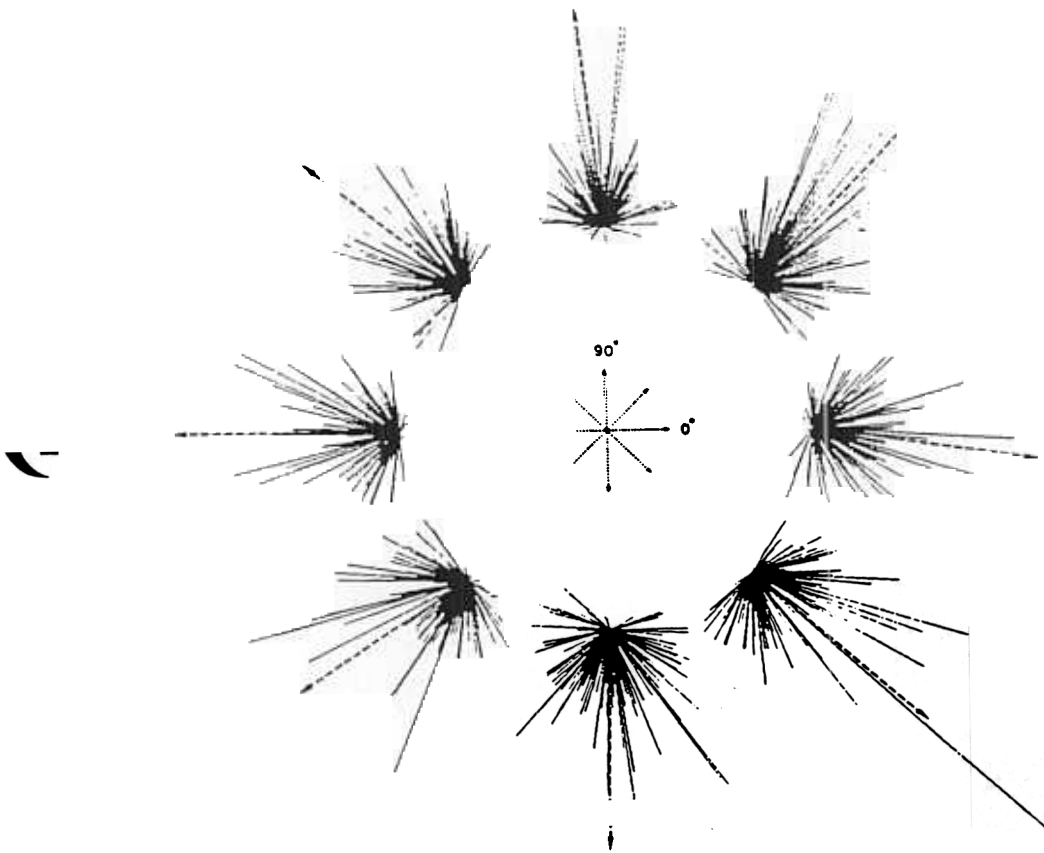
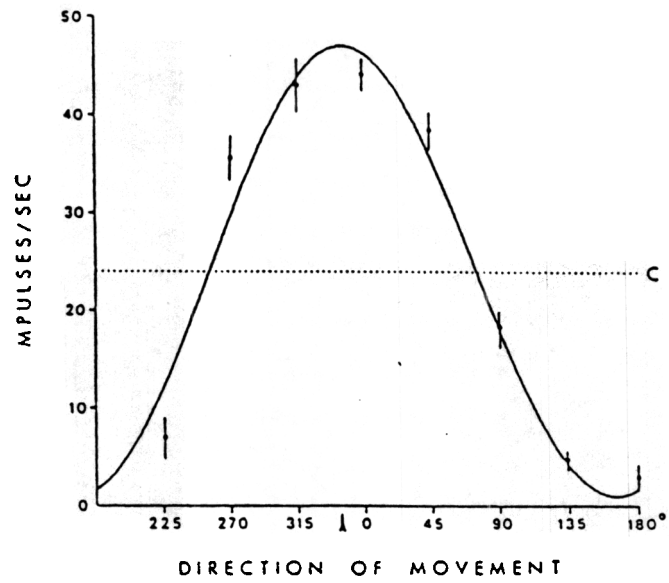


Figure 10. (A) Directional tuning curve for a motor-cortical cell exhibiting peak activity during a 0° (center-to-right) arm movement. (Dotted line indicates control period discharge rate. Thus this cell is inhibited when movement direction falls outside the 180° hemisphere of movements to which it can contribute a

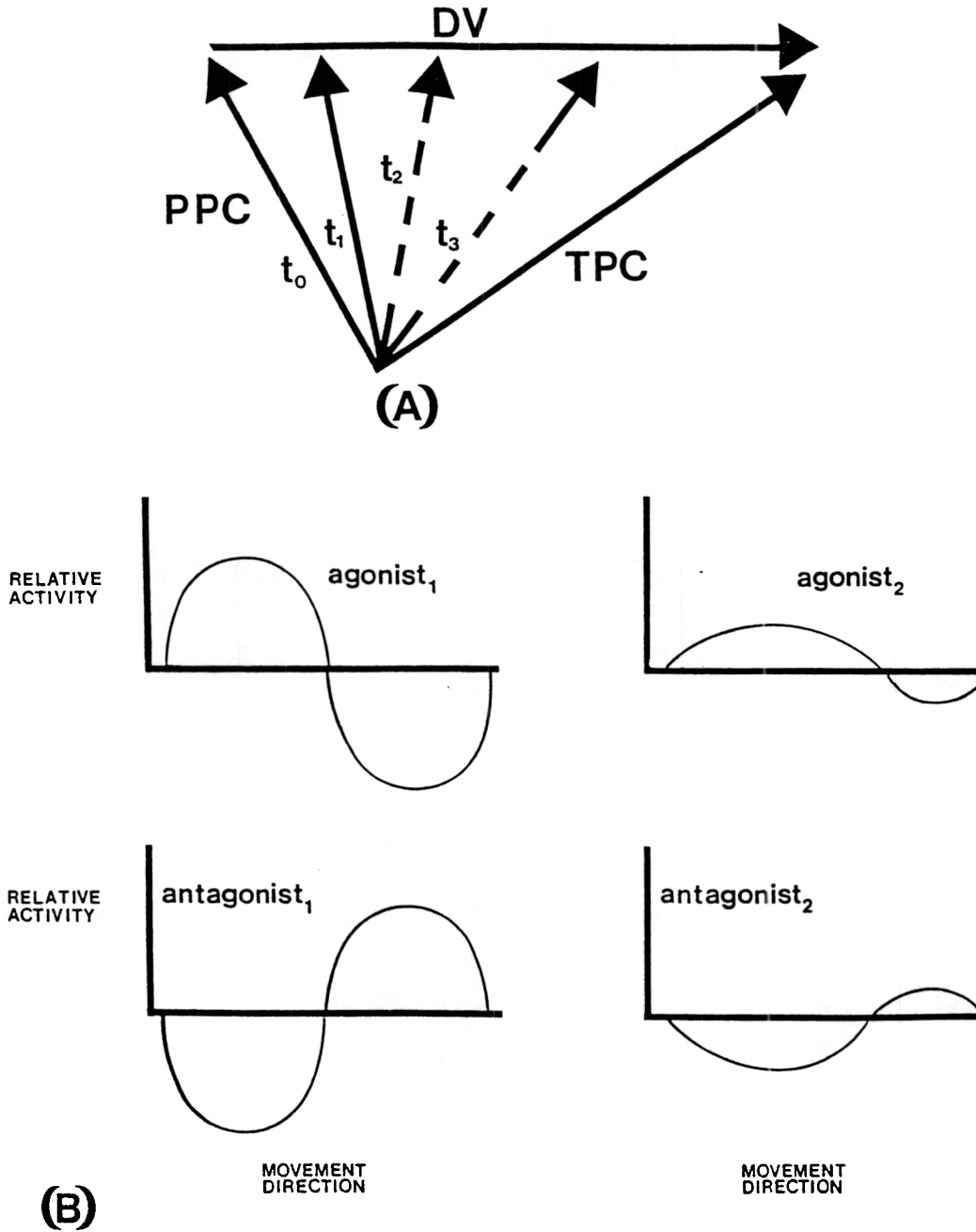


Figure 11. (A) As the movement unfolds through times t_0, t_1, t_2, \dots , the present position command (PPC) approaches the target position command (TPC) in such a way that the difference vector (DV) does not change direction as its length approaches zero. (B) Over a full range of movement directions, DV cells associated with opposing muscles (AG_1 vs. $ANTAG_1$ or AG_2 vs. $ANTAG_2$) show reciprocal patterns of activation and inhibition. (The zero crossings can occur at different points along the direction scale for different opponent pairs— $AG_1 - ANTAG_1$ vs. $AG_2 - ANTAG_2$.)

formation is learned from the parameters of the hand–arm system to the parameters of the eye–head system. A reverse transformation is also learned from parameters of the eye–head system to parameters of the hand–arm system. This reverse

transformation enables an observer intentionally to move its hand to a visually fixated position.

How do these two sensorimotor systems know what parameters are the correct ones to map on each other? This question

not be clear whether these cells' activities code DVs or TPCs. However, further characteristics confirm their status as DV cells. The second bracket for each cell in Figure 13b indicates that their activities decline as movement proceeds in their preferred direction. This decline rules out the TPC interpretation. In the model, it occurs because the movement progressively cancels the difference with which DV cell activity is correlated.

The third bracket for each cell indicates that the initial position perturbations also have the effect they must have if the DV interpretation is correct: Perturbations that make the starting point closer to target subtract from activity levels, whereas contrary perturbations add to activity levels. This occurs automatically in the model because PPCs, and thus the corresponding DVs, are updated by sensory feedback during passive movements (Section 29).

Although the foregoing considerations argue strongly for the existence of DV cells in precentral motor cortex, it might be argued that the DVs could be measuring force rather than positional values. Indeed, Evars interpreted his early experimental data (Evars, 1968) as suggestive of force coding. The data of Schmidt, Jost, and Davis (1975), however, appear to rule out this alternative interpretation. After varying position and force independently, they concluded that "motor cortex cell firing patterns appear to be unrelated to the large values of rate of change of force seen in this experiment" (p. 213).

The data summarized in Sections 6 through 12 weigh heavily against the STE model and models based on optimization principles. So, too, do the formal shortcomings of these models noted in Sections 6 and 11. We now show that the VITE model overcomes these formal shortcomings and provides a parsimonious quantitative explanation of all the behavioral and neural data summarized above and in the subsequent sections.

13. Learning Constraints Mold Arm Control Circuits

Rejecting the STE model does not entail rejecting all dependence on endpoint commands. An analysis of sensorimotor learning during eye-hand coordination enables us to identify processes that supplement endpoint, or target-position, commands to overcome the shortcomings of the STE model (Grossberg, 1978). The central role of learning constraints in the design of sensorimotor systems has been developed elsewhere for the case of the saccadic eye-movement system (Grossberg & Kuperstein, 1986).

We focus our discussion of learning within the arm-movement system on the basic problem of how, when an observer looks at an object, the observer's hand knows where to move in order to touch the object. We discuss this issue from the perspective of eye-hand coordination in a mammal, but the issues that are raised, as well as the conclusions that are drawn, generalize to many other species and sensorimotor systems. Why learning processes are needed to solve this problem is illustrated by the following example.

The movement command that guides the hand to a visual target at a fixed position relative to the body is not invariant under growth. If a young arm, with relatively short limb segments, and an old arm, with relatively long limb segments, react to the same command—that is, assume equal angles at analogous joints—then the tips of the two arm's fingers will be at different loci with respect to the body frame. In short, any animal that grows over an extended period will need to modify adaptively movement commands even if its only ambition is to perform the same act earlier and later in its life cycle. Put the other way, that animals do remain able to reach desired targets throughout periods of limb growth implies plasticity in their sensorimotor commands. Because such growth is slow relative to the rate of learning, failures of sensorimotor coordination are rarely noticeable. In humans, exceptions occur during the first few months of life, prior to experiential tuning of the infant's initially coarse sensorimotor mapping (Fetters & Todd, 1987; von Hofsten, 1979, 1982).

14. Comparing Target Position With Present Position to Gate Intermodality Learning

Thus, as the arm grows, the motor commands that move it to a fixed position in space with respect to the body must also change through learning. Many arm movements are activated in response to visually seen objects that the individual wishes to grasp. We therefore formulate this learning process as follows: How is a transformation learned and adaptively modified between the parameters of the eye-head system and the hand-arm system so that an observer can touch a visually fixated object?

Following Piaget's (1963) analysis of *circular reactions*, imagine that an infant's hand makes a series of unconditional movements, which the infant's eyes unconditionally follow. As the hand occupies a variety of positions that the eye fixates, a trans-

positive motion component. Reprinted with permission from Kalaska, Caminiti, & Georgopoulos, (1983.) (B) Each dotted arrow in the central graphic indicates the direction of a radial (center-out) movement and points to a representation of the cellular activities observed during that movement. (In each plot of cellular activities, the *direction* of each solid black line corresponds to the direction of movement for which a given cell fired maximally, whereas the *length* of each solid black line corresponds to the firing rate of the same cell during the indicated movement. The single dashed line with arrowhead in each plot represents the vector sum of all the neural vectors—solid block lines—generated during the indicated movement. Note the correspondence between the direction of the vector sum—dashed line with arrowhead—and the direction of the actual movement—indicated by the dotted arrow in the central graphic. All cells were related to muscle groups acting at the shoulder, a ball-and-socket joint. Figures reprinted with permission from Georgopoulos, Kalaska, Crutcher, Caminiti, & Massey, 1984.)

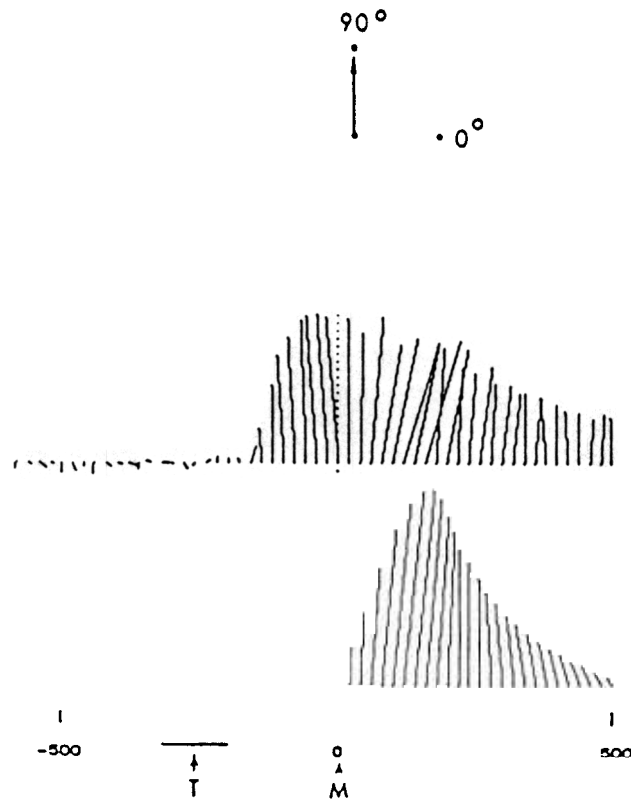


Figure 12. A comparison of the population vector of 241 directionally tuned cells (upper figure) with the velocity vector of the hand (lower figure), each measured at 20-ms intervals during the reaction time and during movement. (Note the asymmetry—longer right tail—in both. Reprinted with permission from Georgopoulos, Kalaska, Crutcher, Caminiti, & Massey, 1984.)

raises the fundamental problem that many neural signals, although large, are unsuitable for being incorporated into behavioral maps and commands. They are “functional noise” to the motor learning process. The learning process needs to be actively modulated, or gated, against learning during inappropriate circumstances.

In the present instance, not all positions that the eye-head system or the hand-arm system assume are the correct positions to associate through learning. For example, suppose that the hand briefly remains at a given position and that the eye moves to foveate the hand. An infinite number of positions are assumed by the eye as it moves to foveate the hand. Only the final, intended, or expected, position of the eye-head system is a correct position to associate with the position of the hand-arm system.

Learning of an intermodal motor map must thus be prevented except when the eye-head system and the hand-arm system are near their intended positions. Otherwise, all possible positions of the two systems could be associated with one another, which would lead to behaviorally chaotic consequences. Four important conclusions follow from this observation (Grossberg, 1978; Grossberg & Kuperstein, 1986): (a) All such

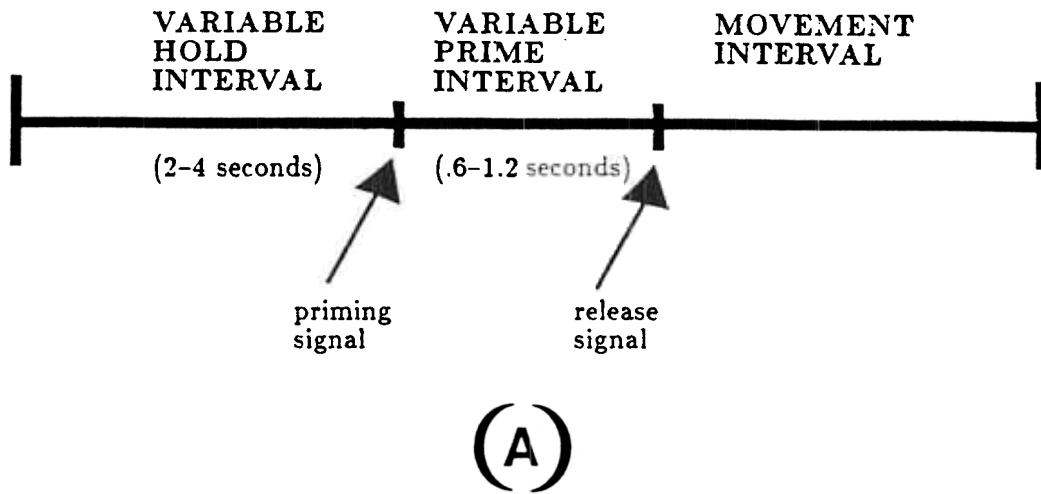
adaptive sensorimotor systems compute a representation of target position (also called expected position or intended position). Thus the importance of endpoint computations is confirmed. This representation is the TPC. (b) All such adaptive sensorimotor systems also compute a representation of present position. This representation is the PPC. (c) During movement, target position is matched against present position. Intermodal map learning is prevented except when target position approximately matches present position (Figure 14). A *gating*, or modulator, signal is thus controlled by the network at which target position is matched with present position. This gating signal enables learning to occur when a good match occurs and prevents learning from occurring when a bad match occurs. This matching process takes place at the match interface that was described in Section 12. The DV controls the gating signal. (d) Finally, to compare target positions with present positions, both types of data must be computed in the same coordinate system. Present eye position is computed with respect to head coordinates. Thus there is an evolutionary pressure to encode target position in head coordinates.

15. Trajectory Formation Using DVs: Automatic Compensation for Present Position

The foregoing discussion of how *intermodality* sensorimotor transformations are learned also sheds light on how *intramodality* movement trajectories are formed. Intermodality transformations associate TPCs because only such transformations can avoid the multiple confusions that could arise through associating arbitrary positions along a movement trajectory. TPCs are not, however, sufficient to generate intramodality movement trajectories. In response to the same TPC, an eye, arm, or leg must move different distances and directions depending on its present position when the target position is registered.

PPCs can be used to convert a single TPC into many different movement trajectories. Computation of the difference between target position and present position at the match interface in Figure 8 generates a DV that can be used to automatically compensate for present position. Such automatic compensation accomplishes a tremendous reduction in the memory load that is placed on an adaptive sensorimotor system. Instead of having to learn whole movement trajectories, the system only has to learn intermodality maps between TPCs. As shall be shown later, DVs computed from target positions and present positions at the match interface can be used to update automatically and continuously the PPC movement commands from which the trajectory is formed. In summary, consideration of the types of information that can be used to learn intermodality commands during motor development leads to general conclusions about the quantities from which intramodality movement trajectories are formed, and thus about the way in which other neural systems, such as sensory, cognitive, and motivational systems, can influence the planning of such trajectories.

Computation of TPCs, PPCs, and DVs is a qualitatively different approach to generating a trajectory than are traditional computations based on a Newtonian analysis of movement kinematics. In a Newtonian analysis, every position within the trajectory is assumed to be explicitly controlled (At-



CELL 1 OPERATING CHARACTERISTICS

| | | |
|--|--|---|
| $\left\{ \begin{array}{l} \uparrow \text{ priming signal} \\ \downarrow \text{ priming signal} \end{array} \right\}$ | $\left\{ \begin{array}{l} \text{produced} \\ \text{produced} \end{array} \right\}$ | $\left\{ \begin{array}{l} \uparrow \text{ activity} \\ \downarrow \text{ activity} \end{array} \right\}$ |
| $\left\{ \begin{array}{l} \uparrow \text{ movement} \end{array} \right\}$ | $\left\{ \begin{array}{l} \text{produced} \end{array} \right\}$ | $\left\{ \begin{array}{l} \downarrow \text{ activity} \end{array} \right\}$ |
| $\left\{ \begin{array}{l} \uparrow \text{ prime} + \downarrow \text{ perturbation} \\ \uparrow \text{ prime} + \uparrow \text{ perturbation} \end{array} \right\}$ | $\left\{ \begin{array}{l} \text{produced} \\ \text{produced} \end{array} \right\}$ | $\left\{ \begin{array}{l} \text{greater } \uparrow \text{ activity} \\ \text{less } \uparrow \text{ activity} \end{array} \right\}$ |

CELL 2 OPERATING CHARACTERISTICS

| | | |
|--|--|---|
| $\left\{ \begin{array}{l} \downarrow \text{ priming signal} \\ \uparrow \text{ priming signal} \end{array} \right\}$ | $\left\{ \begin{array}{l} \text{produced} \\ \text{produced} \end{array} \right\}$ | $\left\{ \begin{array}{l} \uparrow \text{ activity} \\ \downarrow \text{ activity} \end{array} \right\}$ |
| $\left\{ \begin{array}{l} \downarrow \text{ movement} \end{array} \right\}$ | $\left\{ \begin{array}{l} \text{produced} \end{array} \right\}$ | $\left\{ \begin{array}{l} \downarrow \text{ activity} \end{array} \right\}$ |
| $\left\{ \begin{array}{l} \downarrow \text{ prime} + \uparrow \text{ perturbation} \\ \downarrow \text{ prime} + \downarrow \text{ perturbation} \end{array} \right\}$ | $\left\{ \begin{array}{l} \text{produced} \\ \text{produced} \end{array} \right\}$ | $\left\{ \begin{array}{l} \text{greater } \uparrow \text{ activity} \\ \text{less } \uparrow \text{ activity} \end{array} \right\}$ |



Figure 13. (A) The time course of each trial in the push-or-pull task used by Evarts and Tanji (1974). (B) Operating characteristics of two motor-cortical cells. (Solid arrows indicate increases—upward arrow—or decreases—downward arrow—in cell discharge rates. Hollow arrows indicate a push- [upward arrow] or pull- [downward arrow] related event: either the push/pull priming signal, a push/pull movement, or the push/pull perturbation that also served as the release signal.)

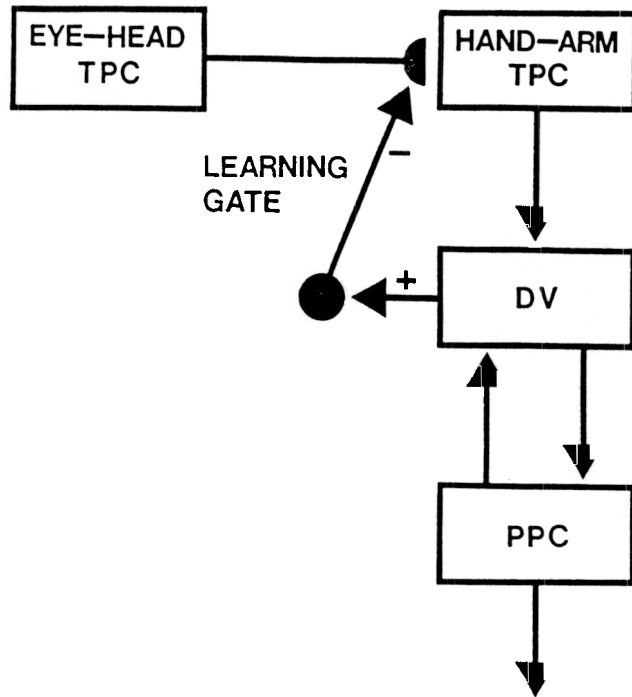


Figure 14. Learning in sensorimotor pathways is gated by a difference vector (DV) process that matches the target position command (TPC) with the present-position command (PPC) to prevent incorrect associations from forming between eye-head TPCs and hand-arm TPCs.

keson & Hollerbach, 1985; Brody & Paul, 1984; Hogan, 1984; Hollerbach, 1984). Such computations lead to a combinatorial explosion that is hard to reconcile with the rapidity of biological movement generation in real time. In a vector computation, the entire trajectory is never explicitly planned. Instead, a TPC is computed that determines where the movement expects, or intends, to terminate. The subtraction of the PPC is an automatic process that compensates for the variability of the starting position. The DV that is hereby computed can be used to generate an accurate movement without ever explicitly computing a planned sequence of trajectory positions for the whole movement. In arm movements, a continuous comparison is made between a fixed TPC and all the PPCs computed during the movement. All of these compensations for changes in present position are automatically registered and therefore place no further burden on the computation of planned movement parameters. In addition, such automatic compensations for present position spontaneously generate the major invariants of arm movements that have been discovered to date (Sections 21–28). Thus the general problem of how DVs are computed is central to understanding trajectory formation in several movement systems.

16. Matching and Vector Integration During Trajectory Formation

We now specify in greater detail a model of how TPCs, PPCs, and DVs interact with one another through time to synthesize

a movement trajectory. Each PPC generates a pattern of outflow movement signals to arm system muscles (Figure 8). Each such outflow pattern acts to move the arm system toward the present positions that it encodes. Thus, were only a single PPC to be activated, the arm system would come to rest at a single physical position. A complete movement trajectory can be generated in the form of a temporal succession of PPCs. Such a movement trajectory can be generated in response to a single TPC that remains active throughout the movement. Although a TPC explicitly encodes only the endpoint of the movement, the process whereby present positions are automatically and continuously updated possesses properties that are much more powerful than those of an STE model.

This process of continuous updating proceeds as follows. At every moment, a DV is computed from the fixed TPC and the PPC (Figure 8). This DV encodes the difference between the TPC and the PPC. In particular, the DV is computed by subtracting the PPC from the TPC at the match interface.

Because a DV computes the difference between the TPC and the PPC, the PPC equals the TPC only when all components of the DV equal zero. Thus if the arm system's commands are calibrated so that the arm attains the physical position in space that is coded by its PPC, then the arm system will approach the desired target position in space as the DVs computed during its trajectory approach zero. This is accomplished as follows.

At each time, the DV computes the direction and amplitude that must still be moved to match the PPC with the TPC. Thus the DV computes an error signal of a very special kind. These error signals are used continuously to update the PPC in such a way that the changing PPC approaches the fixed TPC by progressively reducing the vector error to zero. In particular, the match interface at which DVs are computed sends excitatory signals to the stage where PPCs are computed. This stage integrates, or adds up, these vector signals through time. The PPC is thus a cumulative record of all past DVs, and each DV brings the PPC a little closer to the TPC.

In so doing, the DV is itself updated through negative feedback from the new PPC to the match interface (Figure 8). This process of updating present positions through vector integration and negative feedback continues until the PPC equals the TPC. Several important conclusions follow from this analysis of the trajectory formation process.

Two processes within the arm-control system do double duty: A PPC generates feed-forward, or outflow, movement signals and negative feedback signals that are used to compute a DV. A DV is used to update intramodality trajectory information and to gate intermodality learning of associative transformations between TPCs. Thus the match interface continuously updates the PPC when the arm is moving and disinhibits the intermodality map learning process when the arm comes to rest.

Within the circuit depicted in Figure 8, position and direction information are coded separately. Positional information is coded within the PPC, and directional information is coded by the DV at the match interface. On the other hand, the computations that give rise to positional and directional information are not independent, because DVs are integrated to compute PPCs, and PPCs are subtracted from TPCs to compute DVs.

In Figure 8, the PPC is computed using outflow information, but not inflow information. This property emphasizes the need to mechanize concepts about how present position is computed. The use of an outflow-based PPC clarifies how targets can be reached when sources of inflow information are eliminated (Polit & Bizzi, 1978) without being forced into the erroneous conclusion that no information about present position is needed to form a trajectory. In addition, although the PPC integrates outflow DV signals during active movements, inflow signals are used to update the PPC during passive movements (Section 29), thereby clarifying the data of Polit and Bizzi (1978) concerning failure of monkeys to compensate for passive shifts of their initial upper arm position in the deafferented state. The PPC feedback shown in Figure 8 is an “efference copy” of a premotor command (von Holst & Mittelstaedt, 1950). The VITE model’s use of efferent feedback distinguishes it from an alternative class of models, which propose that present-position information is derived from afferent feedback from sensory receptors in the limb. In particular, the far-reaching consequences of its use of efferent, as opposed to afferent, feedback make the VITE model fundamentally different from the classical closed-loop servo recommended by Adams (1971, 1977) as a model of human motor performance. Further differences are introduced by the VITE model’s use of the time-varying multiplicative GO signal introduced in Section 10 and elaborated below.

17. Intentionality and the GO Signal: Motor Priming Without Movement

The circuit depicted in Figure 8 embodies the concept of intention, or expectation, through its computation of a TPC. The complete movement circuit embodies intentionality in yet another sense, which leads to a circuit capable of variable speed control. The need for such an additional process can also be motivated through a consideration of eye–hand coordination (Grossberg, 1978, 1982).

When a human looks at a nearby object, several movement options for touching the object are available. The object could be grasped with the left hand or the right hand. The object could even be touched with one’s nose or one’s toes! We assume that the eye–head system can simultaneously activate TPCs in several motor systems via the intermodality associative transformations that are learned to these systems. An additional act of will, or GO signal, is required to convert one or more of these TPCs into overt movement trajectories within only the selected motor systems.

There is only one way to implement such a GO signal within the circuit depicted in Figure 8. This implementation is described in Figure 15. The GO signal must act at a stage intermediate between the stages that compute DVs and PPCs: The GO signal must act after the match interface so that it does not disrupt the process whereby DVs become zero as PPCs approach the TPC. The GO signal must act before the stage that computes PPCs so that changes in the GO signal cannot cause further movement after the PPC matches the TPC. Thus, although the GO signal changes the outputs from the match interface before they reach the present-position stage, the very existence of such

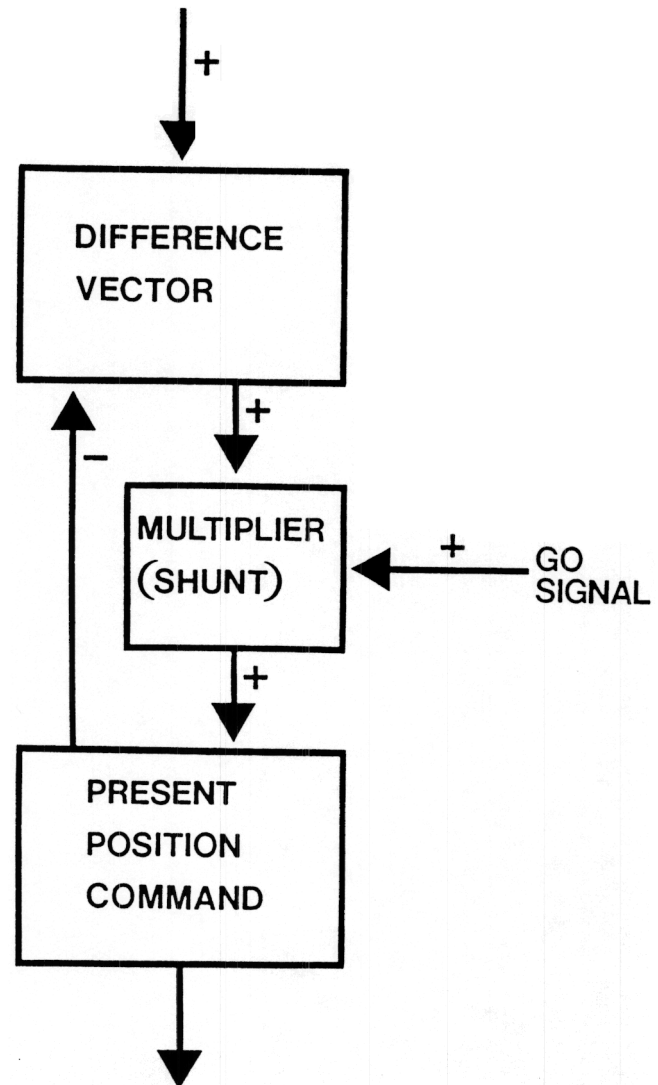


Figure 15. A GO signal gates execution of a primed movement vector and regulates the rate at which the movement vector updates the present-position command.

processing stages for continuous formation of a trajectory enables the GO signal to act without destroying the accuracy of the trajectory.

The detailed computational properties of the GO signal are derived from two other constraints. First, the absence of a GO signal must prevent the movement from occurring. This constraint suggests that the GO signal multiplies, or *shunts*, each output pathway from the match interface. A zero GO signal multiplies every output to zero and, hence, prevents the PPC from being updated. Second, the GO signal must not change the direction of movement that is encoded by a DV. The direction of movement is encoded by the relative sizes of all the output signals generated by the vector. This constraint reaffirms that the GO signal multiplies vector outputs. It also implies that the GO signal is nonspecific: The same GO signal multiplies

each output signal from the matching interface so as not to change the direction encoded by the vector.

In summary, the GO signal takes a particularly simple form. When it equals zero, the present-position signal is not updated. Hence no overt movement is generated. On the other hand, a zero GO signal does not prevent a TPC from being activated, or a DV from being computed. Thus a motor system can become ready, or primed, for movement before its GO signal turns on. When the GO signal does turn on, the movement can be rapidly initiated. The size of the GO signal regulates overall movement speed. Larger GO signals cause faster movements, other things being equal, by speeding up the process whereby directional information from the match interface is integrated into new PPCs. In models of cognitive processing, the functional analog of the GO signal is an attentional gain control signal (Carpenter & Grossberg, 1987, in press; Grossberg, 1987a, 1987b; Grossberg & Stone, 1986).

Georgopoulos et al., (1986) have reported data consistent with this scheme. In their experiment, a monkey was trained to withhold movement for 0.5 to 3 s until a lighted target dimmed. They reported that cells with properties akin to DV cells computed a direction congruent with that of the upcoming movement during the waiting period. These data support the prediction that the neural stage where the GO signal is registered lies between the DV stage and the PPC stage.

18. Synchrony, Variable Speed Control, and Fast Freeze

The circuit in Figure 15 is now easily seen to possess qualitative properties of synchronous synergetic movement, variable speed control, and fast freeze-and-abort. We apply the circuit properties that each muscle synergist's motor command is updated at a rate that is proportional both to the synergist's distance from its target position and to a variable-magnitude GO signal, which is broadcast to all members of the synergy to initiate and sustain the parallel updating process.

To fix ideas, consider a simple numerical example. Suppose that prior to movement initiation, Muscle Synergist A is 4 distance units from its target position and Muscle Synergist B is 2 distance units from its target position. In that case, if the mean rates at which PPCs are updated for the two synergists are in the same proportion as the distance (i.e., 2:1), then the updating of Synergist A will take 4/2 time units while the updating of Synergist B will take 2/1 time units. Thus both processes will consume approximately 2 time units. Although the PPC updating process occurs at different rates for different synergists, it consumes equal times for all synergists. The result is a synchronous movement despite large rate variations among the component motions.

Changing the magnitude of the GO signal governs variable speed control. Because both of the updating rates in the example (2 and 1) are multiplied by the same GO signal, the component motions will remain synchronous, though of shorter or longer duration, depending on whether the GO signal multiplier is made larger or smaller, respectively. In general, the GO signal's magnitude varies inversely with duration and directly with speed. Finally, if the value of the GO signal remains at zero, no updating and no motion will occur. Thus very rapid freezing

can be achieved by completely inhibiting the GO signal at any point in the trajectory. The fact that target position may be very different from present position when the GO signal is withdrawn does not interfere with freezing, as it would using a STE model, because the arm position closely tracks the PPC, which stops changing as soon as the signal shuts off.

Grossberg (1978, Section 54; reprinted in Grossberg, 1982) suggested an alternative scheme whereby actively moving muscles could be opposed by properly scaled antagonist co-contractions in response to a sudden unexpected event. In this scheme, agonist-antagonist motor commands are organized as gated dipole opponent processes, and the unexpected event triggers a burst of nonspecific arousal to all the command sources. Each gated dipole opponent process reacts to such a nonspecific arousal burst by causing an antagonistic rebound whose size is scaled to that of the dipole's prior on-response. The rate of antagonist contraction generated by such a scheme is thus matched to the size of the just-previous rate of agonist contraction. Both types of mechanism—inhibition of GO signal and onset of arousal burst to opponent motor controls—are worthy of further neurophysiological testing. Another role for the opponent organization of motor commands is summarized in the next section.

19. Opponent Processing of Movement Commands

Mammalian motor systems are organized into pairs of agonist and antagonist muscles. We now note a new functional role for such an opponent organization: An opponent organization is needed to convert DVs into PPCs that can eventually match an arbitrary TPC. Figure 16 depicts how opponent organization is joined to the system's other processing constraints.

The need for opponent signals can be seen from the following examples. If a target-position signal is larger than the corresponding present-position signal, then a positive output signal is generated by the corresponding component of the DV. Such positive output signals increase the present-position signal until it matches the target-position signal. Increasing the present-position signal causes the target muscle group to contract. The opponent muscle group must also simultaneously relax. Inhibitory signals to the present-position node of the opponent muscle instate this latter property. When these inhibitory signals are integrated by the present-position node of the opponent muscle, the output signal to the opponent muscle decreases, thereby relaxing the muscle.

The need for opponent processing can also be seen by considering the case in which the target-position signal is smaller than the present-position signal. Then the corresponding component of the DV is negative. Because only nonnegative activities can generate output signals, no output signal is generated by this component of the DV to its corresponding present-position node. How, then, is this present-position signal decreased until it matches the target-position signal? The answer is now obvious, because we have just considered the same problem from a slightly different perspective: If a negative vector component corresponds to an antagonist muscle group, a positive vector component corresponds to its opponent agonist muscle group. This positive vector component generates inhibitory signals to

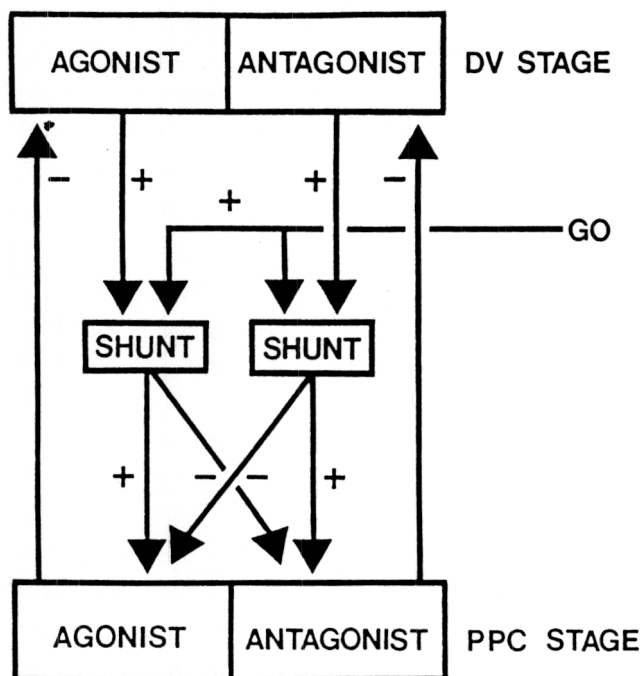


Figure 16. Opponent interactions among channels controlling agonists and their antagonists enable coordinated, automatic updating of their present-position commands (PPCs). (DV = difference vector.)

the PPC of the antagonist muscle, thereby relaxing the antagonist muscle until its PPC equals its TPC.

20. System Equations

A quantitative analysis of movement invariants requires the development of a rigorous real-time mathematical model of the constraints summarized in the preceding sections. Qualitative algebraic analysis is insufficient because the trajectory is an emergent property of a nonlinear integration and feedback process under variable gain control. Our model defines the simplest system that is consistent with these constraints. To fix ideas, we explicitly study how the TPC to an agonist muscle group generates a trajectory of PPC signals to that muscle group. Generalizations to synergetic movement of multiple agonist-antagonist muscle groups follow directly from this analysis. Figure 17 locates the mathematical variables that are defined below. The network depicted in Figure 17 obeys the following system of differential equations:

$$\frac{dV}{dt} = \alpha(-V + T - P) \quad (2)$$

and

$$\frac{dP}{dt} = G[V]^+ \quad (3)$$

In Equations 2 and 3, $T(t)$ is a target position input, $V(t)$ is the activity of the agonist's DV population, $P(t)$ is the activity of the

agonist's PPC population, $G(t)$ is the GO signal, dV/dt is the rate of change of V , and dP/dt is the rate of change of P .

Equation 2 says that the activity $V(t)$ averages the difference of the input signals $T(t)$ and $P(t)$ at a rate α through time. The TPC input $T(t)$ excites $V(t)$, whereas the PPC input $P(t)$ inhibits $V(t)$ as part of the negative feedback loop between $V(t)$ and $P(t)$.

Equation 3 says that $P(t)$ cumulatively adds, or integrates, the product $G[V]^+$, where

$$[V]^+ = \begin{cases} V & \text{if } V > 0 \\ 0 & \text{if } V \leq 0. \end{cases} \quad (4)$$

In other words, the DV population elicits an output signal $[V]^+$ to the PPC population only if the activity V exceeds the output threshold 0. The output signal is a linear function of V at supra-threshold values. The output signal $[V]^+$ is multiplied, or gated, by the GO signal $G(t)$ on its way to the PPC stage. The activity $P(t)$ at the PPC stage integrates the gated signal through time.

In particular, $G(t) = 0$ implies $(dP/dt)(t) = 0$. In other words, if the GO signal is shut off within a given time interval, the $P(t)$ is constant throughout that time interval. Fast freeze can hereby be rapidly obtained by simply switching $G(t)$ quickly to zero no matter how far $P(t)$ may be from $T(t)$ at that time. In addition, this circuit generates compensatory, or error-correcting, trajectories, as described in Section 9. For example, suppose that the GO signal starts out larger than usual or that there is a slight delay in instatement of the TPC relative to onset of the GO signal. In either case, $P(t)$ can initially increase faster than usual. As a result, $T - P(t)$ can rapidly become smaller than usual. Consequently, updating of $P(t)$ terminates earlier than usual.

This compensatory process illustrates two critical features of the VITE model: (a) Trajectories are not pre-formed. (b) Because the GO signal feeds in between the DV stage and the PPC stage and because the DV is continuously inhibited by feedback from the PPC stage, accuracy is largely insulated from random variations in the size or onset time of the GO signal, variations in the onset time of the TPC, or momentary perturbations of the PPC owing to internal noise or inflow signals.

The system of Equations 2 through 4 is explicitly solved for a particular choice of GO signal in Appendix A. In Sections 21 through 28, we display the results of computer simulations that demonstrate that this simple model provides a quantitative explanation of all the data thus far summarized. In most of these simulations, we write the GO signal in the form

$$G(t) = G_0 g(t). \quad (5)$$

Constant G_0 is called the GO amplitude, and function $g(t)$ is called the GO onset function. The GO amplitude parameterizes how large the GO signal can become. The GO onset function describes the transient buildup of the GO signal after it is switched on. In our simulations, we systematically studied the influence of choosing different GO amplitudes G_0 and onset functions from the family

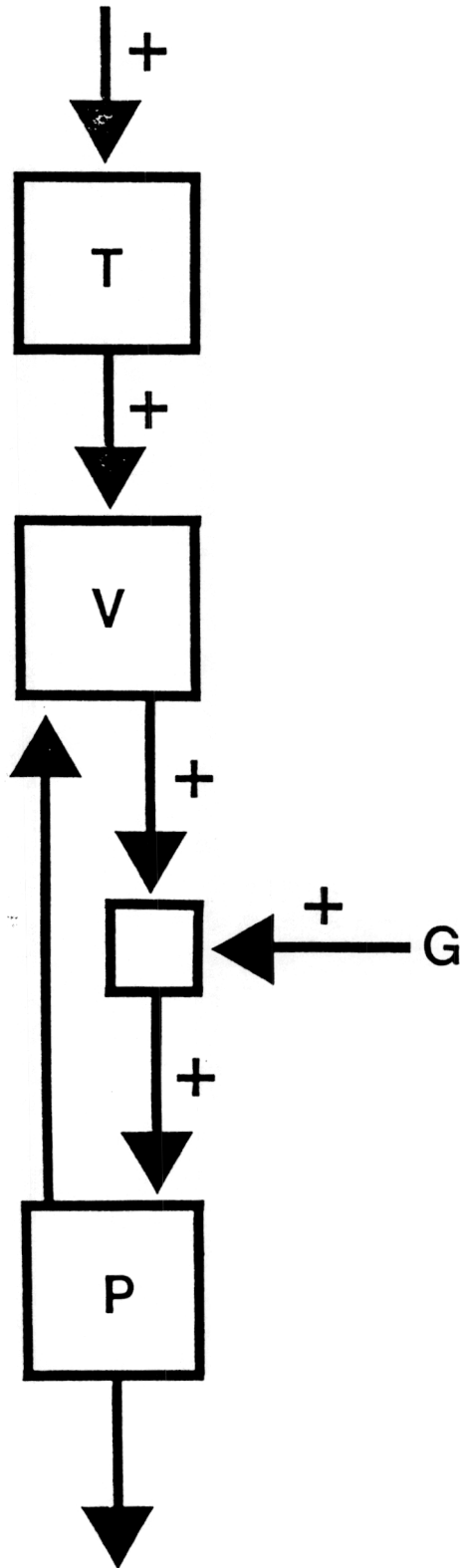


Figure 17. Network variables used in computer simulations. (See Equations 2 and 3 in text.)

$$g(t) = \begin{cases} t^n & \text{if } t \geq 0. \\ \beta^n + \gamma t^n & \text{if } t < 0. \end{cases} \quad (6)$$

In Equation 6, we chose β and γ equal to 1 or 0. If $\beta = 0$ and $\gamma = 1$, then $g(t)$ is a step function that switches from 0 to 1 at time $t = 0$. If $\beta = 1$ and $\gamma = 1$, then $g(t)$ is a slower-than-linear function of time if $n = 1$ and a sigmoid, or S-shaped, function of time if $n > 1$. In both of these cases, function $g(t)$ increases from $g(0) = 0$ to a maximum of 1 and attains the value $1/2$ at time $t = \beta$. If $\beta = 1$ and $\gamma = 0$, then $g(t)$ is a linear function of time if $n = 1$ and a faster-than-linear function of time if $n > 1$. We will soon demonstrate that an onset function that is a faster-than-linear or a sigmoid function of time generates a PPC profile through time that is in quantitative accord with data about the arm's velocity profile through time. On the other hand, if muscle and arm properties attenuate the increase in velocity at the beginning of a movement, then linear, or even slower-than-linear, onset functions could also quantitatively fit the data. Direct physiological measurements of the GO signal and PPC updating processes would enable a more definitive selection of the onset function to be made.

21. Computer Simulation of Movement Synchrony and Duration Invariance

In simulations of synchronous contraction, the same GO signal $G(t)$ is switched on at time $t = 0$ across all VITE circuit channels. We consider only agonist channels whose muscles contract to perform the synergy. Antagonist channels are controlled by opponent signals, as described in Section 19. We assume that all agonist channels start out at equilibrium before their TPCs are switched to new, sustained target values at time $t = 0$. In all agonist muscles, $T(0) > P(0)$. Consequently, $V(t)$ in Equation 2 increases, thereby increasing $P(t)$ in Equation 3 and causing the target muscle to contract. Different muscles may be commanded to contract by different amounts. Then the size of $T(0) - P(0)$ will differ across the VITE channels inputting to different muscles. Thus Equations 2 through 4 describe a generic component of a TPC (T_1, T_2, \dots, T_n), a DV (V_1, V_2, \dots, V_n), and a PPC (P_1, P_2, \dots, P_n). Rather than introduce subscripts 1, 2, . . . , n needlessly, we merely note that our mathematical task is to show how the VITE circuit in Equations 2 through 4 behaves in response to a single GO function $G(t)$ if the initial value $T(0) - P(0)$ is varied. The variation of $T(0) - P(0)$ can be interpreted as the choice of a different setting for each of the components $T_i(0) - P_i(0), i = 1, 2, \dots, n$. Alternatively it can be interpreted as the reaction of the same component to different target- and initial-position values on successive performance trials.

Figure 18 depicts a typical response to a faster-than-linear $G(t)$ when $T(0) > P(0)$. Although $T(t)$ is switched on suddenly to a new value T , $V(t)$ gradually increases then decreases, while $P(t)$ gradually approaches its new equilibrium value, which equals T . The rate of change dP/dt of P provides a measure of the velocity with which the muscle group that quickly tracks $P(t)$ will contract. Note that dP/dt also gradually increases then decreases

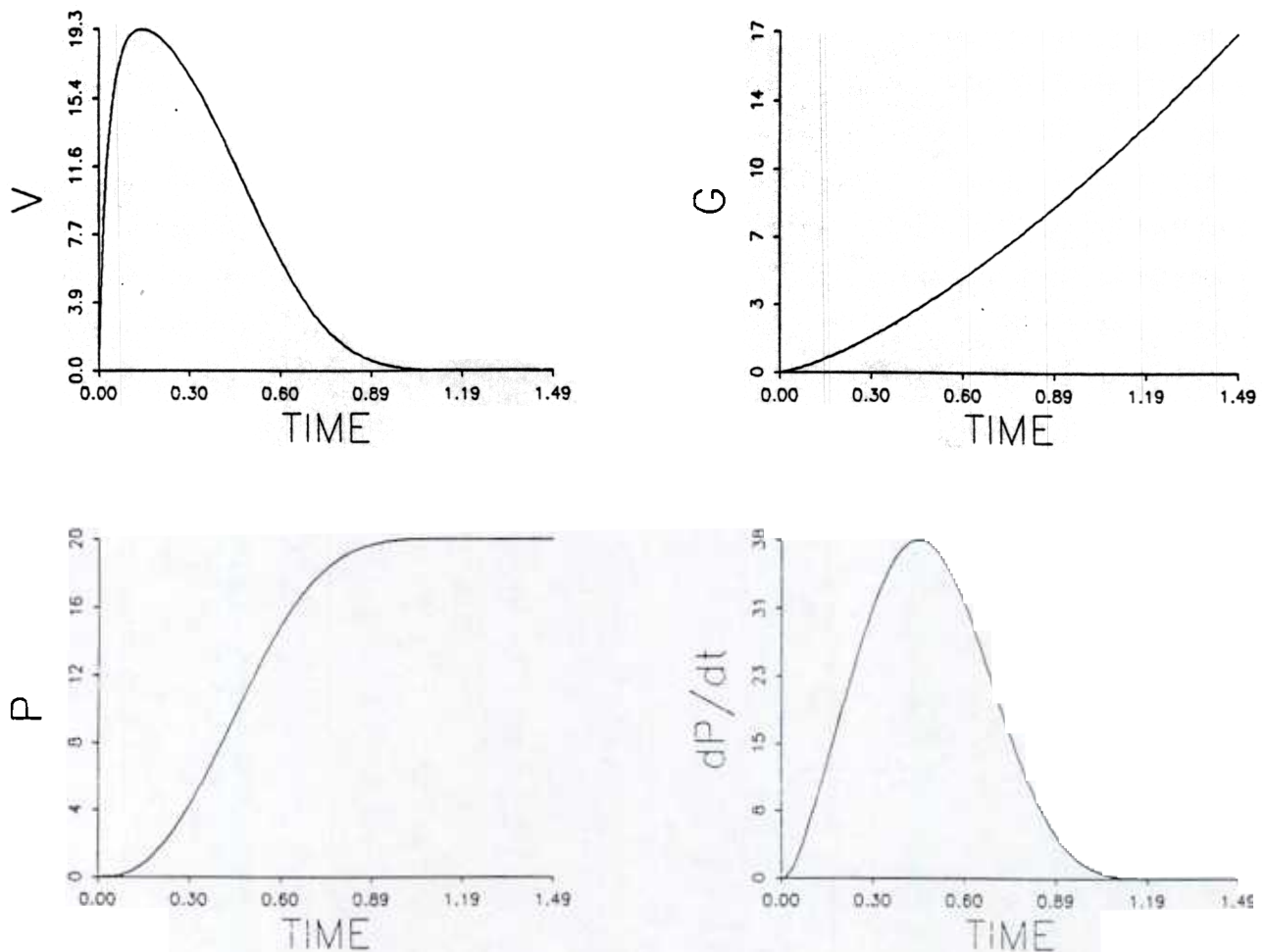


Figure 18. The simulated time course of the neural network activities V , G , and P during an 1100-ms movement. (The variable T [not plotted] had value 0 at $t < 0$, and value 20 thereafter. The derivative of P is also plotted to allow comparison with experimental velocity profiles. Parameters for Equations 2, 3, and 6: $\alpha = 30$, $n = 1.4$, $\beta = 1$, and $\gamma = 0$.)

with a bell-shaped curve whose decelerative portion ($d^2P/dt^2 < 0$) is slightly longer than its accelerative portion ($d^2P/dt^2 > 0$), as in the data described in Sections 7, 8, 11, and 12.

Figure 19 demonstrates movement synchrony and duration invariance. This figure shows that the V curves and the dP/dt curves generated by widely different $T(0) - P(0)$ values and the same GO signal $G(t)$ are perfectly synchronous through time. This property is proved mathematically in Appendix B. The simulated curves mirror the data summarized in Sections 11 and 12. These results demonstrate that the PPC output vector $[P_1(t), P_2(t), \dots, P_n(t)]$ from a VITE circuit dynamically defines a synergy that controls a synchronous trajectory in response to any fixed choice (T_1, T_2, \dots, T_n) of TPC, any initial positions $[P_1(0), P_2(0), \dots, P_n(0)]$, and any GO signal $G(t)$.

22. Computer Simulation of Changing Velocity Profile Asymmetry at Higher Movement Speeds

The next simulations reproduce the data reviewed in Section 11 concerning the greater symmetry of velocity profiles at

higher movement velocities. In these simulations, the initial difference $T(0) - P(0)$ between TPC and PPC was held fixed, and the GO amplitude G_0 was increased. Figure 20a, 20b, and 20c shows that the profile of dP/dt becomes more symmetric as G_0 is increased. At still larger G_0 values, the direction of asymmetry reversed: that is, the symmetry ratio exceeded .5, as in the data of Zelaznik et al. (1986). Figure 20d shows that if both the time axis t and the velocity axis dP/dt are rescaled, then curves corresponding to movements of the same size at different speeds can approximately be superimposed, except for the mismatch of their decelerative portions, as in the data summarized in Section 11.

23. Why Faster-Than-Linear, or Sigmoid, Onset Functions?

The parametric analysis of velocity profiles in response to different values of $T(0) - P(0)$ and G_0 led to the choice of a faster-than-linear, or sigmoid, onset function $g(t)$. In fact, the

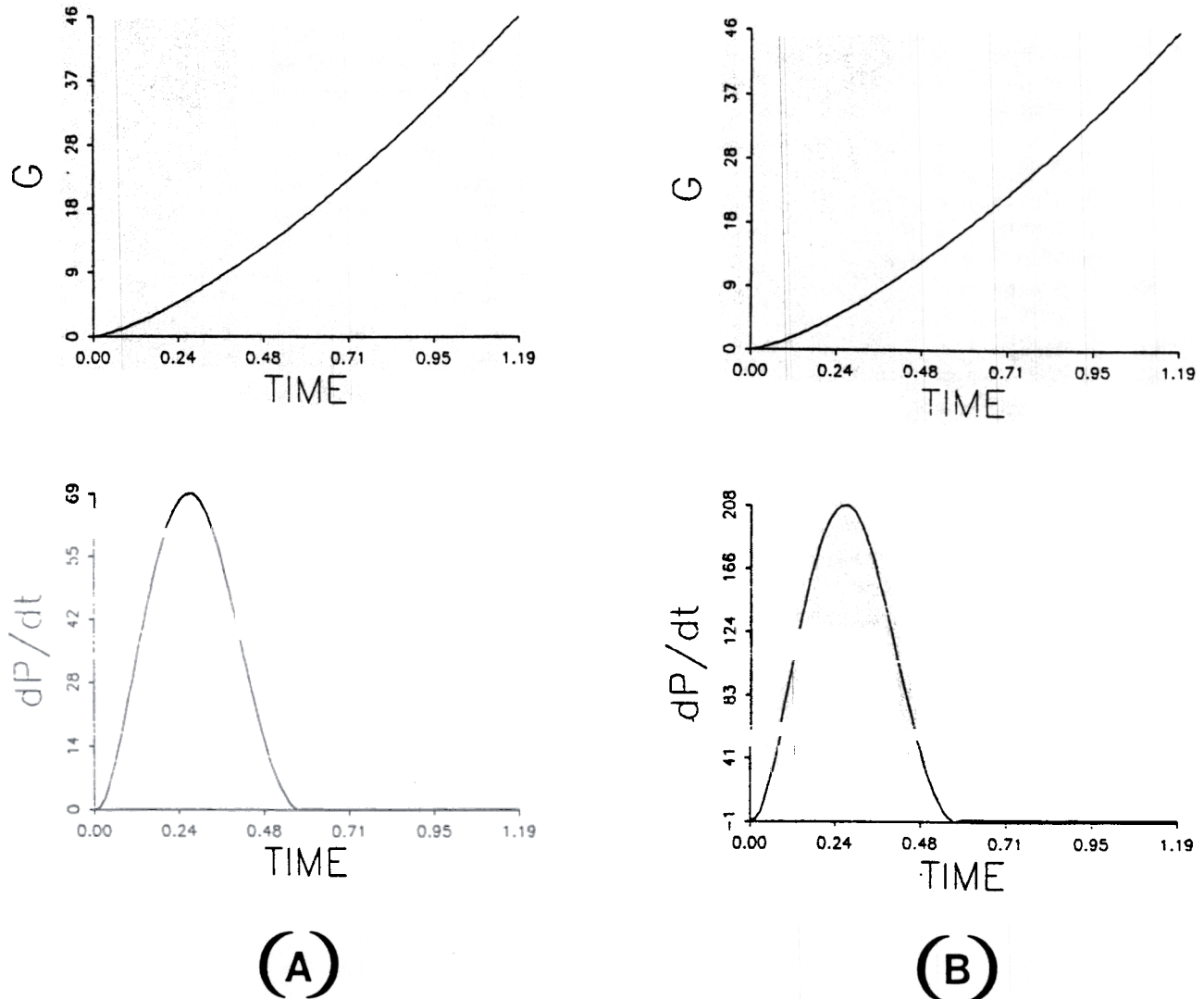


Figure 19. With equal GO signals, movements of different size have equal durations and perfectly superimposable velocity profiles after velocity axis rescaling. (For A and B, respectively, GO signals and velocity profiles are for 20- and 60-unit movements lasting 560 ms. Parameters for Equations 2, 3, and 6: $\alpha = 30$, $n = 1.4$, $\beta = 1$, and $\gamma = 0$.)

faster-than-linear onset function should be interpreted as the portion of a sigmoid onset function whose slower-than-linear part occurs at times after $P(t)$ has already come very close to T .

Figure 21 shows what happens when a slower-than-linear $g(t) = (\beta + t)^{-1}$ or a linear $g(t) = t$ is used. At slow velocities (small G_0), the velocity profile dP/dt becomes increasingly asymmetric when a slower-than-linear $g(t)$ is used. At a fixed slow velocity, the degree of asymmetry increases as the slower-than-linear $g(t)$ is chosen to approximate more closely a step function. A linear $g(t)$ leads to an intermediate degree of asymmetry. A faster-than-linear, or sigmoid, $g(t)$ leads to slight asymmetry at small values of G_0 as well as greater symmetry at large values of G_0 . A sigmoid $g(t)$ can be generated from a sudden

onset of GO signal if at least two cell stages average the GO signal before it gates $[V]^*$ in Equation 3. A sigmoid $g(t)$ contains a faster-than-linear part at small values of t and an approximately linear part at intermediate values of t . Thus a sigmoid $g(t)$ can generate different degrees of asymmetry depending on how much of the total movement time occurs within each of these ranges.

We have also simulated a VITE circuit using sigmoid GO signals whose rate of growth increases with the size of the GO amplitude. Such covariation of growth rate with amplitude is a basic property of neurons that obey membrane, or shunting, equations (Grossberg, 1970, 1973, 1982; Sperling & Sondhi, 1968). Such a sigmoid GO signal $G(t)$ can simply be defined as the output of the second neuron population in a chain of shunt-

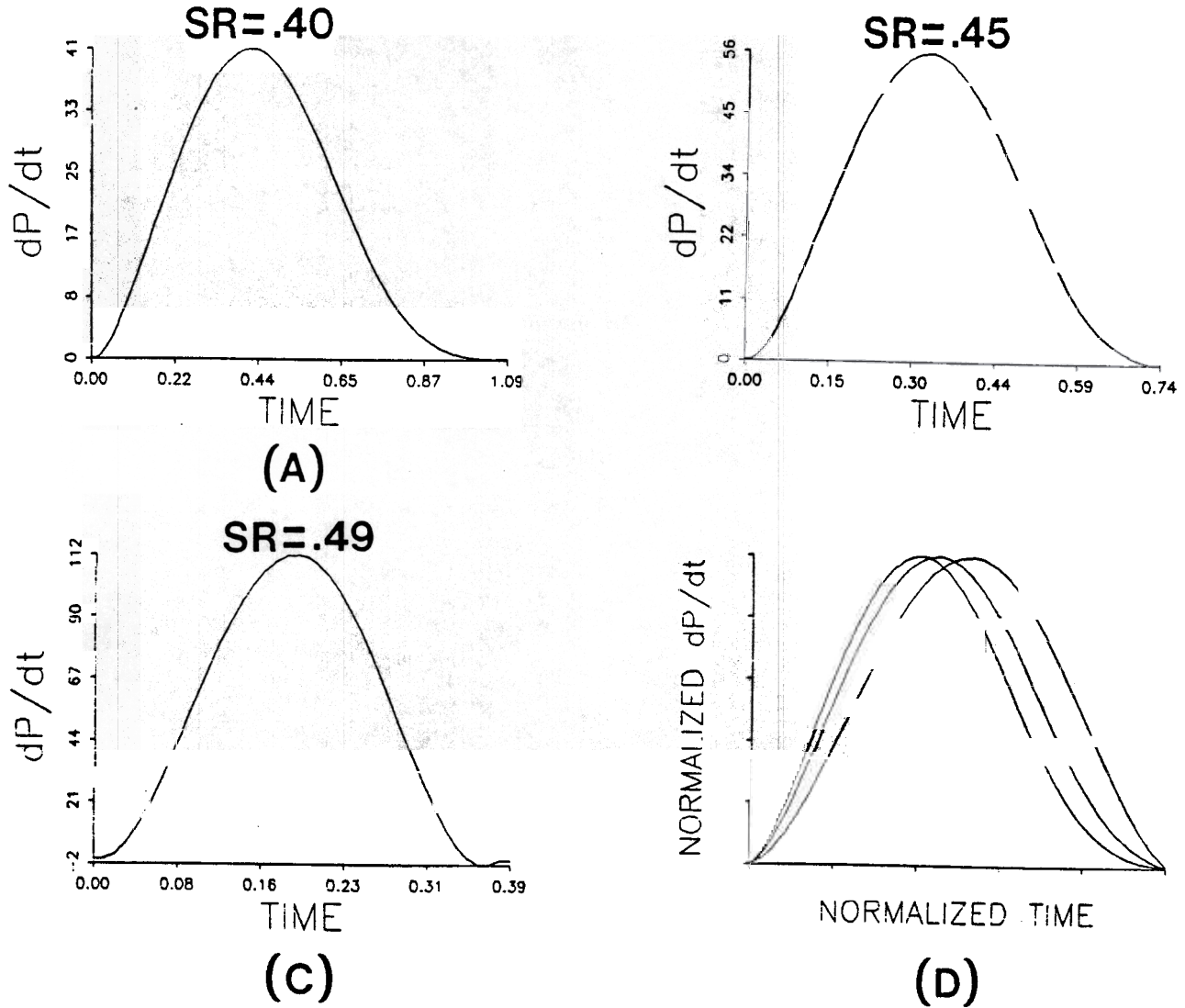


Figure 20. (A, B, and C) Velocity profiles associated with a slow, medium, and fast performance of a 20-unit movement. (Each SR value gives the trajectory's symmetry ratio: that is, the time taken to move half the distance, $.5[T(0) - P(0)]$, divided by the total movement duration, MT . These ratios indicate progressive symmetrization at higher speeds.) (D) The velocity profiles shown in (A), (B), and (C) are not perfectly superimposable. (Parameters for Equations 2, 3, and 6: $\alpha = 30$, $n = 1.4$, $\beta = 1$, and $\gamma = 0$.)

ing equations perturbed by a step function input with amplitude G_0 . Thus, let

$$G_0(t) = \begin{cases} G_0 & \text{if } t \geq 0 \\ 0 & \text{if } t < 0, \end{cases} \quad (7)$$

$$\frac{d}{dt} G_1 = -AG_1 + (B - G_1)G_0, \quad (8)$$

and

$$\frac{d}{dt} G_2 = -AG_2 + (B - G_2)G_1. \quad (9)$$

Then $G_2(t)$ is a sigmoid function of the desired shape. The GO

signal $G(t)$ can be set equal to $G_2(t)$, as we did, or even to a sigmoid signal $f[G_2(t)]$ of $G_2(t)$. A typical result is shown in Figure 22. In the series of simulations exemplified by Figure 22, the range of symmetry ratios, namely .44 to .50, was similar to that found in Figure 19 using a faster-than-linear signal function. Final choice of a best-fitting $G(t)$ awaits a more direct experimental determination of the PPC profile through time.

24. Computer Simulation of Velocity Amplification During Target Switching

Velocity amplification by up to a factor of 3 can be obtained by switching to a new value of T while a previously activated

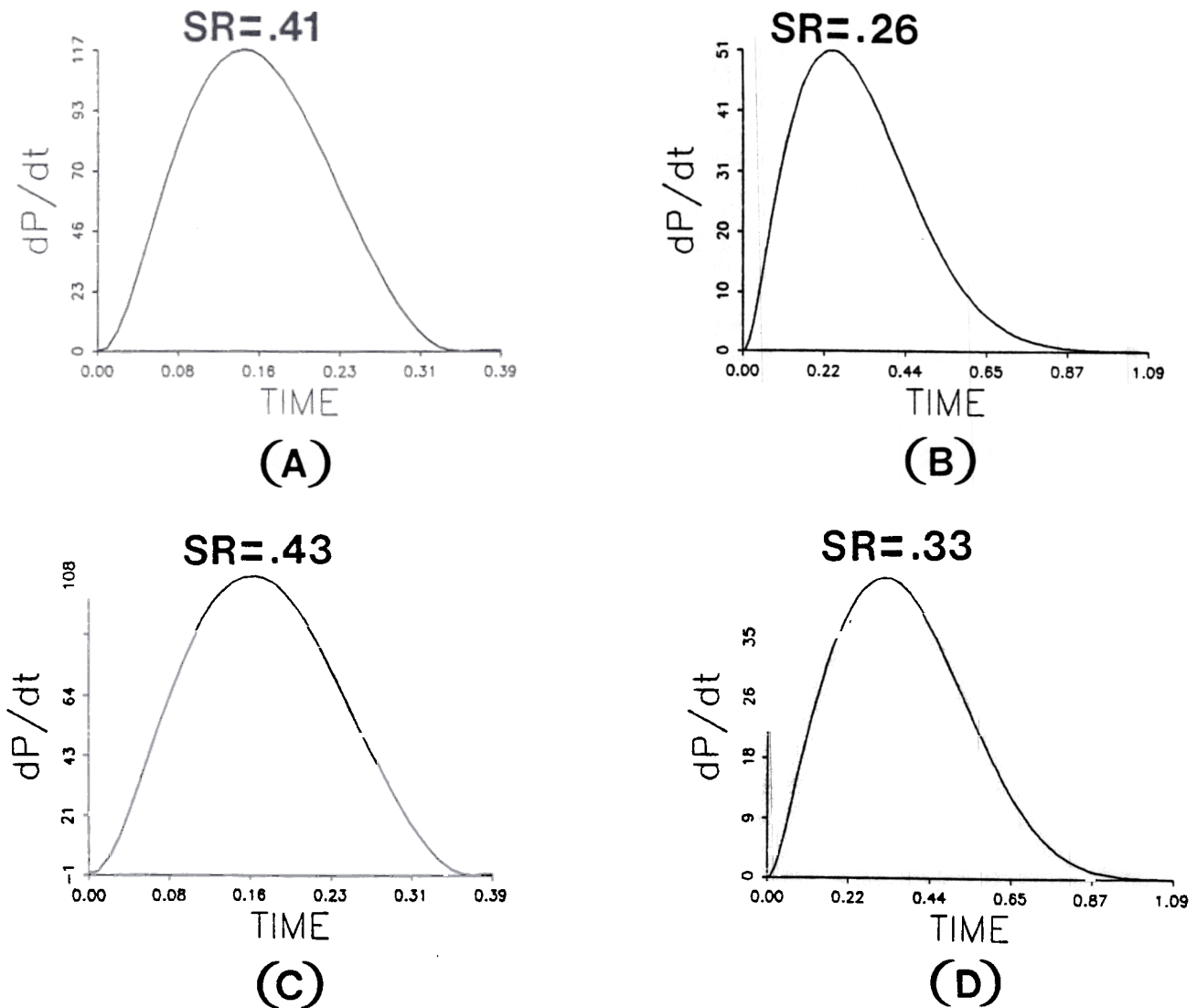


Figure 21. (A and B) Velocity profiles for a slow and a fast movement with a slower-than-linear $g(t)$: $\alpha = 30$, $n = 1$, $\beta = 1$, and $\gamma = 1$. (C and D) Velocity profiles for a slow and a fast movement with a linear $g(t)$: $\alpha = 30$, $n = 1$, $\beta = 1$, and $\gamma = 0$. (SR = symmetry ratio.)

GO signal is still on. Figure 23 demonstrates this effect by comparing two computer simulations. In the first simulation, onset of $T(t)$ and $g(t)$ were both synchronous at time $t = 0$ (Figure 23a). In the second simulation, onset of $g(t)$ preceded onset of $T(t)$ by a time equivalent to about 300 ms (Figure 23b). Note the much higher peak velocity (235 vs. 102) attained in Figure 23b. The effect, which matches the "anomalous" velocity multiplication observed in the target-switching experiments of Georgopoulos et al. (1981), is due to the prior buildup of the GO signal during response execution.

In the ensuing sections, computer simulations will be compared with a variety of data that were not reviewed in the preceding sections.

25. Reconciling Staggered Onset Times With Synchronous Termination Times

Within the context of a target-switching experiment, velocity amplification may appear to be a paradoxical property. On the other hand, such a property has an adaptive function in the many situations where a hand will fail to reach a moving target unless it both changes direction and speeds up. In addition, we now show that the same mechanism can generate synchronous termination times of synergetic muscle components that may individually start to move at staggered onset times.

The need for this latter property has recently been emphasized in a study by Hollerbach et al. (1986), who showed that

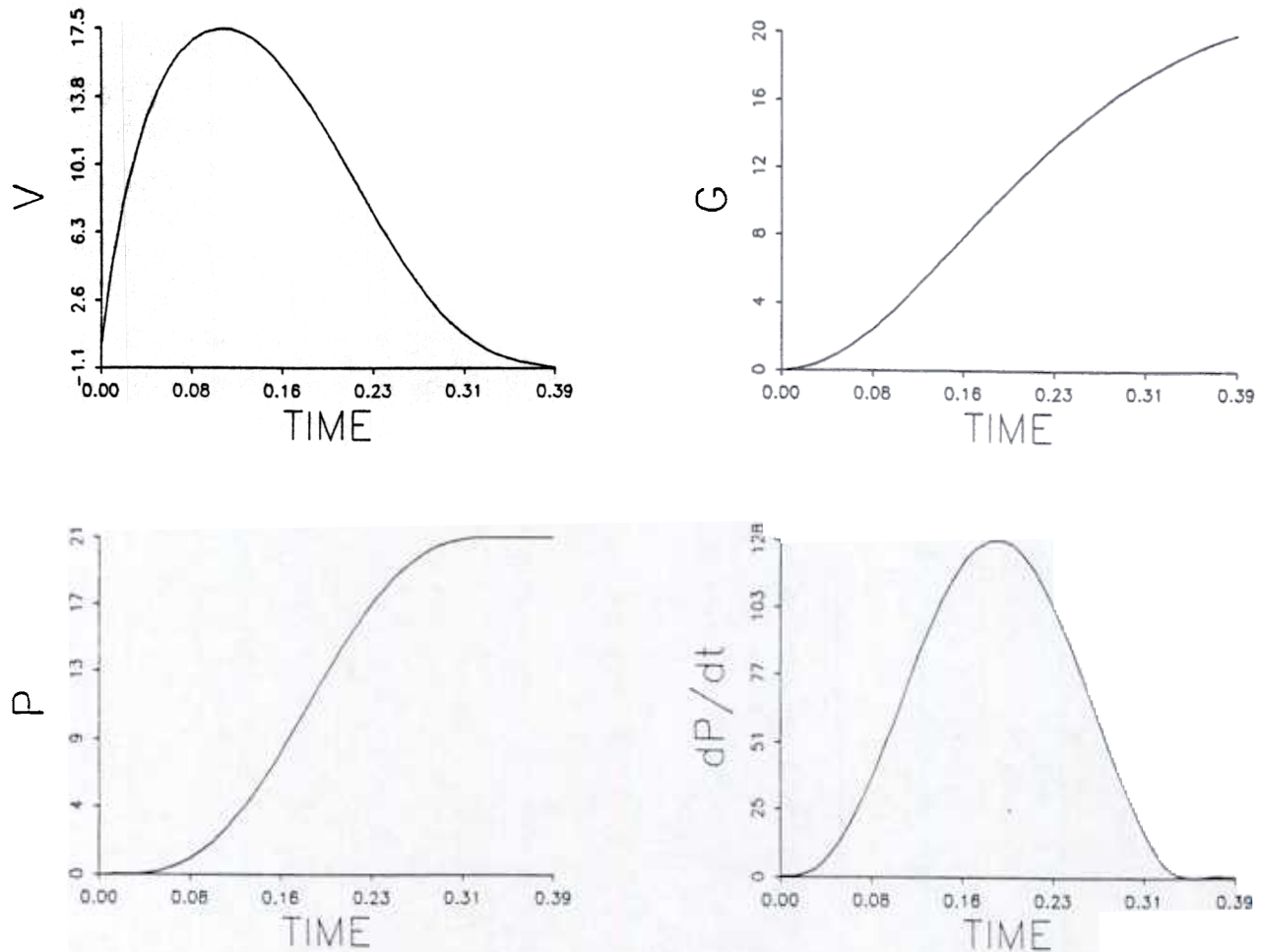


Figure 22. Simulated time course of neural-network activities and dP/dt for a 350-ms movement. (Note the S-shaped growth in G —sigmoid GO signal. Parameter values for Equations 2, 3, 8, and 9: $\alpha = 25$, $A = 1$, and $B = 25$.)

nearly straight movement paths can result from muscle-coordinate planning if the onset times of muscles acting at different joints are appropriately staggered and if all the muscles reach their final positions synchronously. Their study did not, however, explain how a neural mechanism could generate synchronous muscle offsets despite staggered muscle onsets.

We now show that the posited interaction of a growing GO signal with components of a DV that may be switched on at different times automatically generates synchronous offsets as an emergent property of the VITE circuit. Thus the interaction of a GO signal with a DV both helps to linearize the paths generated by individual TPCs and, as in the target-switching experiments, enables the hand to track efficiently a moving target by quickly reacting to readout of an updated TPC.

Figure 24 depicts the results of four blocks, labeled I, II, III, and IV, of computer simulations. Each block represents the onset time, offset time, and duration of three simulations. In the leftmost simulations of each block, onset of a DV component and a GO signal were synchronous. In the other two simulations

of each block, a different DV component was read out at successively longer delays with respect to the onset time of the GO signal. Because of duration invariance (Appendix B), the results are independent of the initial sizes of the $T(0) - P(0)$ values of these components.

The four blocks (I, II, III, and IV) correspond to four increasing values of the GO amplitude G_0 (10, 20, 40, and 80). The approximate invariance of termination times across components with different onset delays is indicated by the nearly equal heights reached by all the bars within the block. The different lengths of bars within each block show that less time is needed to update those components whose onset times are most delayed. Thus, in Block I, all the components terminate almost synchronously even though their onset times are staggered by as much as 26% of the total movement time. In Block II, almost-synchronous terminations occur even though onset times are staggered by as much as 39% of the total movement time. At very large choices of G_0 (Blocks III and IV), synchrony begins to break down because the earliest components have ex-

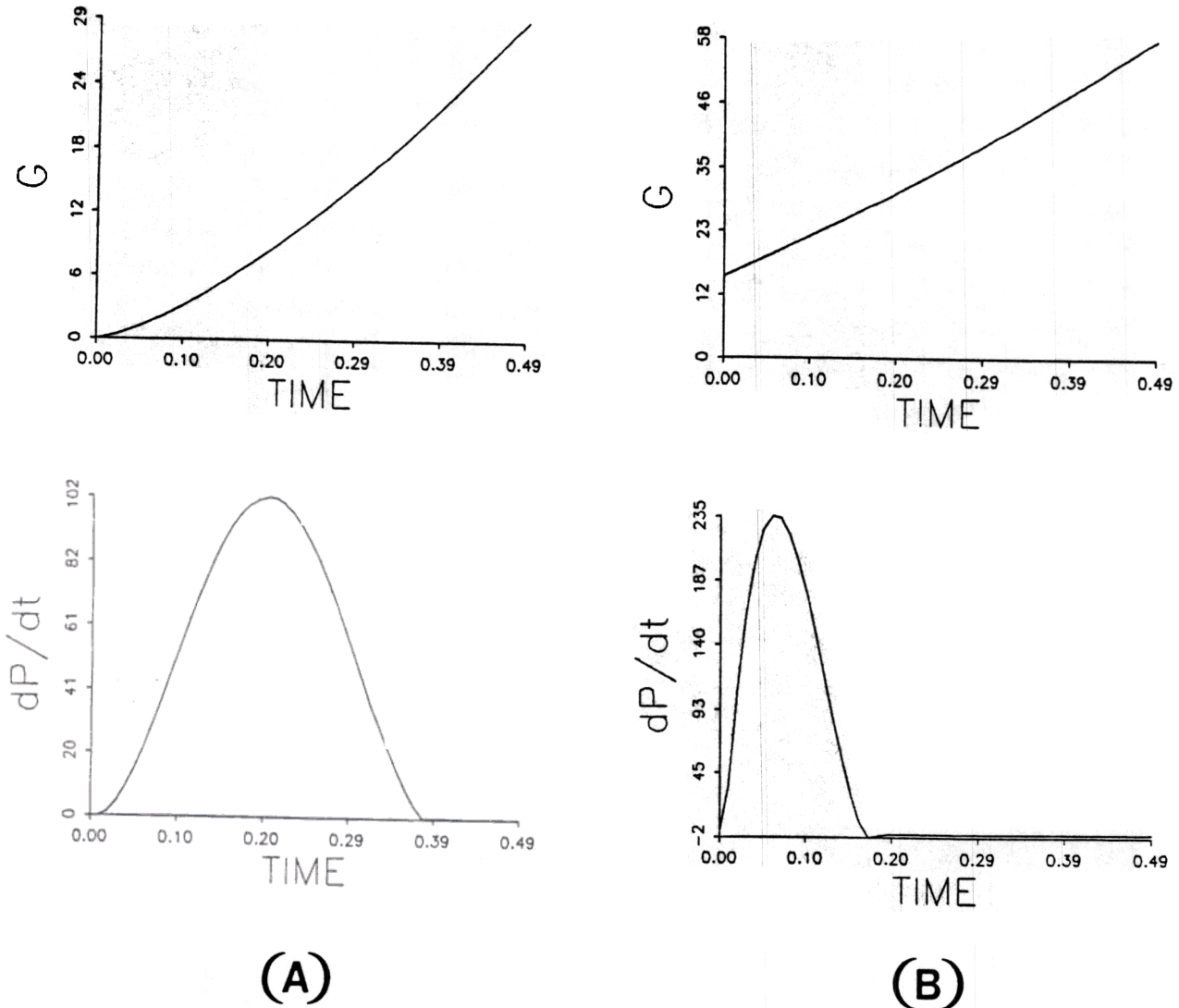


Figure 23. (A) The control condition, in which T and the GO signal growth process are activated synchronously. (B) Same T as in (A), but here T was activated after $G(t)$ had been growing for 300 ms. (A much higher peak velocity is predicted by the model whenever a target is activated after the GO signal has already had time to grow. Parameters for Equations 2, 3, and 6: $\alpha = 30$, $n = 1.4$, $\beta = 1$, and $\gamma = 0$.)

cuted more than 50% of their trajectories before later components even begin to move. These and other results in the article suggest the critical importance of experimentally testing the existence and predicted properties of GO-DV interactions, notably the predicted correlations between the temporal evolution of the GO signal and the DV.

26. Computer Simulation of the Inverse Relation Between Duration and Peak Velocity

Each curve depicted in Figure 25a summarizes a series of simulations in which $T(0) - P(0)$ was held constant while G_0 was varied. In this way, a series of velocity profiles were generated whose peak velocities differed even though their trajec-

tries traversed the same distance. The duration of each movement was computed by measuring the interval between velocity profile zero crossings. The different curves in Figure 25a used different values of the distance parameter $T(0) - P(0)$.

These curves mirror the data of Lestienne (1979) summarized in Figure 25b. Figure 25b plots agonist burst duration against peak velocity. The overall shapes of the plots of simulated durations (Figure 25a) and agonist burst durations (Figure 25b) as a function of peak velocity are similar. This similarity reinforces the postulate that the VITE circuit operates in agonist-antagonist muscle coordinates (Sections 2 and 19). It also suggests that the relation between VITE circuit outputs, motoneuron inputs, and actual muscle activities might be relatively simple (Bullock & Grossberg, 1987).

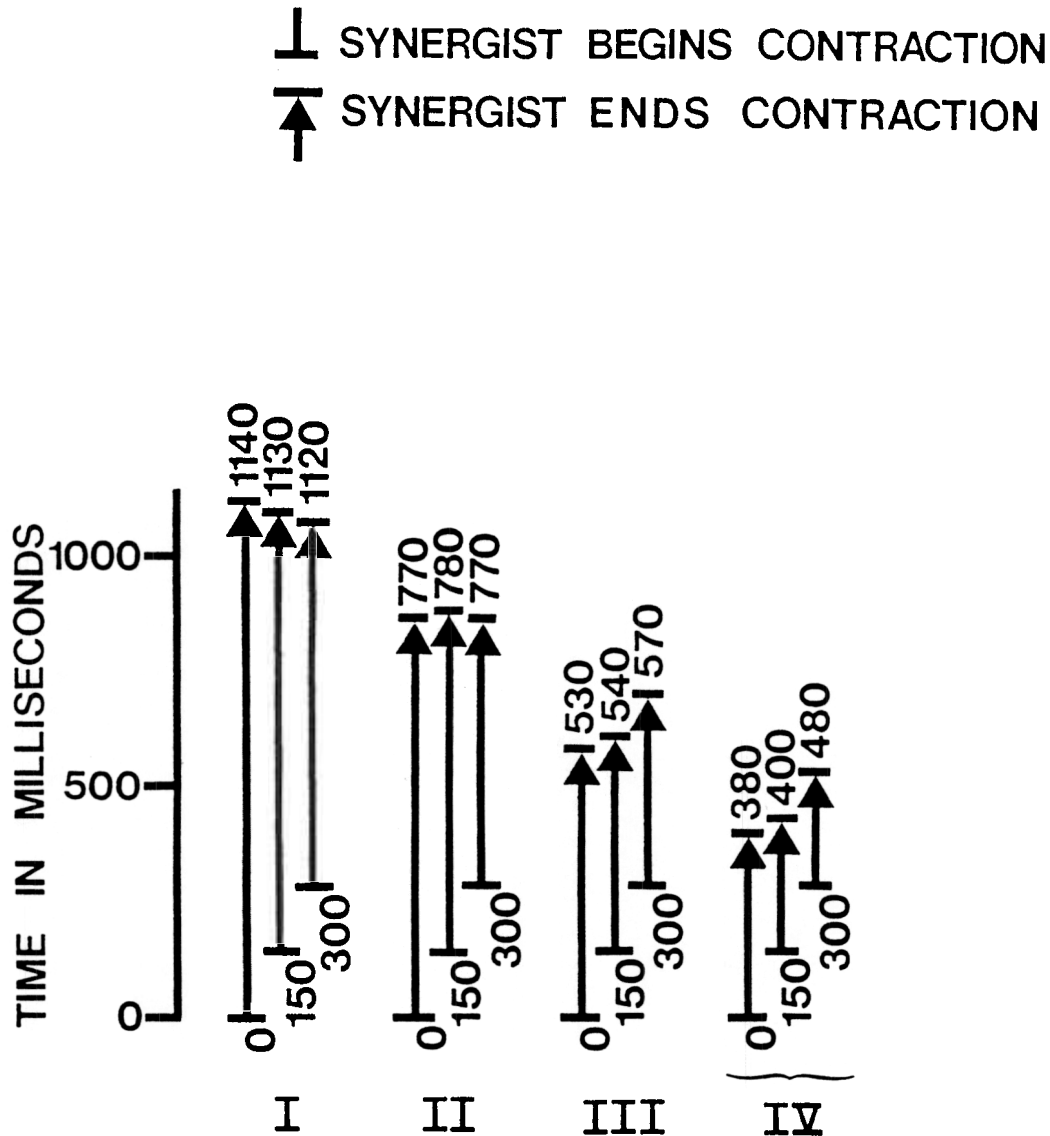


Figure 24. Simulation results showing automatic VITE circuit compensation for contraction-onset-time staggering across components of a synergy. (Each block—I, II, III, and IV—shows results for a different value—10, 20, 40, and 80, respectively—of the GO signal scalar, G_0 . Parameters for Equations 2, 3, and 6: $\alpha = 30$, $n = 1.4$, $\beta = 1$, and $\gamma = 0$.)

Nevertheless, two caveats deserve mention. First, were Figure 25a a plot of movement duration (MT) against mean velocity (\bar{V}), it would necessarily have the shape shown, because by definition,

$$MT = \frac{D}{\bar{V}}, \quad (10)$$

where D denotes the distance. Multiplying by different values of D generates a family of curves similar in shape to those shown in Figure 25a. The VITE model generates the curve in Figure 25a because mean velocity and peak velocity are strongly

correlated in these VITE trajectories owing to the duration invariance described in Section 21.

The second caveat acknowledges that the VITE circuit cooperates with several other circuits to generate a controllable trajectory in response to unexpected loads and to variable velocities (Bullock & Grossberg, 1987). For example, during medium- and high-speed movement, the duration of the initial agonist burst may be only one fourth the duration of the corresponding movement. If we assume that the PPC updating process consumes most of the movement time, then these short duration electromyograph (EMG) bursts are further evidence that the PPC stage must not be identified with—and must be

higher in the outflow channel than—the spinal motoneurons whose suprathreshold activities are directly reflected in the EMG bursts.

This conclusion is consonant with available data on the genesis of EMG burst patterns. In vivo, EMG activities are often sculpted into multiphasic burst patterns by several subnetworks that converge on and embed the spinal motoneurons. In particular, during high-speed movements, muscle changes lag behind neural changes early in response development. This leads to registration of lag errors at model regulatory circuits (Bullock & Grossberg, 1987; Feldman, 1986; Ghez & Martin, 1982; Grossberg & Kuperstein, 1986), including the stretch reflex and cerebellar circuits, which translate these error signals into large agonist activations and antagonist inhibitions. If the large agonist activations accelerate the limb so much that it begins to overshoot the intended position, this overshoot is registered as an error opposite in sign to the initial lag error, and the result is a large antagonist-braking activity in concert with agonist inhibition. Such braking may slow the movement enough that a smaller lag error is once again registered. Although this results in a second agonist burst and transient antagonist inhibition, this last phasic modulation fades quickly and gives way to the tonic EMG pattern required to hold the arm at the final postural position. A similar analysis may be given for isometric contractions.

27. Speed–Accuracy Trade-off: Woodworth's Law and Fitts's Law

The VITE model circuit predicts a speed–accuracy trade-off that quantitatively fits the laws of Woodworth (1899) and Fitts (1954). The existence of a speed–accuracy trade-off per se can be understood by considering the role of the rate parameter α in Equation 1. The case of an overshoot error is considered for definiteness.

Given any finite value of the averaging rate α in Equation 2, $V(t)$ takes some time to react to changes in $P(t)$. In particular, even if $P(t) = T$ at a given time $t = t_0$, $V(t)$ will typically require some extra time after $t = t_0$ to decrease to the value 0, and by Equation 3, $P(t)$ will continue to increase during this extra time. If α is very large, $V(t)$ can approach 0 quickly. Consequently, by Equation 3, $V(t)$ will not allow $P(t)$ to overshoot the target value T by a large amount. On the other hand, given any choice of α , the relative amount whereby $P(t)$ overshoots the target T depends on the size of the GO amplitude G_0 . This is true because a larger value of G_0 causes $P(t)$ to increase faster, because of Equation 3, and thus $P(t)$ can approach T faster. In contrast, $V(t)$ can respond only to the rapidly changing values of $T - P(t)$ at the constant rate α . As a result, $V(t)$ tends to be larger at a time $t = t_0$ when $P(t_0) = T$ if G_0 is large than if G_0 is small. It therefore takes $V(t)$ longer to equal 0 after $t = t_0$ if G_0 is large. Thus $P(t)$ overshoots T more if G_0 is large. This covariation of amount of overshoot with overall movement velocity is a speed–accuracy trade-off.

Fitts's law, as described in Equation 1, relates movement time, distance, and target width. The target width may be thought of as setting the criterion for what counts as an error. The law may be given two complementary readings. The first

notes that for a fixed movement time, error grows in proportion to amplitude. This component of the law was discovered by Woodworth (1899). Table 1 presents simulation results based on the same parameter choices used in Figure 18. The results show that in a parameter range where model overshoot errors occur, the model's error also grows in proportion to amplitude. In these simulations, G_0 was held fixed, and $T(0) - P(0)$ was varied.

The second way of reading the law notes that to maintain a fixed absolute-error size, or to fall within a target zone of fixed width, while increasing movement distance, it is necessary to allow more time for completing the movement. In particular, every doubling of distance will add a constant amount, b , to the time needed to perform the movement with the same level of accuracy. Allowing less than b more time for a movement of twice the distance will lead to a less accurate movement.

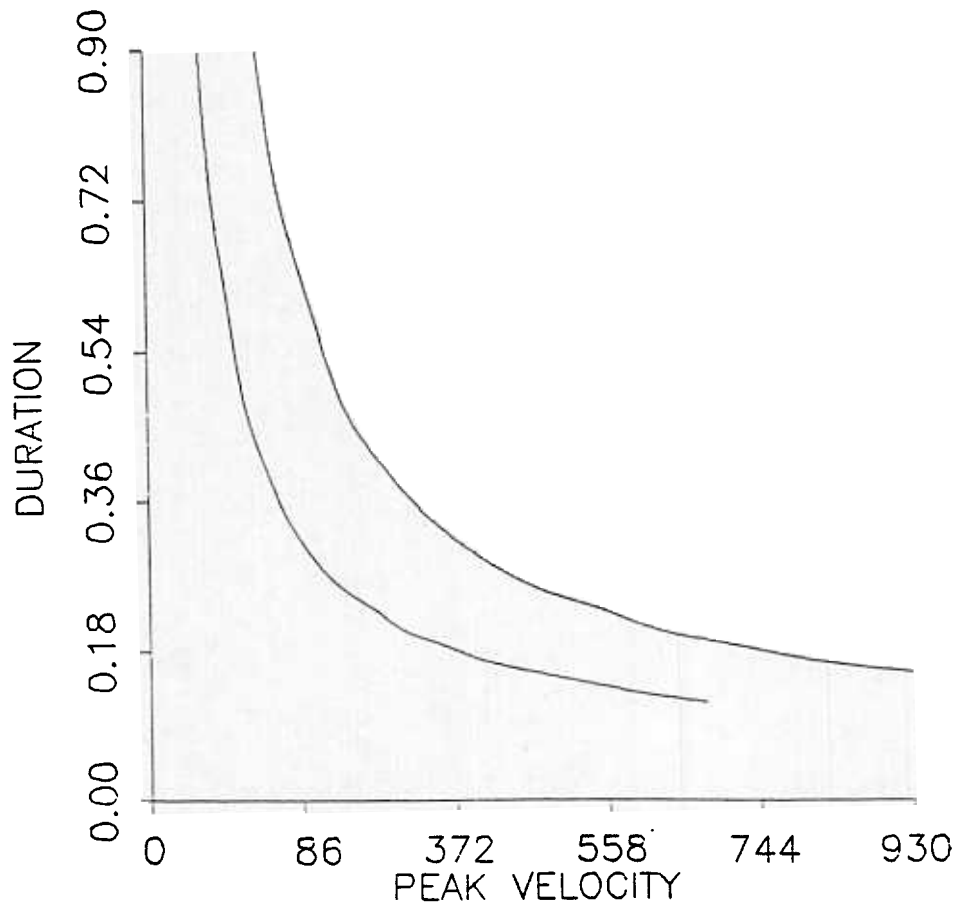
Table 2 presents the results of a simulation (parameters as in Figure 18) in which the rate parameter α was small enough that modest error resulted even at the smallest distance, or initial value of $T(0) - P(0)$, that was tested, namely a distance of two units. Then the distance $T(0) - P(0)$ was repeatedly doubled, and the value of G_0 progressively decreased, such that the error level was held approximately constant. As can be seen, movement time increased approximately linearly with each doubling of distance, as required by a logarithmic relation between movement time and distance moved. Note that the "errors" shown in Tables 1 and 2 are defined relative to a mathematical point, that is a target having zero width along the direction of motion. If subjects adjust their GO signal so that expected error is no greater than the width of a physical target, then by choosing a TPC corresponding to the near side of the target, they can produce the "errorless" movements required in the Fitts task. The model's striking replication of the laws of Woodworth and Fitts, together with its other successes in experimental results, increases our confidence that the VITE model captures some of the basic neural design principles that underly trajectory generation in vivo.

Woodworth's law is a consequence of duration invariance in the model. This can be seen from the mathematical analysis provided in Appendix B. There it is proved that the PPC value $P(t)$ can be written in the form

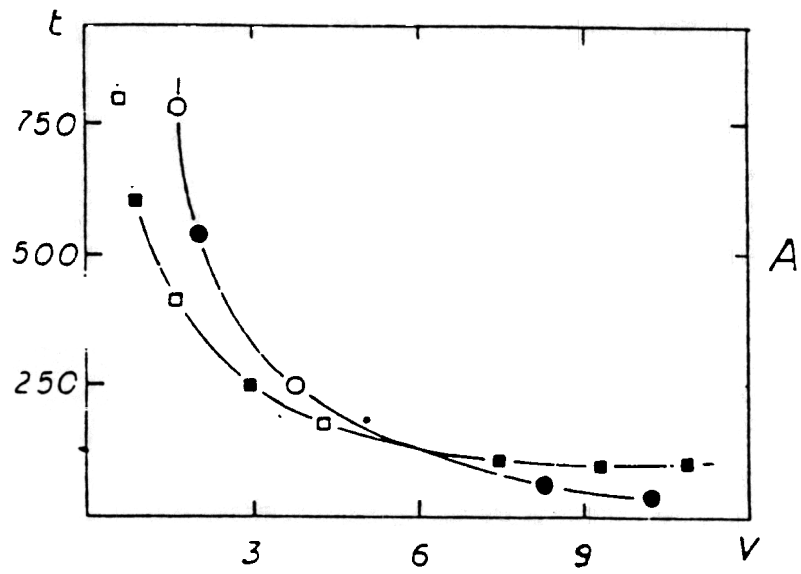
$$P(t) = P(0) + [T(0) - P(0)]q(t), \quad (11)$$

given any continuous GO signal $G(t)$. In Equation 11, $T(0) - P(0)$ represents the amount of contraction, or "distance" to be moved, that is mandated by the TPC value $T(0)$ and the initial PPC value $P(0)$. Function $q(t)$ is independent of $P(0)$ and $T(0)$. By Equation 11, $P(t)$ approaches $T(0)$ as $q(t)$ approaches 1, and $P(t)$ overshoots or undershoots if $q(t)$ approaches a value greater or less than 1, respectively. Because $q(t)$ is multiplied by $T(0) - P(0)$, the amount of error (undershoot or overshoot), is proportional to distance, as in Woodworth's law.

Whereas the proof of Woodworth's law is a general consequence of duration invariance in the model, Fitts's law has been mathematically proved in only one case as of the present time (Appendix A), although our computer simulations demonstrate that it occurs with greater generality. In this case, the GO signal



(A)



(B)

Table 1
For Fixed Duration, Error Grows in Proportion to Distance

| Movement time | Distance | Error |
|---------------|----------|-------|
| .56 | 10 | .084 |
| .56 | 20 | .170 |
| .56 | 40 | .349 |
| .56 | 80 | .700 |

Table 2
For Fixed Error Level, Duration Grows Linearly With Distance Doubling

| Error | Distance | Movement time |
|-------|----------|---------------|
| .059 | 2 | .39 |
| .057 | 4 | .49 |
| .058 | 8 | .59 |
| .059 | 16 | .70 |
| .057 | 32 | .80 |
| .059 | 64 | .91 |

$G(t)$ switches on from value 0 at times $t < 0$ to the constant value $G_0 > 0$ at times $t \geq 0$. In addition, G_0 is chosen sufficiently large to generate overshoot errors. In particular, when $4G_0 > \alpha$,

$$MT = \frac{2}{\alpha} \log\left(\frac{T(0) - P(0)}{E}\right) \quad (12)$$

where E is the amount of overshoot error in the VITE command.

These instances of Woodworth's law and Fitts's law are generated by the VITE circuit itself, without the intervention of visual feedback. A number of authors have commented on the applicability of these laws when visual feedback is inoperative. For example, Keele (1982, pp. 152-153) has written,

What is the underlying nature of the movement system that yields Fitts' Law? . . . One factor is the intrinsic accuracy of the motor control system when visual feedback is unavailable. When the eyes are closed during a movement (or the lights are turned off), an average movement will miss target by about 7% of the total distance moved.

R. A. Schmidt (1982, pp. 253-254) summarized error functions for sighted and blind movements across various movement times from studies by Keele and Posner (1968) and Zelaznik, Hawkins, and Kisselburgh (1983). A clear speed-accuracy trade-off was observed. Meyer et al., (1982, p. 450) have reviewed data comparing the initial impulse phase of a movement, where visual feedback is unimportant, with the subsequent current-control phase, where visual feedback may be used to improve accuracy. They noted that

the initial-impulse phase was found to contribute directly to the speed-accuracy trade-off. Even when subjects had to perform with their eyes closed and relied on just this phase to execute their movements, they still produced a trade-off . . . Models that attempt to account for the speed-accuracy trade-off . . . must include mechanisms that modulate the trade-off during the initial-impulse phase, not just during the current-control phase.

The VITE circuit's ability to reproduce both Woodworth's law

and Fitts's law as emergent properties of the PPC updating process satisfies this requirement.

It should be emphasized that the VITE circuit is also capable of generating a PPC that approaches the TPC without error in some parameter ranges (Appendix A). In these parameter ranges, an undershoot error will occur if the GO signal is prematurely terminated or if the effects of small DV signals get lost in ambient cellular noise. A range effect has also been reported (Georgopoulos, 1986, p. 151) such that "subjects tended to overshoot the target in small movements (2.5 cm) and to undershoot in large movements (40 cm)." A number of factors may influence this result. For example, during high-speed small movements, auxiliary circuits for controlling the arm's inertial effects may not have a sufficient opportunity to act (Grossberg & Kuperstein, 1986, chapters 3 and 5). During large movements, the distance to be moved may be visually underestimated, thereby leading to instatement of an incorrect TPC. The choice of GO signal amplitude as a function of target distance may contribute to the range effect. The relative importance of such factors will be easier to assess as new experiments and the theory are progressively elaborated with the aid of the quantitative VITE circuit analysis that is provided herein.

Even the definition of what constitutes a movement error during ecologically useful motor behavior deserves further commentary. For example, Carlton (1979) asked subjects to keep their movement errors below 5%. Subjects typically chose a two-part movement strategy whose first velocity component undershot the target and whose second velocity component made the final approach to the target at a much lower speed. Such results suggest that subjects found it easier to achieve greater accuracy by breaking up the movement into parts than by launching the movement ballistically over the full distance. The first movement part, albeit strictly speaking an "undershoot error," provides the occasion for updating TPCs and choosing small GO signals during the final part of the movement, thereby achieving high accuracy without too great an in-

Figure 25. (A) Simulation of movement duration (in seconds) as a function of peak velocity (degree/s) for a 30° (lower curve) and a 60° (upper curve) movement. (Parameters for Equations 2, 3, and 6: $\alpha = 30$, $n = 1.4$, $\beta = 1$, and $\gamma = 0$.) (B) Data on agonist burst duration (squares) and antagonist burst onset time (dots) as a function of peak velocity (radians/s) for a 60° movement. (Reprinted with permission from Lestienne, 1979.)

Table 3
Comparison of Three Models' Abilities to Predict Data on Peak Acceleration (\ddot{P})

| Distance | Movement time | Peak \ddot{P} (per s^2) | Peak \ddot{P} source |
|----------|---------------|------------------------------|--|
| 20° | .554 | | Bizzi, Accornero, Chapple, & Hogan (1984) (Experimental data) |
| 60° | .692 | | |
| 20° | .554 | 376* | Minimum-jerk model (Simulation) |
| 60° | .692 | 722* | |
| 20° | .554 | 394* | VITE model (Simulation) |
| 60° | .692 | 854* | |
| 20° | .554 | 396* | VITE ⁺ model (Simulation) |
| 60° | .692 | 1127* | |

Note. VITE = Vector-integration-to-endpoint.

crease in total movement duration. Because GO signal adjustments may also be necessary during the final components of such composite movements, these components may also obey a speed-accuracy tradeoff, as Carlton (1979) found.

28. Computer Simulation of Peak Acceleration Data

Bizzi et al. (1984) measured the peak accelerations of medium-speed forearm movements by monkeys. They considered movements around the elbow that swept out 20° and 60°. In Table 3, a computer simulation is compared with their data. To make this comparison, we scaled 1 time unit in our simulation to equal 10 ms. We then chose two values of the GO amplitude parameter G_0 that generated trajectories of duration approximately equal to 554 ms and 692 ms, respectively. Because of duration invariance (Section 21), the same durations obtain given these choices of G_0 over a wide range of choices of the distance measure $T(0) - P(0)$. The fact that movements were 20° or 60° was translated into the constraint that the $T(0) - P(0)$ value corresponding to the smaller choice of G_0 must be chosen 3 times larger than the $T(0) - P(0)$ value corresponding to the larger choice of G_0 . Then we searched for values of $T(0) - P(0)$ that gave the best fit to the peak acceleration data subject to this constraint.

The result is compared in Table 3 with the data and with the fit of Hogan's (1984) minimum-jerk model. The VITE model fit these data substantially better than the minimum-jerk model. The values associated with the VITE⁺ model indicate that a perfect fit can be obtained (with Figure 18 parameters) if DV readout to the shunting stage, rather than being instantaneous, occurs over a brief interval whose length is proportional to the size of the DV.

As noted in Section 11, the minimum-jerk model also erroneously predicts a symmetric velocity profile, at least at the level of the central controller. Moreover, it is hard to see how this model could explain the velocity amplification that occurs during target switching (Section 10). Finally, the minimum-jerk model does not contain any representation that may be com-

pared with the existence of vector cells or with the manner in which vector cell activities are integrated into outflow movement commands (Section 12). We therefore believe that the VITE model provides a better foundation for developing a quantitative neurally based theory of arm movements than does the minimum-jerk model. The VITE model, in addition to the model circuits developed in Grossberg and Kuperstein (1986), also provides a mechanistic neural explanation of some of the types of invariant behaviors for whose analysis the task-dynamic approach to motor control was developed (Saltzman & Kelso, 1987).

29. Updating the PPC Using Inflow Signals During Passive Movements

Despite these successes, the VITE model, as described, is far from complete. In this section we outline a solution to one additional design problem. Bullock and Grossberg (1987) suggested solutions to a number of the other design problems whereby a VITE circuit can effectively move an arm of variable mass subjected to unexpected perturbations at variable velocities through a Newtonian world.

In Section 5, we noted that inflow signals are needed to update the PPC during a passive movement. For example, Gellmann, Gibson, and Houk (1985) have described cells in the cat inferior olive that are sensitive to passive body displacement but not to active movement, and Clark, Burgess, Chapin, and Lipscomb (1985) have analyzed muscle proprioceptive contributions to position sense during passive finger movements in humans. Two basic problems motivate our model of PPC updating by inflow signals. First, the process of updating the PPC during passive movements must continue until the PPC registers the position coded by the inflow signals. Thus a difference vector of inflow signals minus PPC outflow signals updates the PPC during passive movements. We denote this difference vector by DI'_p to distinguish it from the DV that compares TPCs with PPCs. At times when $DI'_p = 0$, the PPC is fully updated. Although the DI'_p is not the same as the DV that compares a TPC with a PPC, the PPC is a source of inhibitory signals, as will be seen shortly, in computing both difference vectors.

Second, PPC outflow signals and inflow signals may, in principle, be calibrated quite differently. We will show how corollary discharges of the PPC outflow signals are adaptively recalibrated until they are computed in the same numerical scale as the inflow signals to which they are compared. We also show that the adaptive recalibration mechanism automatically computes a DI'_p that updates the PPC by just the correct amount.

Figure 26 schematizes a model circuit for adaptively computing this DI'_p . We call this circuit the *passive update of position* (PUP) model. In Figure 26, the PPC sends inhibitory corollary discharge signals toward the outflow-inflow match stage where the inflow signals are registered. It is assumed that this stage is inhibited except when the movement command circuit is inactive. A simple way to achieve this property is to assume that the GO signal in the movement command circuit inhibits the outflow-inflow match stage, as in Figure 26. Thus the mismatches of outflow and inflow signals that occur during every active movement do not erroneously update the outflow-inflow

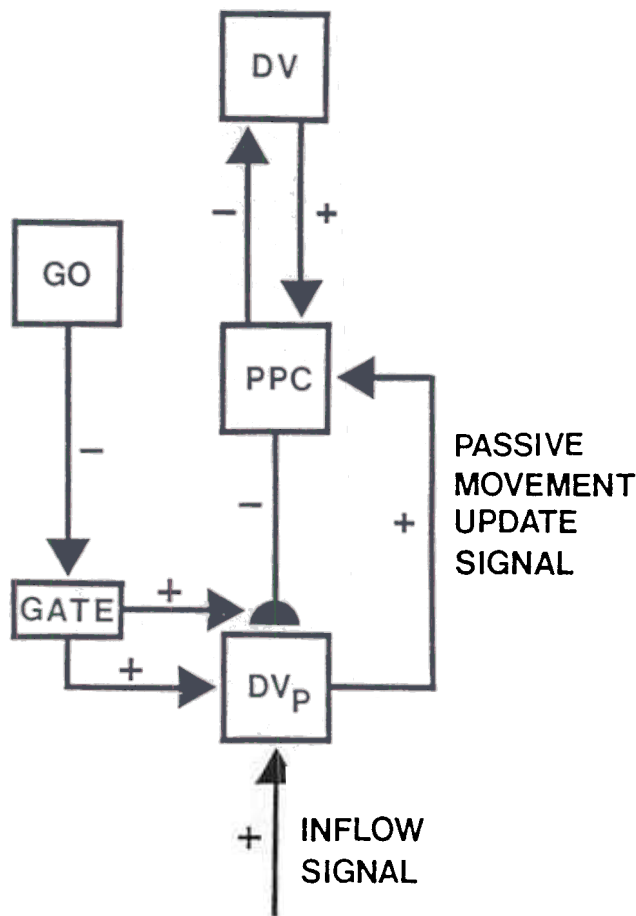


Figure 26. A passive update of position (PUP) circuit. PPC = present-position command. DV = difference vector. (An adaptive pathway $PPC - DV_p$ calibrates PPC-outflow signals in the same scale as inflow signals during intervals of posture. During passive movements, output from DV equals zero. Hence the passive difference vector DV_p updates the PPC until it equals the new position caused by any passive movements that may occur because of the application of external forces.)

match stage. In addition, the GO signal is assumed to inhibit learning at the long-term memory (LTM) traces that multiply the PPC signals on their way to the outflow-inflow match stage.

This assumption is consistent with the arm movement results of Evarts and Fromm (1978), which showed greater modulation of vector cells in precentral motor cortex by inflow signals during small slow movements than during posture, and strongly attenuated modulation during large fast movements. In the model, the amount of attenuation increases with the size of the GO signal. The gating signal that attenuates the inflow process may be a nonlinear (e.g., sigmoid) function of the GO signal. Parametric analysis of the degree of inflow attenuation as a function of overall active movement speed would provide valuable information about the form of this hypothesized gating signal.

After a movement is over, both the outflow-inflow match stage and the LTM traces are released from inhibition. Typi-

cally, the PPC represents the same position as the inflow signals, but perhaps in a different numerical scale. The learning laws described in Appendix C define LTM traces that change until the PPC multiplied by the LTM trace equals the inflow signal. After a number of such learning trials during stable posture, $DV_p = 0$ and the PPC signals are rescaled by the LTM traces to match correctly the inflow signals.

During a passive movement, the PPC does not change, but the inflow signal may change. If the DV_p becomes positive, it causes an increase in the PPC until the DV_p decreases to 0 and the PPC is correctly updated by the inflow signals. If the DV_p becomes negative, then the DV_p of the opponent muscle can decrease the PPC until a match again occurs.

30. Concluding Remarks

The present article introduces a circuit for automatically translating a target-position command into a complete movement trajectory via a mechanism of continuous vector updating and integration. A wide variety of behavioral and neural data can be explained quantitatively by this mechanism. The model also provides a foundation for clarifying some of the outstanding classic issues in the motor-control literature, highlights the relevance of learning constraints to the design of neural circuitry, and may be viewed as a specialized version of a more general architecture for movement control.

The VITE circuit and the PUP circuit do not, however, exhaust the total neural machinery needed for the control of arm movements. Mechanisms for properly timed sequential readout of TPCs in a serial motor plan, such as during reaching and grasping or during a dance (Grossberg & Kuperstein, 1986, chapter 9), for adaptive linearization of a nonlinear muscle plant (Grossberg & Kuperstein, 1986, chapter 5), and for automatically or predictively adapting to the inertial properties generated by variable loads and velocities (Bullock & Grossberg, 1987) also form essential parts of the arm-control system. When all of these systems are joined together, however, one can begin to understand quantitatively how the arm system achieves its remarkable flexibility and versatility and can begin to build a new type of biologically inspired adaptive robot whose design is qualitatively different from the algorithms offered by traditional approaches to artificial intelligence.

References

- Abend, W., Bizzi, E., & Morasso, P. (1982). Human arm trajectory formation. *Brain*, *105*, 331-348.
- Adams, J. A. (1971). A closed-loop theory of motor learning. *Journal of Motor Behavior*, *3*, 111-149.
- Adams, J. A. (1977). Feedback theory of how joint receptors regulate the timing and positioning of a limb. *Psychological Review*, *84*, 504-523.
- Albus, J. A. (1971). A theory of cerebellar function. *Mathematical Biosciences*, *10*, 25-61.
- Atkeson, C. G., & Hollerbach, J. M. (1985). Kinematic features of unrestrained vertical arm movements. *Journal of Neuroscience*, *5*, 2318-2330.
- Beggs, W. D. A., & Howarth, C. I. (1972). The movement of the hand towards a target. *Quarterly Journal of Experimental Psychology*, *24*, 448-453.

- Bernstein, N. A. (1967). *The coordination and regulation of movements*. London: Pergamon Press.
- Bizzi, E. (1980). Central and peripheral mechanisms in motor control. In G. E. Stelmach & J. Requin (Eds.), *Tutorials in motor control* (pp. 131-144). Amsterdam: North-Holland.
- Bizzi, E., Accornero, N., Chapple, W., & Hogan, N. (1982). Arm trajectory formation in monkeys. *Experimental Brain Research*, *46*, 139-143.
- Bizzi, E., Accornero, N., Chapple, W., & Hogan, N. (1984). Posture control and trajectory formation during arm movement. *Journal of Neuroscience*, *4*, 2738-2744.
- Brindley, G. S. (1964). The use made by the cerebellum of the information that it receives from sense organs. *International Brain Research Organization Bulletin*, *3*, 80.
- Brody, M., & Paul, R. (Eds.). (1984). *Robotics research: The first international symposium*. Cambridge: MIT Press.
- Brooks, V. B. (1979). Motor programs revisited. In R. E. Talbot & D. R. Humphrey (Eds.), *Posture and movement: Perspective for integrating sensory and motor research on the mammalian nervous system* (pp. 13-49). New York: Raven Press.
- Brooks, V. B. (1986). *The neural basis of motor control*. New York: Oxford University Press.
- Buchanan, T. S., Almdale, D. P. J., Lewis, J. L., & Rymer, W. Z. (1986). Characteristics of synergic relations during isometric contractions of human elbow muscles. *Journal of Neurophysiology*, *56*, 1225-1241.
- Bullock, D., & Grossberg, S. (1986, August). *Neural dynamics of planned arm movements: Synergies, invariants, and trajectory formation*. Paper presented at the meeting of the Society for Mathematical Psychology, Cambridge, MA.
- Bullock, D., & Grossberg, S. (1987). *Neuromuscular realization of planned trajectories: Adaptive and automatic mechanisms*. Unpublished manuscript.
- Carlton, L. G. (1979). Control processes in the production of discrete aiming responses. *Journal of Human Movement Studies*, *5*, 115-124.
- Carpenter, G. A., & Grossberg, S. (1987). A massively parallel architecture for a self-organizing neural pattern recognition machine. *Computer Vision, Graphics, and Image Processing*, *37*, 54-115.
- Carpenter, G. A., & Grossberg, S. (in press). Neural dynamics of category learning and recognition: Attention, memory consolidation, and amnesia. In J. Davis, R. Newburgh, & E. Wegman (Eds.), *Brain structure, learning, and memory*.
- Clark, F. J., Burgess, R. C., Chapin, J. W., & Lipscomb, W. T. (1985). Role of intramuscular receptors in the awareness of limb position. *Journal of Neurophysiology*, *54*, 1529-1540.
- Cooke, J. D. (1980). The organization of simple, skilled movements. In G. E. Stelmach & J. Requin (Eds.), *Tutorials in motor behavior* (pp. 199-212). Amsterdam: North-Holland.
- Evarts, E. V. (1968). Relation of pyramidal tract activity to force exerted during voluntary movement. *Journal of Neurophysiology*, *31*, 14-27.
- Evarts, E. V., & Fromm, C. (1978). The pyramidal tract neuron as summing point in a closed-loop control system in the monkey. In J. E. Desmedt (Ed.), *Cerebral motor control in man: Long loop mechanisms* (pp. 56-69). Basel, Switzerland: Karger.
- Evarts, E. V., & Tanji, J. (1974). Gating of motor cortex reflexes by prior instruction. *Brain Research*, *71*, 479-494.
- Feldman, A. G. (1974). Change in the length of the muscle as a consequence of a shift in equilibrium in the muscle-load system. *Biofizika*, *19*, 534-538.
- Feldman, A. G. (1986). Once more on the equilibrium-point hypothesis (λ model) for motor control. *Journal of Motor Behavior*, *18*, 17-54.
- Fetters, L., & Todd, J. (1987). Quantitative assessment of infant reaching movements. *Journal of Motor Behavior*, *19*, 147-166.
- Fitts, P. M. (1954). The information capacity of the human motor system in controlling the amplitude of movement. *Journal of Experimental Psychology*, *47*, 381-391.
- Fitts, P. M., & Peterson, J. R. (1964). Information capacity of discrete motor responses. *Journal of Experimental Psychology*, *67*, 103-112.
- Flash, T., & Hogan, N. (1985). The coordination of arm movements: An experimentally confirmed mathematical model. *Journal of Neuroscience*, *5*, 1688-1703.
- Freund, H.-J., & Büdingen, H. J. (1978). The relationship between speed and amplitude of the fastest voluntary contractions of human arm muscles. *Experimental Brain Research*, *31*, 1-12.
- Fujita, M. (1982a). Adaptive filter model of the cerebellum. *Biological Cybernetics*, *45*, 195-206.
- Fujita, M. (1982b). Simulation of adaptive modification of the vestibulo-ocular reflex with an adaptive filter model of the cerebellum. *Biological Cybernetics*, *45*, 207-214.
- Gellmann, R., Gibson, A. R., & Houk, J. C. (1985). Inferior olivary neurons in the awake cat: Detection of contact and passive body displacement. *Journal of Neurophysiology*, *54*, 40-60.
- Georgopoulos, A. P. (1986). On reaching. *Annual Review of Neuroscience*, *9*, 147-170.
- Georgopoulos, A. P., Kalaska, J. F., Caminiti, R., & Massey, J. T. (1982). On the relations between the direction of two-dimensional arm movements and cell discharge in primate motor cortex. *Journal of Neuroscience*, *2*, 1527-1537.
- Georgopoulos, A. P., Kalaska, J. F., Crutcher, M. D., Caminiti, R., & Massey, J. T. (1984). The representation of movement direction in the motor cortex: Single cell and population studies. In G. M. Edelman, W. E. Gall, & W. M. Cowan (Eds.), *Dynamic aspects of neocortical function* (pp. 501-524). New York: Wiley.
- Georgopoulos, A. P., Kalaska, J. F., & Massey, J. T. (1981). Spatial trajectories and reaction times of aimed movements: Effects of practice, uncertainty, and change in target location. *Journal of Neurophysiology*, *46*, 725-743.
- Georgopoulos, A. P., Schwartz, A. B., & Kettner, R. E. (1986). Neuronal population coding of movement direction. *Science*, *233*, 1416-1419.
- Ghez, C., & Martin, J. H. (1982). The control of rapid limb movement in the cat. III: Agonist-antagonist coupling. *Experimental Brain Research*, *45*, 115-125.
- Ghez, C., & Vicario, D. (1978). The control of rapid limb movement in the cat. II: Scaling of isometric force adjustments. *Experimental Brain Research*, *33*, 191-202.
- Gordon, J., & Ghez, C. (1984). EMG patterns in antagonist muscles during isometric contraction in man: Relations to response dynamics. *Experimental Brain Research*, *55*, 167-171.
- Gordon, J., & Ghez, C. (1987a). Trajectory control in targeted force impulses. II: Pulse height control. *Experimental Brain Research*, *67*, 241-252.
- Gordon, J., & Ghez, C. (1987b). Trajectory control in targeted force impulses. III: Compensatory adjustments for initial errors. *Experimental Brain Research*, *67*, 253-269.
- Grossberg, S. (1969). On learning of spatiotemporal patterns by networks with ordered sensory and motor components. I. Excitatory components of the cerebellum. *Studies in Applied Mathematics*, *48*, 105-132.
- Grossberg, S. (1970). Neural pattern discrimination. *Journal of Theoretical Biology*, *27*, 291-337.
- Grossberg, S. (1972). Neural expectation: Cerebellar and retinal analogs of cells fired by learnable or unlearned pattern classes. *Kybernetik*, *10*, 49-57.
- Grossberg, S. (1973). Contour enhancement, short-term memory, and constancies in reverberating neural networks. *Studies in Applied Mathematics*, *52*, 217-257.
- Grossberg, S. (1978). A theory of human memory: Self-organization

- and performance of sensory-motor codes, maps, and plans. In R. Rosen & F. Snell (Eds.), *Progress in theoretical biology* (Vol. 5, pp. 233–374). New York: Academic Press.
- Grossberg, S. (1982). *Studies of mind and brain: Neural principles of learning, perception, development, cognition, and motor control*. Boston: Reidel Press.
- Grossberg, S. (1986). Adaptive compensation to changes in the oculomotor plant. In E. Keller & D. Zee (Eds.), *Adaptive processes in the visual and oculomotor systems* (pp. 341–345). New York: Pergamon Press.
- Grossberg, S. (Ed.). (1987a). *The adaptive brain. I: Cognition, learning, reinforcement, and rhythm*. Amsterdam: Elsevier/North-Holland.
- Grossberg, S. (Ed.). (1987b). *The adaptive brain. II: Vision, speech, language, and motor control*. Amsterdam: Elsevier/North-Holland.
- Grossberg, S. (1987c). Cooperative self-organization of multiple neural systems during adaptive sensory-motor control. In D. M. Guthrie (Ed.), *Aims and methods in neuroethology*. Manchester, England: Manchester University Press.
- Grossberg, S., & Kuperstein, M. (1986). *Neural dynamics of adaptive sensory-motor control: Ballistic eye movements*. Amsterdam: Elsevier/North-Holland.
- Grossberg, S., & Stone, G. O. (1986). Neural dynamics of word recognition and recall: Attentional priming, learning, and resonance. *Psychological Review*, 93, 46–74.
- Helmholtz, H. von. (1866). *Handbook of physiological optics*. East Germany: Leipzig: Voss.
- Hofsten, C. von. (1979). Development of visually directed reaching: The approach phase. *Journal of Human Movement Studies*, 5, 160–178.
- Hofsten, C. von. (1982). Eye-hand coordination in the newborn. *Developmental Psychology*, 18, 450–461.
- Hogan, N. (1984). An organizing principle for a class of voluntary movements. *Journal of Neuroscience*, 4, 2745–2754.
- Hollerbach, J. M. (1982). Computers, brain, and the control of movement. *Trends in Neuroscience*, 5, 189–192.
- Hollerbach, J. M. (1984). Dynamic scaling of manipulator trajectories. *Journal of Dynamic Systems, Measurement, and Control*, 106, 102–106.
- Hollerbach, J. M., Moore, S. P., & Atkeson, C. G. (1986). Workspace effect in arm movement kinematics derived by joint interpolation. In G. Gantchev, B. Dimitrov, & P. Gatev (Eds.), *Motor control*. New York: Plenum Press.
- Holst, E. von, & Mittelstaedt, H. (1950). The reafference principle: Interaction between the central nervous system and the periphery. *Naturwissenschaften*, 37, 464–476.
- Houk, J. C., & Rymer, W. Z. (1981). Neural control of muscle length and tension. In *Handbook of physiology: The nervous system II* (pp. 257–322). Bethesda, MD: American Physiological Society.
- Howarth, C. I., & Beggs, W. D. A. (1971). The relationship between speed and accuracy of movement aimed at a target. *Acta Psychologica*, 35, 207–218.
- Howarth, C. I., & Beggs, W. D. A. (1981). Discrete movements. In D. Holding (Ed.), *Human skills* (pp. 91–117). New York: Wiley.
- Humphrey, D. R., & Reed, D. J. (1983). Separate cortical systems for control of joint movement and joint stiffness: Reciprocal activation and coactivation of antagonist muscles. In J. E. Desmedt (Ed.), *Motor control mechanisms in health and disease* (pp. 347–372). New York: Raven Press.
- Ito, M. (1974). The control mechanisms of cerebellar motor systems. In F. O. Schmitt & F. G. Worden (Eds.), *The neurosciences third study program* (pp. 293–303). Cambridge: MIT Press.
- Ito, M. (1982). Cerebellar control of the vestibulo-ocular reflex—Around the flocculus hypothesis. *Annual Review of Neuroscience*, 5, 275–296.
- Ito, M. (1984). *The cerebellum and neural control*. New York: Raven Press.
- Jagacinski, R. J., & Monk, D. L. (1985). Fitts' Law in two dimensions with hand and head movements. *Journal of Motor Behavior*, 17, 77–95.
- Jeannerod, M. (1984). The timing of natural prehension movements. *Journal of Motor Behavior*, 16, 235–254.
- Kalaska, J. F., Caminiti, R., & Georgopoulos, A. P. (1983). Cortical mechanisms related to the direction of two-dimensional arm movements: Relations in parietal area 5 and comparison with motor cortex. *Experimental Brain Research*, 51, 247–260.
- Keele, S. W. (1981). Behavioral analysis of movement. In V. B. Brooks (Ed.), *Handbook of physiology: Motor control* (Vol. 2, pp. 1391–1414). Bethesda, MD: American Physiological Society.
- Keele, S. W. (1982). Component analysis and conceptions of skill. In J. A. S. Kelso (Ed.), *Human motor behavior* (pp. 143–159). Hillsdale, NJ: Erlbaum.
- Keele, S. W., & Posner, M. I. (1968). Processing of visual feedback in rapid movements. *Journal of Experimental Psychology*, 77, 155–158.
- Kelso, J. A. S. (Ed.). (1982). *Human motor behavior*. Hillsdale, NJ: Erlbaum.
- Kelso, J. A. S., & Holt, K. G. (1980). Exploring a vibratory systems analysis of human movement production. *Journal of Neurophysiology*, 28, 45–52.
- Kelso, J. A. S., Southard, D. L., & Goodman, D. (1979). On the nature of human interlimb coordination. *Science*, 203, 1029–1031.
- Kerr, B., & Langolf, G. D. (1977). Speed of aimed movements. *Quarterly Journal of Experimental Psychology*, 29, 475–481.
- Knight, A. A., & Dagnall, P. R. (1967). Precision in movements. *Ergonomics*, 10, 327–330.
- Lestienne, F. (1979). Effects of inertial load and velocity on the braking process of voluntary limb movements. *Experimental Brain Research*, 35, 407–418.
- Luschei, E. S., & Fuchs, A. F. (1972). Activity of brain stem neurons during eye movements of alert monkeys. *Journal of Neurophysiology*, 35, 445–461.
- Marr, D. (1969). A theory of cerebellar cortex. *Journal of Physiology*, 202, 437–470.
- Marteniuk, R. G., & MacKenzie, C. L. (1980). A preliminary theory of two-hand co-ordinated control. In G. E. Stelmach & J. Requin (Eds.), *Tutorials in motor behavior* (pp. 185–197). Amsterdam: Elsevier/North-Holland.
- Massey, J. T., Schwartz, A. B., & Georgopoulos, A. P. (1986). On information processing and performing a movement sequence. In H. Heuer & C. Fromm (Eds.), *Generation and modulation of action patterns*. Berlin: Springer-Verlag.
- McCormick, D. A., & Thompson, R. F. (1984). Cerebellum: Essential involvement in the classically conditioned eyelid response. *Science*, 223, 296–299.
- Meyer, D. E., Smith, J. E. K., & Wright, C. E. (1982). Models for the speed and accuracy of aimed movements. *Psychological Review*, 89, 449–482.
- Morasso, P. (1981). Spatial control of arm movements. *Experimental Brain Research*, 42, 223–227.
- Nichols, T. R. (1985). Is "the mass-spring model" a testable hypothesis? *Journal of Motor Behavior*, 17, 499–500.
- Optican, L. M., & Robinson, D. A. (1980). Cerebellar-dependent adaptive control of primate saccadic system. *Journal of Neurophysiology*, 44, 1058–1076.
- Piaget, J. (1963). *The origins of intelligence in children*. New York: Norton.

- Polit, A., & Bizzi, E. (1978). Processes controlling arm movements in monkeys. *Science*, *201*, 1235-1237.
- Polit, A., & Bizzi, E. (1979). Characteristics of the motor programs underlying arm movements in monkeys. *Journal of Neurophysiology*, *42*, 183-194.
- Raybourn, M. S., & Keller, E. L. (1977). Colliculoreticular organization in primate oculomotor system. *Journal of Neurophysiology*, *40*, 861-878.
- Ron, S., & Robinson, D. A. (1973). Eye movements evoked by cerebellar stimulation in the alert monkey. *Journal of Neurophysiology*, *36*, 1004-1021.
- Ruffini, A. (1898). On the minute anatomy of the neuro-muscular spindles of the cat, and on their physiological significance. *Journal of Physiology*, *23*, 190-208.
- Sakitt, B. (1980). A spring model and equivalent neural network for arm posture control. *Biological Cybernetics*, *37*, 227-234.
- Saltzman, E. L., & Kelso, J. A. S. (1987). Skilled actions: A task-dynamic approach. *Psychological Review*, *94*, 84-106.
- Schmidt, E. M., Jost, R. G., & Davis, K. K. (1975). Reexamination of the force relationship of cortical cell discharge patterns with conditioned wrist movements. *Brain Research*, *83*, 213-223.
- Schmidt, R. A. (1982). *Motor control and learning*. Champaign, IL: Human Kinetics Press.
- Schmidt, R. A., Zelaznik, H. N., & Frank, J. S. (1978). Sources of inaccuracy in rapid movement. In G. E. Stelmach (Ed.), *Information processing in motor control and learning* (pp. 183-203). New York: Academic Press.
- Sherrington, C. S. (1894). On the anatomical constitution of nerves of skeletal muscles; with remarks on recurrent fibres in the ventral spinal nerve-root. *Journal of Physiology*, *17*, 211-258.
- Soechting, J. F., & Lacquaniti, F. (1981). Invariant characteristics of a pointing movement in man. *Journal of Neuroscience*, *1*, 710-720.
- Sperling, G., & Sondhi, M. M. (1968). Model for visual luminance distribution and flicker detection. *Journal of the Optical Society of America*, *58*, 1133-1145.
- Tanji, J., & Evarts, E. V. (1976). Anticipatory activity of motor cortex units in relation to direction of an intended movement. *Journal of Neurophysiology*, *39*, 1062-1068.
- Vilis, T., & Hore, J. (1986). A comparison of disorders in saccades and in fast and accurate elbow flexions during cerebellar dysfunction. In H. J. Freund, U. Büttner, B. Cohen, & J. Noth (Eds.), *The oculomotor and skeletal motor systems: Differences and similarities* (pp. 207-215). New York: Elsevier.
- Vilis, T., Snow, R., & Hore, J. (1983). Cerebellar saccadic dysmetria is not equal in the two eyes. *Experimental Brain Research*, *51*, 343-350.
- Viviani, P., & Terzuolo, C. (1980). Space-time invariance in learned motor skills. In G. E. Stelmach & J. Requin (Eds.), *Tutorials in motor behavior* (pp. 525-533). Amsterdam: North-Holland.
- Welford, A. T., Norris, A. H., & Schock, N. W. (1969). Speed and accuracy of movement and their changes with age. In W. G. Koster (Ed.), *Attention and performance II* (pp. 3-15). Amsterdam: North-Holland.
- Woodworth, R. S. (1899). The accuracy of voluntary movement. *Psychological Review*, *3*, 1-114.
- Zelaznik, H. N., Hawkins, B., & Kisselburgh, K. (1983). Rapid visual feedback processing in single-aiming movements. *Journal of Motor Behavior*, *15*, 217-236.
- Zelaznik, H. N., Schmidt, R. A., & Gielen, S. C. A. M. (1986). Kinematic properties of rapid aimed hand movements. *Journal of Motor Behavior*, *18*, 353-372.

Appendix A

Bell-Shaped Velocity Profile, Fitts's Law, and Staggered Onset Times

This Appendix solves the system of equations

$$\frac{d}{dt} V' = \alpha(-V' + T - P) \quad (\text{A1})$$

$$\frac{d}{dt} P = G[V']^+ \quad (\text{A2})$$

under the simplifying assumption that the GO signal G is a step function. Then the system can easily be integrated to demonstrate some basic properties.

In many situations, the system starts out in an equilibrium state such that the present-position command (PPC) equals the target-position command (TPC). Then a new TPC is switched on, and the system approaches a new equilibrium. Before the new TPC is switched on, $P = T$ in Equation A1. Because the system is at equilibrium, $dV'/dt = 0$. Thus by Equation A1, it also follows that $V' = 0$ under these circumstances.

Suppose that a new TPC value is switched on at time $t = 0$. If the system represents an agonist muscle, then $T(0) > P(0)$ so that the PPC increases when $T(0)$ turns on, thereby causing more contraction of its target muscle group. Thus by Equation A1,

$$\dot{V}'(0) = 0, \quad (\text{A3})$$

and

$$\frac{d}{dt} V'(0) = \alpha[T(0) - P(0)] > 0. \quad (\text{A4})$$

Consequently $V'(t) \geq 0$ for all times t such that $0 \leq t \leq T$, where T is the first positive time, possibly infinite, at which $V'(T) = 0$. While $V'(t) \geq 0$, it follows by Equation A2 that

$$\frac{d}{dt} P = G1 \quad (\text{A5})$$

To solve Equations A1 and A5, we differentiate Equation A1 at times $t \geq 0$. Then

$$\frac{d^2}{dt^2} V' = \alpha \left(-\frac{dV'}{dt} - \frac{dP}{dt} \right), \quad (\text{A6})$$

because T is constant. Substituting Equation A5 into Equation A6 yields

$$\frac{d^2}{dt^2} V' + \alpha \frac{d}{dt} V' + \alpha G1 = 0, \quad (\text{A7})$$

subject to the initial data in Equations A3 and A4.

This equation can be solved by standard methods. The solution takes the form

$$V'(t) = [T(0) - P(0)]f(t), \quad (\text{A8})$$

where $f(t)$ is independent of $T(0)$ and $P(0)$. Thus $V'(t)$ equals the initial difference between the new TPC and the initial PPC multiplied by a function $f(t)$, which is independent of the new TPC and the initial PPC. By Equation A2,

$$\frac{d}{dt} P = [T(0) - P(0)]g(t), \quad (\text{A9})$$

where $g(t) = Gf(t)$. Integration of Equation A9 yields

$$P(t) = P(0) + [T(0) - P(0)] \int_0^t g(v)dv. \quad (\text{A10})$$

Because dP/dt provides an estimate of the arm's velocity profile, Equation A9 illustrates the property of duration invariance in the special case that $G(t)$ is constant. Duration invariance is proved using a general $G(t)$ in Appendix B. Equation A9 also illustrates how the velocity profile can respond to a sudden switch in the TPC with a gradual increase then decrease in its shape, although $g(t)$ assumes a different form if $\alpha > 4G$, $\alpha = 4G$, or $\alpha < 4G$. When $\alpha > 4G$,

$$g(t) = \frac{\alpha G}{\sqrt{\alpha^2 - 4\alpha G}} e^{-\alpha/2t} [e^{t/2\sqrt{\alpha^2 - 4\alpha G}} - e^{-t/2\sqrt{\alpha^2 - 4\alpha G}}], \quad (\text{A11})$$

Term $\left[\exp\left(\frac{t}{2}\sqrt{\alpha^2 - 4\alpha G}\right) \right] - \left[\exp\left(-\frac{t}{2}\sqrt{\alpha^2 - 4\alpha G}\right) \right]$ in Equation A11 increases exponentially from the value 0 at $t = 0$, whereas term $\exp\left[-\frac{\alpha}{2}t\right]$ decreases exponentially toward the value 0 at a faster rate.

The net effect is a velocity function that increases then decreases with an approximately bell-shaped profile. In addition, $g(t) \geq 0$ and

$$\int_0^\infty g(t)dt = 1. \quad (\text{A12})$$

By Equations A10 and A12, $P(t)$ increases toward T as t increases. Thus $P(t)$ either approaches $T(0)$ with an arbitrarily small error, or an undershoot error occurs if the GO signal is switched off prematurely.

If $\alpha = 4G$, then

$$g(t) = \alpha G t e^{-\alpha/2t}. \quad (\text{A13})$$

Again, the velocity profile gradually increases then decreases, but it starts to increase linearly before it decreases exponentially. The function in Equation A13 also satisfies Equation A12, so that accurate movement or undershoot occur, depending on the duration of the GO signal.

The case of $\alpha < 4G$ deserves special attention. In this case, the rate G with which P is updated in Equation A2 exceeds the ability of the rate α in Equation A1 to keep up. As a result, an overshoot error can occur. In particular,

$$g(t) = \frac{2\alpha G}{\sqrt{4\alpha G - \alpha^2}} e^{-\alpha/2t} \sin\left(\frac{\sqrt{4\alpha G - \alpha^2}}{2}t\right) \quad (\text{A14})$$

if $0 \leq t \leq \frac{2\pi}{\sqrt{4\alpha G - \alpha^2}}$. When t exceeds $\frac{2\pi}{\sqrt{4\alpha G - \alpha^2}}$, function $g(t)$, and thus $V'(t)$, becomes negative. By Equation A2, $[V'(t)]^+ = 0$ when t exceeds $\frac{2\pi}{\sqrt{4\alpha G - \alpha^2}}$, so that by Equation A2, $P(t)$ stops moving at this time. The movement time (MT) in this case thus satisfies

$$MT = \frac{2\pi}{\sqrt{4\alpha G - \alpha^2}}. \quad (\text{A15})$$

Within this time frame, the velocity profile is the symmetric function $\sin\left(\frac{\sqrt{4\alpha G - \alpha^2}}{2}t\right)$ multiplied by the decaying, hence asymmetric, function $e^{-\alpha/2t}$. Greater overall symmetry of $g(t)$ is achieved if the rate

$\frac{\sqrt{4\alpha G - \alpha^2}}{2}$ with which the sine function changes is rapid relative to the rate $\frac{\alpha}{2}$ with which the exponential function changes; namely, if $2G \gg \alpha$.

Because $P(t)$ stops changing at time $t = \frac{2\pi}{\sqrt{4\alpha G - \alpha^2}}$, the final PPC value found from Equation A10 is

$$P\left(\frac{2\pi}{\sqrt{4\alpha G - \alpha^2}}\right) = P(0) + [T(0) - P(0)](1 + e^{-(\alpha\pi/\sqrt{4\alpha G - \alpha^2})}). \quad (\text{A16})$$

Thus an overshoot error occurs of size

$$E = [T(0) - P(0)]e^{-(\alpha\pi/\sqrt{4\alpha G - \alpha^2})}. \quad (\text{A17})$$

In accordance with Woodworth's law, the error is proportional to the distance $[T(0) - P(0)]$. Fitts's law can be derived by holding E constant in Equation A17 and varying $[T(0) - P(0)]$ to test the effect on the MT in Equation A15. Substituting Equation A15 into A17 shows that

$$E = [T(0) - P(0)]e^{-\alpha MT/2}, \quad (\text{A18})$$

which implies Fitts's law

$$MT = \frac{2}{\alpha} \log\left(\frac{T(0) - P(0)}{E}\right). \quad (\text{A19})$$

The initial condition $V(0) = 0$ in Equation A3 obtains if the system has actively tracked a constant TPC until its PPC attains this TPC value. Under other circumstances, $V(0)$ may be negative. When this occurs, $(d/dt)P$ in Equation A2 may remain 0 during an initial interval, while $V(t)$ increases to nonnegative values. Thus P begins to change only after a staggered onset time. A derivation of some properties of staggered onset times follow.

A negative initial value of $V(0)$ may obtain if a particular muscle group has been passively moved to a new position either by an external force or by the prior active contraction of other muscle groups. In such a situation, $P(t)$ may be changed by the passive update of position (PUP) circuit (Section 29) even if $T(t) = 0$, and $V(t)$ may track $P(t)$ via Equation A1 until a new equilibrium is reached. Under these circumstances, Equation A1 implies that

$$0 = \frac{d}{dt}V = \alpha(-V + 0 - P). \quad (\text{A20})$$

If we assume that this equilibrium value obtains at time $t = 0$, then

$$V(0) = -P(0) < 0, \quad (\text{A21})$$

and Equation A2 implies that

$$\frac{d}{dt}P = G[V]^+ = 0. \quad (\text{A22})$$

Thus P remains constant until V becomes positive. If a new TPC is switched on at time $t = 0$ to an agonist muscle that satisfies Equation A21, then $T(0) > P(0)$. By Equation A1, V increases according to the equation

$$\frac{d}{dt}V + \alpha V = \alpha[T(0) - P(0)], \quad (\text{A23})$$

where $\alpha[T(0) - P(0)]$ is a positive constant, until the time $t = t_1$ at which $V(t_1) = 0$. Thereafter $[V]^+ = V > 0$ so that V and P mutually influence each other through Equations A1 and A5.

Time t_1 is computed by integrating Equation A10. We find

$$V(t) = V(0)e^{-\alpha t} + [T(0) - P(0)](1 - e^{-\alpha t}) \quad (\text{A24})$$

for $0 \leq t \leq t_1$. By Equation 21,

$$V(t) = -P(0) + T(0)(1 - e^{-\alpha t}). \quad (\text{A25})$$

Thus

$$t_1 = \frac{1}{\alpha} \ln \left[1 - \left(\frac{P(0)}{T(0)} \right) \right]^{-1}. \quad (\text{A26})$$

By Equation A26, t_1 is a function of the ratio of the initial PPC value to the new TPC value.

For times $t \geq t_1$, Equations A1 and A5 can be integrated just as they were in the preceding case. Indeed,

$$V'(t_1) = 0 \quad (\text{A27})$$

by the definition of t_1 , and

$$\frac{d}{dt}V'(t_1) = \alpha[T(0) - P(0)] \quad (\text{A28})$$

by Equations A23 and A28. The initial data in Equations A27 and A28 are the same as the initial data in Equations A3 and A4 except for a shift of t_1 time units. Consequently if the GO signal onset time is also shifted by t_1 time units, then it follows from Equation A8 that at times $t \geq t_1$,

$$V'(t) = [T(0) - P(0)]f'(t - t_1). \quad (\text{A29})$$

An estimate of such a velocity profile is found by piecing together Equations A24 and A29. Thus

$$\frac{d}{dt}P = \begin{cases} 0 & \text{for } 0 \leq t < t_1 \\ G[T(0) - P(0)]f'(t - t_1) & \text{for } t_1 \leq t \end{cases} \quad (\text{A30})$$

Equation A30 illustrates how a velocity profile with a staggered onset time can occur if $V(0) < 0$. As shown in Section 25, the vector-integration-to-endpoint (VITE) command to a muscle group can compensate for a staggered onset time if its difference vector is multiplied by the same GO signal as other muscles in the synergy. In this case, the GO signal onset time is not shifted to match the onset time of each component of the VITE command.

Appendix B

Synchrony and Duration Invariance

Consider Equations A1 and A2 under the influence of an arbitrary nonnegative and continuous GO function $G(t)$. As in Appendix A, let

$$V(0) = 0 \quad (\text{B1})$$

and $P = T$ before T is switched to a new value. Suppose for definiteness that $T(t)$ switches from the value T_0 to T_1 at time $t = 0$ and that

$$T_1 > T_0 = P(0). \quad (\text{B2})$$

Consequently, equations

$$\frac{d}{dt} V = \alpha(-V + T - P) \quad (\text{B3})$$

and

$$\frac{d}{dt} P = GV \quad (\text{B4})$$

hold for $T \geq t \geq 0$. Define the new present-position command variable

$$Q(t) = P(t) - T_0. \quad (\text{B5})$$

and the new target-position constant

$$T_2 = T_1 - T_0. \quad (\text{B6})$$

Then Equations B3 and B4 can be replaced by equations

$$\frac{d}{dt} V = \alpha(-V + T_2 - Q) \quad (\text{B7})$$

and

$$\frac{d}{dt} Q = GV \quad (\text{B8})$$

for $t \geq 0$. By Equation B2,

$$Q(0) = 0. \quad (\text{B9})$$

Thus by Equations B1 and B9, both V and Q start out with 0 values at $t = 0$.

Now define new variables

$$v(t) = \frac{V(t)}{T_2}$$

and

$$q(t) = \frac{Q(t)}{T_2}.$$

By Equations B7 and B8, these variables obey the equations

$$\frac{d}{dt} v = \alpha(-v + 1 - q) \quad (\text{B12})$$

and

$$\frac{d}{dt} q = Gv$$

In addition,

$$v(0) = q(0) = 0 \quad (\text{B14})$$

by Equations B1 and B9. It is obvious that a unique solution of Equations B12 through B14 obtains no matter how T_2 and T_1 are chosen, if $T_2 > T_1$.

By combining Equations B2, B5, B6, and B11, we find that

$$P(t) = P(0) + [T_1 - P(0)]q(t), \quad (\text{B15})$$

where $q(t)$ is independent of T_1 and $P(0)$. Equation B15 proves duration invariance given a general GO function $G(t)$. Indeed, differentiating Equation B15 yields

$$\frac{d}{dt} P = [T_1 - P(0)] \frac{d}{dt} q(t), \quad (\text{B16})$$

which shows that function dq/dt generalizes function $g(t)$ in Equation A9.

Appendix C

Passive Update of Position

Descriptions of mathematical equations for a passive update of position (PUP) circuit follow. As in our description of a vector-integration-to-endpoint (VITE) circuit, equations for the control of a single muscle group will be described. Opponent interactions between agonist and antagonist muscles also exist and can easily be added once the main ideas are understood.

The PUP circuit supplements Equation C1

$$\frac{d}{dt}P = G[I]^+, \quad (C1)$$

whereby the present-position command (PPC) integrates difference vectors through time. A PUP circuit obeys the following equations: present-position command.

$$\frac{d}{dt}P = G[I]^+ + G_p[M]^+, \quad (C2)$$

outflow-inflow interface.

$$\frac{d}{dt}M = -\beta M + \gamma I - zP, \quad (C3)$$

adaptive gain control.

$$\frac{d}{dt}z = \delta G_p(-\epsilon z + [M]^+), \quad (C4)$$

The match function M in Equation C3 rapidly computes a time average of the difference between inflow (γI) and gated outflow (zP) signals. Thus

$$M \approx \frac{1}{\beta}(\gamma I - zP). \quad (C5)$$

If the inflow signal γI exceeds the gated outflow signal zP , then $[M]^+ > 0$ in Equation C5. Otherwise $[M]^+ = 0$. The *passive gating function* G_p in Equation C2 is positive only when the muscle is in a passive, or postural, state. In particular, $G_p > 0$ only when the GO signal $G(t) \approx 0$ in the VITE circuit. Figure 26 assumes that a signal $f[G(t)]$ inhibits a tonically active source of the gating signal G_p . Thus G_p is the output from a "pauser" cell, which is a tonically active cell whose output is attenuated during an active movement. Such cells are well-known to occur in saccadic eye-movement circuits (Grossberg & Kuperstein, 1986; Luschei & Fuchs, 1972; Raybourn & Keller, 1977). If both G_p and $[M]^+$ are positive in Equation C2, then $dP/dt > 0$. Consequently, P increases until $M = 0$, that is, until the gated outflow signal zP equals the inflow signal γI . At such time, the PPC is updated to match the position attained by the muscle during a passive movement. To see why this is true, we need to consider the role of function z in Equations C3 and C4.

Function z is a long-term memory (LTM) trace, or associative weight, which adaptively recalibrates the scale, or gain, of outflow signals until they are in the same scale as inflow signals. Using this mechanism, a

match between inflow and outflow signals accurately encodes a correctly updated PPC. Adaptive recalibration proceeds as follows.

In Equation C4, the learning-rate parameter δ is chosen to be a small constant to assure that z changes much more slowly than M or P . The passive gating function G_p also modulates learning, because z can change only at times when $G_p > 0$. At such times, term $-\epsilon z$ describes a very slow forgetting process that prevents z from getting stuck in mistakes. The forgetting process is much slower than the process whereby z grows when $[M]^+ > 0$. Because function M reacts quickly to its inputs γI and $-zP$, as in Equation C5, term $[M]^+ > 0$ only if

$$\gamma I > zP. \quad (C6)$$

The outflow signal P is multiplied, or gated, by z on its way to the match interface where M is computed (Figure 26).

Because z changes only when the muscle is in a postural, or a passive, state, terms γI and P typically represent the same position, or state of contraction, of the muscle group. Then Inequality C6 says that the scale γI for measuring position I using inflow signals is larger than the scale zP for measuring the same position using outflow signals. When this happens, z increases until $M = 0$; namely, until outflow and inflow measurement scales are equal.

On an occasion when the arm is passively moved by an external force, the inflow signal γI may momentarily be greater than the outflow signal zP . Because of past learning, however, the inflow signal satisfies

$$\gamma I = zP^*, \quad (C7)$$

where P^* is the outflow command typically associated with I . Thus by Equation C5,

$$M \approx \frac{\epsilon}{\beta}(P^* - P). \quad (C8)$$

By Equations C2 and C8, P quickly increases until it equals P^* . Thus, after learning occurs, P approaches P^* , and M approaches 0 very quickly, so quickly that any spurious new learning which might have occurred because of the momentary mismatch created by the onset of the passive movement has little opportunity to occur, because z changes slowly through time. What small deviations may occur tend to average out because of the combined action of the slow forgetting term $-\epsilon z$ in Equation C4 and opponent interactions.

Equations C3 and C4 use the same formal mechanisms as the *head-muscle interface* (HMI) described by Grossberg and Kuperstein (1986). The HMI adaptively recodes a visually activated target position coded in head coordinates into the same target position coded in agonist-antagonist muscle coordinates. Such a mechanism for adaptive matching of two measurement scales may be used quite widely in the nervous system. We therefore call all such systems *adaptive vector encoders*.

Received October 10, 1986

Revision received June 1, 1987

Accepted June 10, 1987 ■